NON-UNIFORM EXCITABILITY OF HIPPOCAMPAL NEURONS AFFORDS WEAK PREDICTABILITY OF FUTURE IMMEDIATE-EARLY GENE EXPRESSION PATTERNS

AUBREY MARISSA DEMCHUK
Bachelor of Science, University of Alberta, 2008

A Thesis
Submitted to the School of Graduate Studies
of the University of Lethbridge
in Partial Fulfillment of the
Requirements for the Degree

MASTER OF SCIENCE

Department of Neuroscience
University of Lethbridge
LETHBRIDGE, ALBERTA, CANADA

NON-UNIFORM EXCITABILITY OF HIPPOCAMPAL NEURONS AFFORDS WEAK PREDICTABILITY OF FUTURE IMMEDIATE-EARLY GENE EXPRESSION PATTERNS

AUBREY MARISSA DEMCHUK

Date of Defence: December 1, 2014

Dr. Bruce L. McNaughton *Supervisor*	*Professor*	*Ph.D.*
Dr. Robert J. Sutherland *Thesis Examination Committee Member*	*Professor*	*Ph.D.*
Dr. Igor Kovalchuk *Thesis Examination Committee Member*	*Professor*	*Ph.D.*
Dr. Robbin Gibb *Chair, Thesis Examination Committee*	*Associate Professor*	*Ph.D.*

ABSTRACT

Early immediate-early gene (IEG) studies and electrophysiological data support the "uniform random sample with replacement" (URSWR) model for the orthogonalization of memory representations in the rodent hippocampus. This model is challenged, however, by the observed "preplay" of place cell firing sequences and recent IEG studies that fail to demonstrate the proportionate increase in neuron recruitment predicted to accompany multiple environments. Thus, the purpose of this study was to assess preplay at the molecular level. Utilizing *Arc*/*Homer1a* fluorescent *in situ* hybridization, this study compared patterns of rat neural activity during rest in a familiar environment and during the subsequent exploration of a novel environment. The observed overlap between IEG expression patterns was statistically equivalent to that expected by the URSWR model in both CA1 and CA3 but became significantly higher when analysis was restricted to presumably highly active cells, effectively uniting both the URSWR and preselection models of hippocampal pattern separation.

ACKNOWLEDGEMENTS

First and foremost, I owe tremendous thanks to my supervisor, Dr. Bruce McNaughton, for his continuous support, encouragement, comments and criticisms. Bruce has a contagious drive for excellence in this field and it is an honour to have been mentored by someone with such extensive experience and great passion. I would also like to thank my other committee members, Dr. Robert Sutherland and Dr. Igor Kovalchuk, for their comments and discussion over the course of this project.

In addition, I would like to acknowledge the following people for their technical or administrative assistance: Dr. Michael Eckert, Dr. Ben Clark, and Lilia Mesina for forgiving my considerably inferior FARSIGHT and Matlab knowledge and lending both their scripts and expertise; Valérie Lapointe for providing an extra pair of hands during animal handling, perfusions and tissue preparation; the entire animal care staff (particularly our veterinarian, Isabelle Gauthier, and our senior animal health technician, Karen Dow-Cazal); Dr. Neal Melvin for designing the *Arc* primers; Doug Bray for general microscope maintenance; and Amanda Mauthe-Kaddoura for (seemingly single-handedly) keeping the Canadian Centre for Behavioural Neuroscience functioning.

Of course, I am also extremely grateful to my partner, my friends, and my family (especially my parents, Robert and Susan Demchuk, and grandmother, Margaret Ross) for providing healthy distractions and the mental, physical and financial support necessary to help me achieve my goals. Thank you!

TABLE OF CONTENTS

LIST OF TABLES

LIST OF FIGURES

LIST OF ABBREVIATIONS

CA1	*Cornu Ammonis* subfield 1
CA3	*Cornu Ammonis* subfield 3
Cy3	Cyanine 3
DAPI	4’,6’-diamidino-2-phenylindole
DIG	Digoxigenin
DNA	Deoxyribonucleic acid
EC	Entorhinal cortex
EGFP	Enhanced green fluorescent protein
HC	Home cage
HRP	Horseradish peroxidase
HV	High voltage
IEG	Immediate-early gene
INF	Intranuclear foci
mRNA	Messenger ribonucleic acid
NE	Novel environment
NeuN	Neuronal nuclei
PBS	Phosphate buffered saline
PCR	Polymerase chain reaction
PFA	Paraformaldehyde
POD	Peroxidase
RNA	Ribonucleic acid
SE	Standard error
TSA	Tyramide signal amplification
URSWR	Uniform random sample with replacement
3D	Three-dimensional

FULL ABSTRACT

The hippocampus is believed to minimize similarities between novel and familiar memory representations by amplifying small variations in cortical input patterns, a process referred to as pattern separation (for example, McNaughton & Nadel, 1990). Early immediate-early gene (IEG) studies (Guzowski, McNaughton, Barnes, & Worley, 1999; Vazdarjanova & Guzowski, 2004) and electrophysiological data (Leutgeb, Leutgeb, Moser & Moser, 2007; Leutgeb, Leutgeb, Treves, Moser & Moser, 2004; Muller & Kubie, 1987) tend to support the "uniform random sample with replacement" model, which postulates that hippocampal neurons have a uniform probability of activation and are assigned for activation by random selection. This "default" model is challenged, however, by the observed "preplay" of place cell firing sequences (Dragoi & Tonegawa, 2013; Dragoi & Tonegawa, 2011), recent IEG studies that fail to demonstrate the proportionate increase in neuron recruitment predicted to accompany multiple environments (for example, Alme et al., 2010), and the observation that both the firing rates of hippocampal neurons and the number of place fields expressed in a given environment (or over multiple environments) follow log-normal distributions (Maurer, Cowen, Burke, Barnes & McNaughton, 2006; Mizuseki & Buzsáki, 2013; Rich, Liaw & Lee, 2014). Altogether, these studies propose an alternative "preselection" model for neural activation where some cells have an intrinsically higher probability than others of being active in any given environment or brain state. Given such evidence against the uniform random sample with replacement model, the purpose of this study was to assess the concept of preselection using molecular markers of neural activity that permit analysis of co-activity patterns. Specifically, double-label *Arc/Homer1a* fluorescent *in*

situ hybridization and automated nuclear segmentation coupled with automated mRNA foci detection were utilized to analyze extensive populations of rat hippocampal and cortical neurons during both home cage rest and during the subsequent exploration of a remote novel environment. Based on the overall mRNA expression patterns of the IEGs *Arc* and *Homer1a*, the active CA1, CA3 and dorsolateral entorhinal cortex neuronal populations during rest or sleep in a familiar environment and during the subsequent exploration of a novel environment were only weakly correlated and the observed pattern overlap could statistically be attributed to random chance (as dictated by the uniform random sample with replacement model). However, when analysis was restricted to presumably more active neurons (that is, those with above average nuclear IEG mRNA focus volumes), the observed overlap between IEG expression patterns became significantly higher than that expected by random chance in both CA1 and CA3 hippocampal subregions after exploration of a novel environment (as predicted by the preselection model). Altogether, it appears that a minority of hippocampal cells have a higher propensity for activation but are masked by the immense population of less active cells in IEG studies that do not take into account the magnitude of activation at the cellular level. Hence, this study unites the uniform random sample with replacement and preselection models of hippocampal pattern separation and emphasizes the necessity of taking into account the highly skewed nature of activity distributions when assessing neural ensemble representations.

INTRODUCTION

Memory traces in the hippocampus

Spatial and episodic memory rely on a network of cortical and subcortical structures for memory encoding, consolidation and retrieval. In mammals, the hippocampus is functionally critical to such cognitive processes (O'Keefe & Nadel, 1978; Scoville & Milner, 1957; Squire & Alvarez, 1995) and both electrophysiological and molecular traces of recent experience can be detected in hippocampal neurons. "Place cells" are hippocampal neurons that fire action potentials (that is, exhibit "place fields") when an animal is in a specific location within a particular environment (O'Keefe & Dostrovsky, 1971). During exploration of a novel environment, the active ensemble of place cells and their temporally-specific sequence of firing become the underlying framework for a corresponding spatial map in the hippocampus. In addition, the proportion of neurons in CA1, CA3 and the dentate gyrus of the hippocampus exhibiting place fields varies systematically by region and is consistent with the proportion of neurons expressing the immediate-early genes (IEGs) *Arc* and *Homer1a* (Barnes, McNaughton, Mizumori, Leonard, & Lin, 1990; Guzowski et al., 1999; Vazdarjanova, McNaughton, Barnes, Worley & Guzowski, 2002; Vazdarjanova & Guzowski, 2004; Wilson & McNaughton, 1993). *Arc* (or *Arg3.1*) and *Homer1a* are rapidly and dynamically regulated by synaptic activity and may cooperatively function to modify synaptic efficacy in the hippocampal and neocortical networks responsible for encoding memories (Brakeman et al., 1997; for review, see Guzowski, 2002; Link et al., 1995; Lyford et al., 1995; McClelland, McNaughton & O'Reilly, 1995). Hence, detection of IEG expression patterns has emerged as a surrogate for recording neural spiking activity

directly that offers not only increased cellular resolution but also the potential for large-scale mapping of behaviourally relevant circuits with both temporal and spatial specificity (for review, see Guzowski, Timlin, Roysam, McNaughton, Worley, & Barnes, 2005).

Patterns of neural activity are recapitulated during rest

Following spatial exploration, a reactivation of both electrophysiological and molecular patterns of neural memory traces can be detected in the hippocampus. Hippocampal place cells that fire during spatial exploration tend to stay active during subsequent slow-wave sleep (Kudrimoti, Barnes, & McNaughton, 1999; Pavlides & Winson, 1989; Wilson & McNaughton, 1994) or quiet wakefulness (Foster & Wilson, 2006; O'Neill, Senior, & Csicvari, 2006) and the firing pattern often maintains temporal specificity (Lee & Wilson, 2002; Skaggs & McNaughton, 1996). The strength of memory trace reactivation considerably deteriorates over thirty minutes following an experience but, nevertheless, can still intermittently be detected at least 24 hours later (Kudrimoti et al., 1999). Marrone, Schaner, McNaughton, Worley, and Barnes (2008) demonstrated that subsets of patterns of neuronal IEG activity generated by recent experience are also recapitulated during subsequent periods of rest. The reactivation of memory traces is theorized to contribute to the gradual modification of synaptic strengths and the conversion of recent experience into long-term memory (Marr, 1971; for review see Sutherland & McNaughton, 2000).

Neurons may be preselected for activation prior to experience

Interestingly, patterns of neuronal activity in the hippocampus may also be observed in advance of spatial exploration. Dragoi and Tonegawa (2011; 2013) observed that temporal sequences of place cell firing exhibited during a novel spatial experience also occurred during periods of rest preceding the experience and were independent of the replay of previous familiar experiences. Accordingly, it has also been shown that place cells have intrinsically lower spike thresholds than silent cells from the onset of spatial exploration and future place cells display higher burst propensities than silent cells even prior to sensory input (Epsztein, Brecht & Lee, 2011). In fact, firing rate during the slow-wave sleep preceding exploration of a novel environment is moderately correlated with the subsequent number of place fields expressed per cell (Rich et al, 2014). Furthermore, the firing rates of hippocampal neurons follow a persistent, highly skewed distribution (log-normal; Mizuseki & Buzsáki, 2013), as does the number of place fields expressed in a given environment (or over multiple environments; Maurer et al., 2006; Rich et al., 2014), which supports that a highly active minority of cells may be inherently biased for activity. Altogether, these phenomena suggest that neural dynamics during rest or sleep may coordinate hippocampal cell assemblies and that at least a fraction of cells may be designated for activation prior to an experience.

Pattern separation in the hippocampus

The hippocampus is believed to minimize similarities between novel and familiar memory representations by amplifying small variations in cortical input patterns and thereby creating discrete maps of the locations or firing rates of place cells between

distinct environments, a process referred to as pattern separation (Marr, 1971; McNaughton & Morris, 1987; McNaughton & Nadel, 1990). Early IEG studies (Guzowski et al., 1999; Vazdarjanova & Guzowski, 2004) and electrophysiological data (Leutgeb et al., 2007; Leutgeb et al., 2004; Muller & Kubie, 1987) tend to support the "uniform random sample with replacement" model for orthogonalization of neural memory representations, which postulates that hippocampal neurons have a uniform probability of activation and are assigned for activation by random selection.

This model is challenged, however, by the recently observed preplay of place cell firing sequences (Dragoi & Tonegawa, 2011; Dragoi & Tonegawa, 2013) and the highly skewed distributions of firing rate and number of place fields exhibited by hippocampal neurons (Maurer et al., 2006; Mizuseki & Buzsáki, 2013; Rich et al., 2014). There is also mounting evidence that, regardless of the magnitude of an experience, there may be a "ceiling effect" with relation to the number of neurons that can be recruited to represent an environment. While fewer cells may express place fields in simple environments, additional spatial coverage in larger environments is achieved primarily through expression of multiple fields by a limited number of place cells rather than by a proportionate increase in total active place cells (Davidson, Kloosterman, & Wilson, 2009; Epsztein et al., 2011; Fenton et al., 2008; Rich et al., 2014; Thompson & Best, 1989). Similarly, Alme et al. (2010) and Chawla et al. (unpublished data, 2013) failed to demonstrate the proportionate increase in the number of dentate gyrus, CA1 and CA3 neurons expressing *Arc* predicted by the uniform random sample with replacement model following successive exploration of multiple familiar environments. In addition, Witharana et al. (unpublished data, 2013) confirmed, in five separate studies based on the

expression of the IEG *Homer1a*, that there is a significant under-recruitment of hippocampal neurons after exposure to environments of different size and after exploration of multiple novel environments (compared to that expected by the uniform random sample with replacement model). Thus, it seems that some hippocampal cells possess a higher probability of IEG activation than other cells, which is reminiscent of the intrinsic spike threshold and burst propensity differences of place cells observed by Epsztein et al. (2011) and Mizuseki and Buzsáki (2013).

Preplay of molecular neural memory representations

Altogether, the mounting evidence against the uniform random sample with replacement hypothesis suggests that the hippocampus may operate, at least partially, as a preconfigured network where neurons do not have an equal probability of activation in any given environment (McNaughton et al., 1996). Given that the recent electrophysiological evidence of preplay in CA1 (Dragoi & Tonegawa, 2011; Dragoi & Tonegawa, 2013) is a substantial (and unverified) component of this argument, the focus of this study was to assess preselection at the molecular level. More specifically, based on the expression of IEGs, is a hippocampal neuron more likely to be active in a completely novel environment if it was also recently active during rest or sleep in a familiar environment?

To address this question, this study utilized double-label *Arc*/*Homer1a* fluorescent *in situ* hybridization to visually discriminate and quantify the IEG mRNA expression pattern overlap in active CA1, CA3 and dorsolateral entorhinal cortex neuronal populations during rest in a familiar environment and during the subsequent exploration

of a remote novel environment. This method capitalizes on the vastly different but predictable time frames of *Arc* mRNA transcription (5 minutes) and *Homer1a* mRNA transcription (30 minutes) as a detectable measure of neural activity related to information processing following two separate behaviours or experiences (Guzowski et al., 2005; Vazdarjanova et al., 2002). Briefly, after a prolonged period of home cage rest or sleep, rats explored a remote novel environment for five minutes immediately before sacrifice and the observed overlap of the *Homer1a* mRNA expression pattern (representing home cage activity approximately thirty minutes prior to sacrifice) and the *Arc* mRNA expression pattern (representing activity during exploration of the novel environment approximately five minutes prior to sacrifice) was compared to that predicted by the uniform random sample with replacement model (Figure 1).

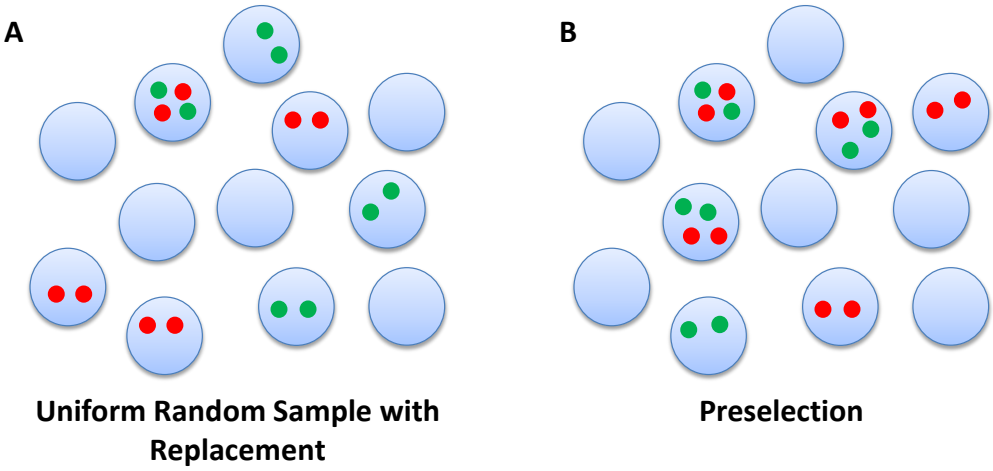

Figure 1: Patterns of *Arc* and *Homer1a* mRNA expression predicted by the uniform random sample with replacement model compared with the preselection model of hippocampal pattern separation. A. The nuclear IEG mRNA expression patterns (where *Arc* expression is represented by red foci while *Homer1a* expression is represented by green foci) elicited in an ensemble of neurons (represented as blue nuclei) after exploration of a novel environment five minutes prior to sacrifice as predicted by the uniform random sample with replacement model. Since it is assumed that all cells have a uniform excitability, expected pattern overlap (proportion of double *Arc*/*Homer1a*-labeled nuclei) is determined based on the probability of the same cell being active twice based on random chance and is equal to the product of the proportions of cells active during each behavioural epoch (that is, the product of the proportion of *Arc*-labeled nuclei and that of *Homer1a*-labeled nuclei). B. If preselection can be observed using IEGs, pattern overlap is predicted to be significantly higher than that expected by the uniform random sample with replacement model. That is, more nuclei should be double-labeled than expected by random chance alone due to the non-uniform excitability of the neural population.

MATERIALS AND METHODS

Animals

Male Long-Evans rats (3-4 months of age) were housed individually under constant humidity, temperature and a twelve hour light/dark cycle with food and water available *ad libitum* throughout the experiment. Rats were acclimated to handling and covered transport over the 3-4 weeks prior to behavioural testing. In total, twelve animals were used for the study: six home cage control animals and six animals exposed to a single novel environment. Animals were handled, tested and sacrificed during the light cycle. All procedures were performed in accordance with the Canadian Council on Animal Care guidelines and following protocols approved by the Institutional Animal Care and Use Committee at the University of Lethbridge.

Behavioural testing

Prior to testing and sacrifice, rats were quiescent in their home cage environment (though sleep versus quiet wakefulness was not monitored). In two cohorts (each consisting of three home cage controls and three experimental animals), six rats were sacrificed directly from home cage and an additional six rats were allowed to explore a remotely-located novel environment without interference for five minutes and sacrificed immediately after the exploration session (Figure 2). The first cohort was sacrificed alternating control and experimental animals (rats 1-3 of each treatment group in that order) and, a week later, the second cohort was sacrificed beginning with all control animals and finishing with all experimental animals (rats 4-6 of each treatment group in

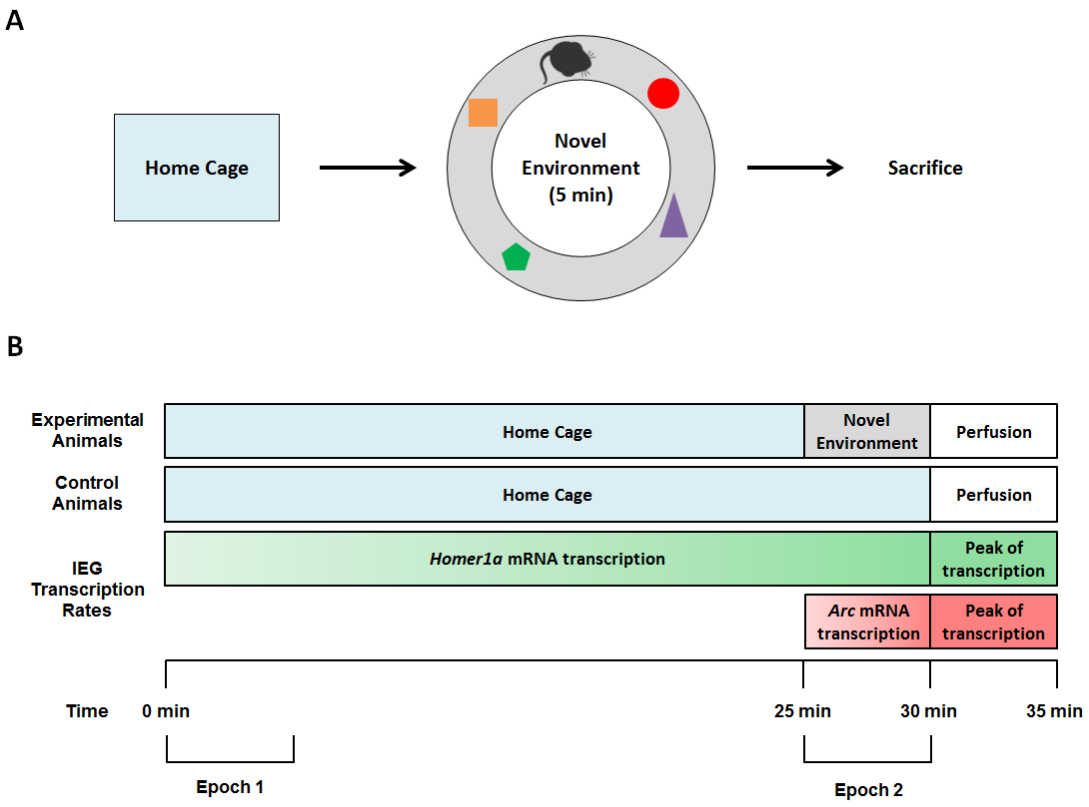

Figure 2: Schematic and timeline of experimental and control paradigms and the corresponding rates of IEG transcription. A. Schematic of the experimental paradigm (not to scale). Rats were allowed to explore a novel circular track containing novel objects for five minutes prior to sacrifice after a prolonged period of home cage rest. Note: the approximate locations of the objects on the track are indicated by coloured shapes that are not representative of the actual objects used. B. Timeline of the experimental and control paradigms relative to the rates of *Arc* and *Homer1a* mRNA transcription and detection (five minutes versus thirty minutes, respectively). Nuclear *Homer1a* mRNA expression at the time of sacrifice (perfusion) indicates IEG transcription initiation during the first behavioural epoch (beginning at approximately 0 minutes) which corresponds to neural activity during home cage rest in both treatment groups. Nuclear *Arc* mRNA expression at the time of sacrifice indicates IEG transcription initiation during the second behavioural epoch (beginning at 25 minutes) which corresponds to either more recent home cage neural activity (in control animals) or exploration of a novel environment (in experimental animals). Thus, a double *Arc/Homer1a*-labeled cell at the time of sacrifice was active during both epochs of activity.

that order). The novel environment consisted of a grey-painted, wooden, circular track (12.7cm wide with a 5.1cm lip along the edges and a circumference of 342.8cm) elevated 16.8cm above a larger circular field. Four novel plastic objects (a toy horse, a toy figurine, a sprinkles bottle and a toy radio) were placed on the track at approximately each of the cardinal points (Figure 3). Exploration sessions were video recorded and the number of laps completed by each experimental rat (in both the clockwise and counterclockwise directions) were subsequently scored.

Sacrifice and tissue preparation

Rats were deeply anesthetized with an intraperitoneal injection of sodium pentobarbital (100mg/kg) and perfused transcardially with phosphate buffered saline (PBS) and 4% paraformaldehyde (PFA). Following fixation, brains were extracted, post-fixed in 4% PFA for 2 hours and subsequently cryoprotected in a 30% sucrose solution. Brains were hemisected along the midline and the right hemisphere was embedded in Tissue-Tek O.C.T. compound (Sakura Finetek USA). Coronal sections (40µm) were prepared using a Leica CM3050S cryostat (Leica Biosystems), placed in PBS, manually mounted in series on Superfrost Plus slides (Fisher Scientific), dried and stored at -80°C until use.

Fluorescent in situ *hybridization*

Primers flanking portions of *Arc* intron 1, exon 2 and intron 2 were designed using online software (National Center for Biotechnology Information Primer-Blast). The exact sequences of the primers are as follows and base pair designations match those of

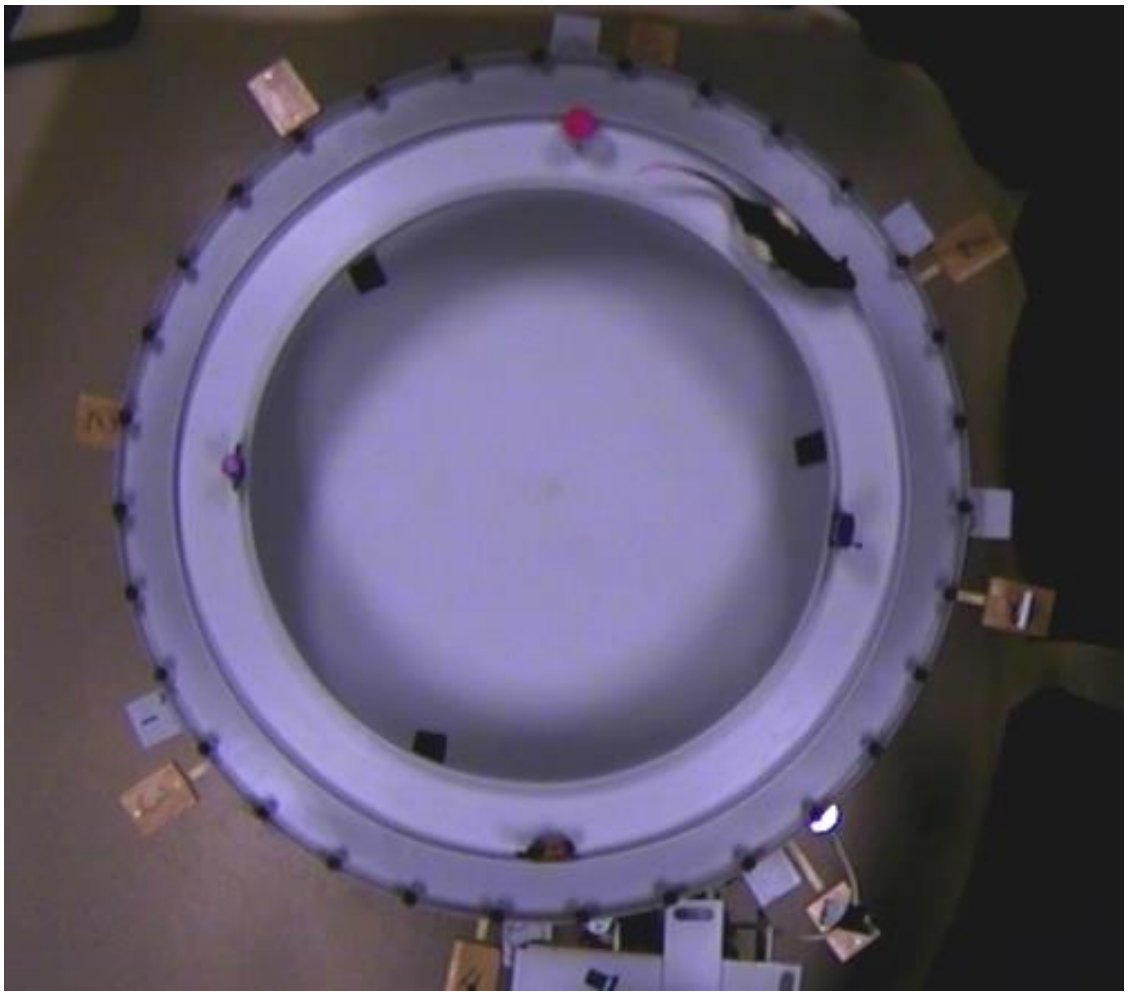

Figure 3: A still image from the video of an experimental rat exploring the novel environment. The novel environment consisted of a grey-painted, wooden, circular track elevated above a larger circular field with four novel plastic objects placed on the track at approximately each of the cardinal points. Rats were allowed to explore freely without interference for five minutes.

GenBank accession number NC_005106: 5'-CTTAGAGTTGGGGGAGGGCAGCAG-3' (forward primer, base pairs 2022-2045) and 5'-ATTAACCCTCACTAAAGGG-CCCTGGGGCCTGTCAGATAGCC-3' (reverse primer tagged with T3 polymerase binding site on 5' end, base pairs 2445-2466). Polymerase chain reaction (PCR) was performed with these primers on genomic rat DNA template using a *Taq* PCR Kit (New England Biolabs) as per the manufacturer's protocol. PCR product was purified using a Qiagen PCR Purification Kit (Life Technologies Inc.) and verified by gel electrophoresis. A commercial transcription kit (MAXIscript T3; Life Technologies Inc.) and Digoxigenin (DIG) RNA Labeling Mix (Roche Diagnostics) were used as per the manufacturer's protocols to generate DIG-labeled *Arc* intron-specific antisense riboprobes from the PCR template. Fluorescein-labeled *Homer1a* probes targeting the 3' untranslated region were generated as previously described (Montes-Rodríguez, Lapointe, Trivedi, Lu, Demchuk & McNaughton, 2013). Riboprobes were purified with mini QuickSpin columns (Roche Diagnostics) and yield was verified by gel electrophoresis.

Fluorescent *in situ* hybridization was performed as previously described (Guzowski et al., 1999; Marrone et al., 2008; Montes-Rodríguez et al., 2013). Three sections separated by 200µm along the coronal axis (centered at approximately -3.30mm from Bregma; Paxinos & Watson, 1997) were processed from each animal (Figure 4A). DIG-labeled *Arc* riboprobe signal was amplified with anti-digoxigenin-POD (1:300; Roche Diagnostics), Tyramide Signal Amplification (TSA) Biotin Tyramide Reagent Pack (1:100; PerkinElmer) and Streptavidin-Texas Red (1:200; PerkinElmer). Fluorescein-labeled *Homer1a* probe was detected with anti-Fluorescein-HRP antibody

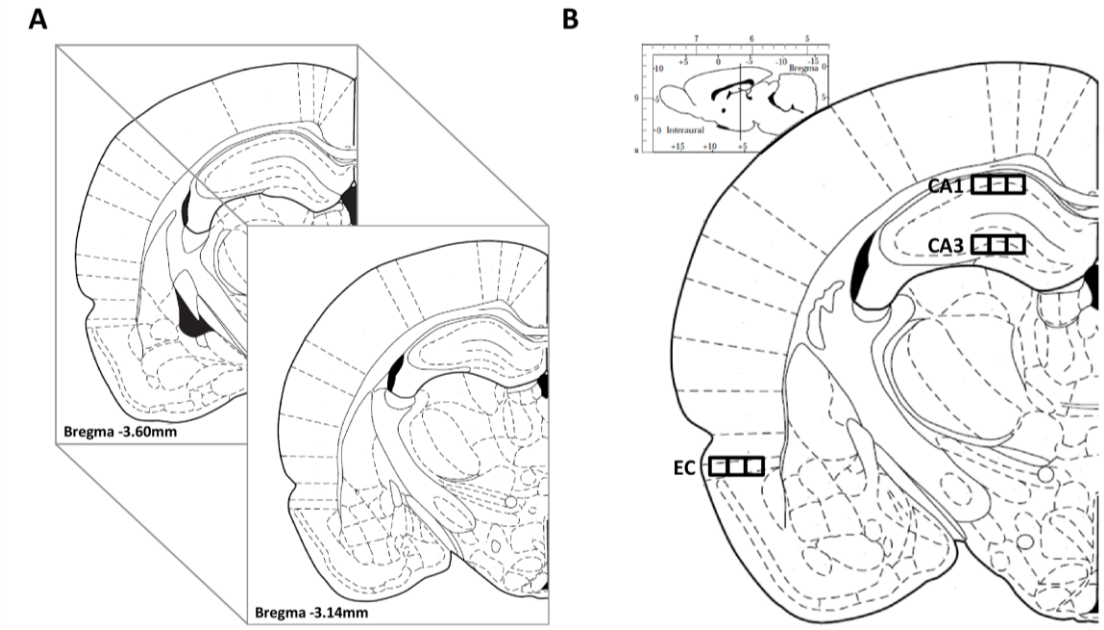

Figure 4: Range of sampled positions along coronal axis and locations of imaged subregions. A. Three sections separated by 200µm along the coronal axis were processed from each animal. Analyzed sections ranged from approximately -3.14mm to -3.60mm from Bregma (Paxinos & Watson, 1997). B. Position of imaged *z*-stacks (317µm x 317µm) in CA1, CA3 and dorsolateral entorhinal cortex (EC). Images adapted from Figures 30-32 of The Rat Brain in Stereotaxic Coordinates (Paxinos & Watson, 1997).

(1:1000; Jackson ImmunoResearch Labs) and amplified with a Fluorescein TSA kit (1:100; PerkinElmer). Nuclei were counterstained with 4',6'-diamidino-2-phenylindole (DAPI; 1:2000; Sigma-Aldrich).

Image acquisition

Post-processing, an Olympus FluoView FV1000 confocal laser scanning microscope (Olympus America Inc.) was used to acquire three adjacent 40x magnification *z*-stacks of 1.0µm optical sections per brain section each of the dorsolateral entorhinal cortex, dorsal CA1, and dorsal CA3 (Figure 4B). Imaging parameters were kept constant for all sections. Dorsolateral entorhinal cortex was included not only for convenience (this region is evident in the same coronal sections selected to represent dorsal CA1 and CA3) but also because the entorhinal cortex is anatomically and functionally connected with the hippocampus (for review, see Knierim, Lee & Hargreaves, 2006; Witter, Wouterlood, Naber & Van Haeften, 2000). While the medial entorhinal cortex is known to be populated with "grid cells" that demonstrate location-specific firing at regular intervals (and consequently it would be unsurprising to observe at least partially preconfigured patterns of activity in this region; Hafting, Fyhn, Molden, Moser & Moser, 2005), the more lateral region does not demonstrate this potentially biasing spatially-tuned pattern of neural activity (Hargreaves, Rao, Lee & Knierim, 2005) and thus is a more suitable region for comparison against hippocampal subregions. It should be noted that, due to the difficulty in discriminating cortical regions based on DAPI-stained nuclei, it is possible that there was minor overlap of imaged regions of the dorsolateral entorhinal cortex with the piriform and/or perirhinal cortices.

Nuclear segmentation and foci-based analysis

Images of *z* optical planes were converted into image stacks using ImageJ (National Institutes of Health) and processed for automated three-dimensional (3D) intranuclear foci quantification using software plug-ins developed in Java for ImageJ as previously described (Montes-Rodríguez et al., 2013; Appendix A). The following pixel thresholds were used for foci detection: minimum green intensity = 40, minimum red intensity = 40, and minimum blue intensity = 50. Subsequently, the image stacks were preprocessed in ImageJ (colour channels were separated and blurred) and subjected to automated 3D nuclear segmentation using FARSIGHT and Matlab (Bjornsson et al., 2008; MathWorks, R2011b; Appendix A; Figure 5B). Using the FARSIGHT Nucleus Editing Tool, all segmented nuclei outside of the CA1 and CA3 regions were deleted and obvious under-segmentation errors were corrected manually. The foci coordinates were overlaid with the nuclear segmentation results in Matlab and guard zones were applied (seven optical sections from the top and bottom of the *z* plane and 30 pixels from each edge of the *x* and *y* planes; Appendix A). The number of *Arc* mRNA only expressing cells, *Homer1a* mRNA only expressing cells, "double-labeled" *Arc* and *Homer1a* mRNA expressing cells, and total nuclei were automatically scored (Figure 5C). *Arc*- and *Homer1a*-labeled nuclei counts were corrected by adding the number of double-labeled cells to each.

Glial correction

The number of total nuclei detected by FARSIGHT included glia, which do not demonstrate an activity-regulated upregulation of *Arc* or *Homer1a* and thus may

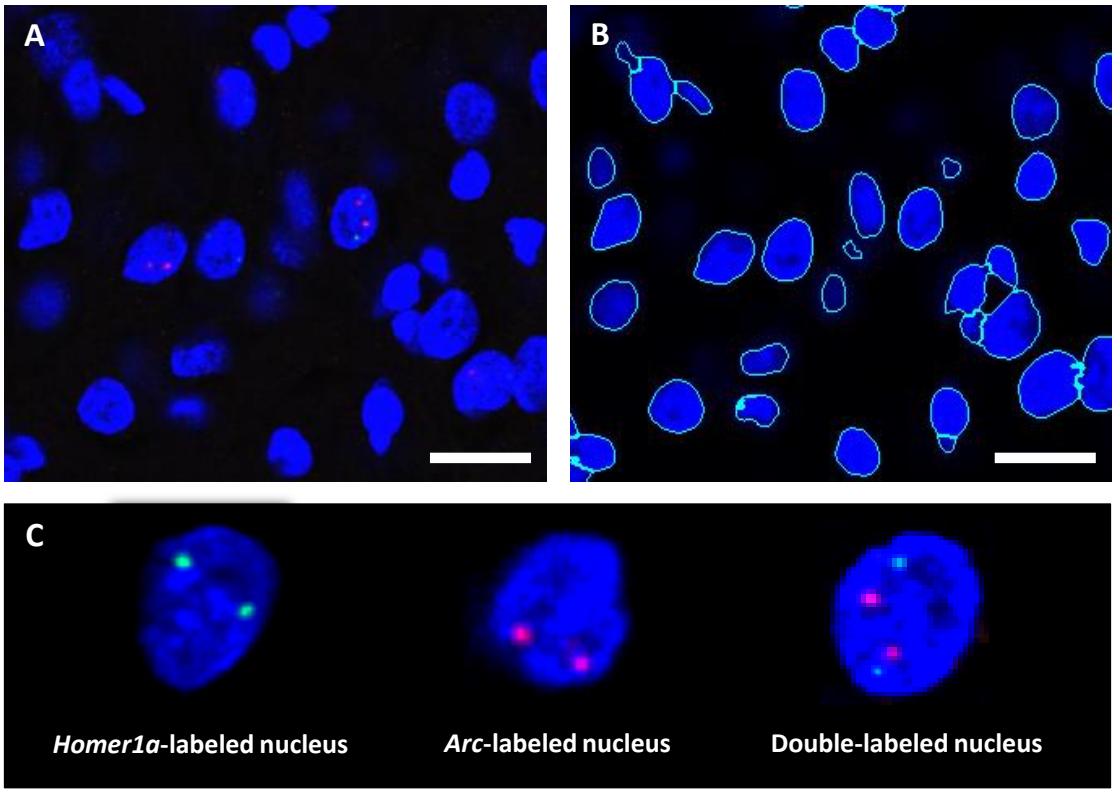

Figure 5: Single-layer confocal images from CA3 demonstrating *Arc* and *Homer1a* transcription foci and FARSIGHT automated nuclear segmentation results. A. Subset of a single layer of a confocal *z*-stack from the CA3 region of a rat from the experimental treatment group. Nuclei were counterstained with DAPI (blue). Single *Arc*- and *Homer1a*-labeled nuclei as well as double-labeled nuclei are evident. Scale bar: 20µm. B. Corresponding preprocessed single layer image demonstrating FARSIGHT nuclear segmentation results. Detected nuclear borders are indicated with light blue outlines. Scale bar: 20µm. C. Enlarged DAPI-stained nuclei demonstrating a *Homer1a*-labeled nucleus (green foci only; active during first behavioural epoch), an *Arc*-labeled nucleus (red foci only; active during second behavioural epoch) and a double-labeled nucleus (both red and green foci; active during both epochs).

contribute to false positive effects. To determine a "glial correction factor" for each analyzed brain region, additional slides of tissue (from within the sampled range of anatomical positions) were stained with rabbit anti-NeuN-Cy3 (1:100; Millipore) overnight and nuclei were subsequently counterstained with DAPI (1:2000; Sigma-Aldrich). Sections were imaged as previously described. Automated FARSIGHT classification of glial and neuronal nuclei was attempted but produced a very modest representation of the total glial population (Appendices A and B). Thus, to determine a more accurate glial correction factor, the total number of neurons and glia were manually scored in ImageJ (within the regions of interest applied to the experimental tissue) in three *z*-stacks each from CA1, CA3 and dorsolateral entorhinal cortex of two animals (one home cage control and one animal that explored a novel environment). Expression of NeuN (a neuron-specific protein), DAPI saturation and nuclear size and shape were used to visually discriminate neurons from glia such that nuclei classified as neuronal had extensive cytosolic NeuN labeling, less DAPI saturation and were generally of larger size and more regular (round) shape than glial nuclei (Figure 6). The average proportion of glia observed in each region was subtracted from the experimental total cell counts.

Blobless analysis

Using the FARSIGHT segmentation results and Matlab, the volume, total pixel intensity (sum of all pixel intensities), average pixel intensity (total intensity/volume), fano factor (variance/mean), tail (mean intensity value at the top 0.1% of histogram), skewness (asymmetry of distribution), and sparsity (how diffuse the intensity was) was determined for each segmented nucleus in each of the blue (DAPI), red (*Arc*) and green

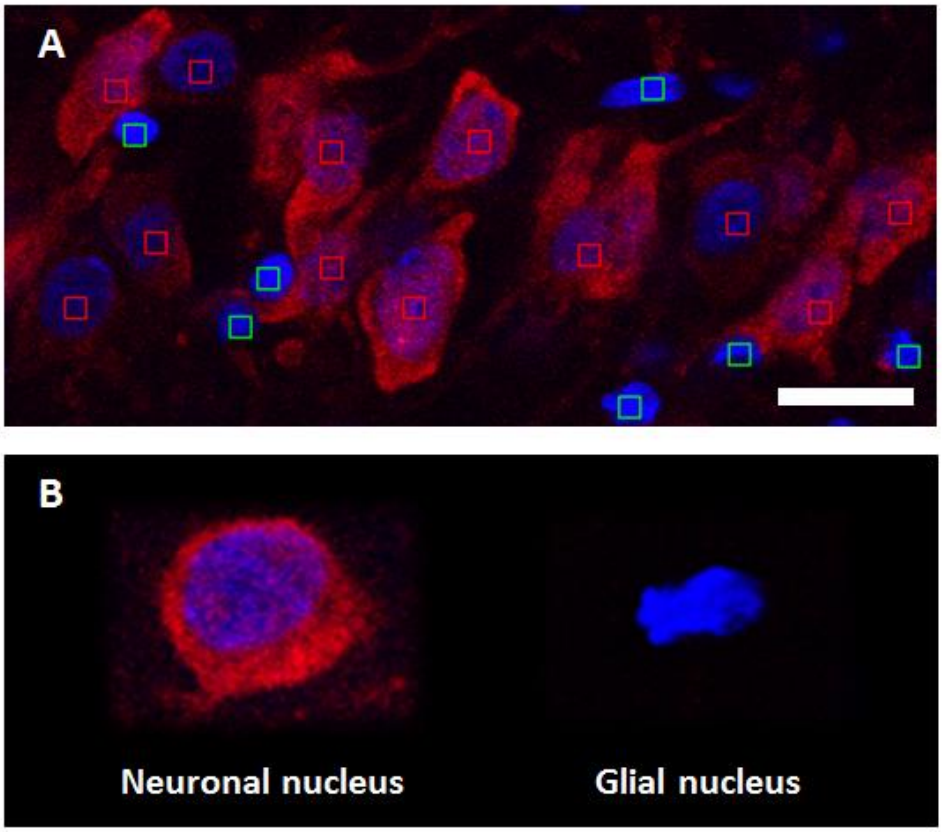

Figure 6: Single-layer confocal images from CA3 demonstrating the visual differences between neuronal and glial nuclei after staining with anti-NeuN-Cy3 and DAPI. A. Subset of a single layer of a confocal *z*-stack from the CA3 region of a home cage control rat. Tissue was labeled with anti-NeuN-Cy3 (red) and nuclei were counterstained with DAPI (blue). Nuclei were manually classified in ImageJ as neuronal (red square marker) or glial (green square marker) based on visual differences in nuclear size and shape, NeuN-labeling and DAPI saturation. Scale bar: 20µm. B. Enlarged NeuN- and DAPI-stained nuclei demonstrating the visual differences between neuronal and glial nuclei used as classification parameters. Neuronal nuclei are typically large and round, demonstrate less DAPI saturation than glial nuclei and have elevated cytosolic NeuN-labeling (a neuron-specific marker). Conversely, glial nuclei are smaller and often have a more irregular shape, demonstrate high DAPI saturation and do not exhibit NeuN-labeling.

(*Homer1a)* channels (Appendix A). To reduce the influence of segmentation errors and glial nuclei, further analysis was restricted to nuclei with volumes within one standard deviation of the mean volume (Appendix A). The analyzed population of nuclei included glial cells with volumes that fell within that range.

Statistical analyses

Random pattern overlap for each region of interest of each animal was determined by calculating the product of the proportion of cells active during the first epoch of home cage rest (that is, those expressing *Homer1a* foci) and the proportion of cells active during the second epoch of either home cage rest or spatial exploration (that is, those expressing *Arc* foci). The estimated overlap based on random chance was compared with the observed overlap (proportion of "double-labeled" cells) across animals within treatment groups for each analyzed region using a paired one-tailed *t*-test. The null hypothesis was rejected at the 0.05 level of significance. For correlation analyses, the Pearson product moment correlation coefficient (*r*) was determined.

RESULTS

Sampled populations of CA1, CA3 and cortical neurons were extensive

Across all regions of all animals, a total of 87302 nuclei (including glia) were sampled. Manual counts of NeuN-stained tissue revealed, on average, 14% ± 2% of CA1 nuclei were glia, 49% ± 1% of CA3 nuclei were glia and 62% ± 4% of cortical nuclei were glia (within the selected regions of interest). After correction for glia, a total of 23161 neuronal nuclei were analyzed from CA1, 15367 neuronal nuclei from CA3 and 11467 neuronal nuclei from the dorsolateral entorhinal cortex. On average, 1930 ± 152 neuronal nuclei were sampled per rat from CA1, 1281 ± 114 neuronal nuclei per rat from CA3 and 956 ± 300 neuronal nuclei per rat from entorhinal cortex.

Proportion of IEG-labeled nuclei increased after exploration of a novel environment

Home cage control animals, on average, did not show a significant difference in the proportion of nuclei exhibiting IEG foci between epochs of home cage rest in CA1 nor in dorsolateral entorhinal cortex (CA1, $p = 0.06$; EC, $p = 0.09$). However, there was a significant increase in the proportion of nuclei exhibiting *Arc* foci (corresponding to the second epoch of home cage rest) relative to that exhibiting *Homer1a* foci (corresponding to the first epoch of home cage rest) observed in CA3 ($p < 0.01$). Approximately 11% ± 10% of CA1 neurons, 4% ± 3% of CA3 neurons and 17% ± 10% of dorsolateral entorhinal cortical neurons demonstrated *Homer1a* mRNA expression during the first behavioural epoch. In comparison, 20% ± 5% of CA1 neurons, 12% ± 5% of CA3 neurons and 23% ± 5% of entorhinal cortex neurons demonstrated *Arc* mRNA expression

during the second epoch of home cage rest (Figure 7; Appendix B).

Rats that explored a novel environment during the second epoch of activity demonstrated a significant increase in the proportion of nuclei exhibiting *Arc* foci (corresponding to novel environment exploration) relative to that exhibiting *Homer1a* foci (corresponding to home cage rest) in CA1, CA3 and dorsolateral entorhinal cortex (CA1, $p < 0.0001$; CA3 & EC, $p < 0.001$). Approximately 11% ± 8% of CA1 neurons, 4% ± 2% of CA3 neurons and 17% ± 7% of dorsolateral entorhinal cortex neurons demonstrated *Homer1a* mRNA expression during the first behavioural epoch. Based on an unpaired, two-tailed t-test, the proportion of *Homer1a*-labeled nuclei observed during home cage rest in experimental animals is not significantly different from that during the first epoch in home cage controls (in all analyzed regions). In comparison, 40% ± 7% of CA1 neurons, 18% ± 5% of CA3 neurons and 34% ± 6% of entorhinal cortex neurons demonstrated *Arc* mRNA expression during the second behavioural epoch in experimental animals. Compared to *Arc* expression during the second epoch of home cage rest in control animals, the proportion of *Arc*-labeled cells was significantly elevated after exploration of a novel environment in CA1 and dorsolateral entorhinal cortex (CA1, $p < 0.001$; EC, $p < 0.01$) but not in CA3 ($p = 0.07$; Figure 7; Appendix B).

In all animals, the average proportion of double-labeled cells was significantly lower than that of *Homer1a*-labeled nuclei (CA1, $p < 0.05$; CA3 & EC, $p < 0.01$) and *Arc*-labeled nuclei (HC CA1 & CA3, $p < 0.001$; HC EC, $p < 0.01$; NE CA1, $p < 0.00001$; NE CA3 & EC, $p < 0.0001$). Approximately 2% ± 3% of CA1 neurons, 0.8% ± 0.7% of CA3 neurons and 3% ± 2% of dorsolateral entorhinal cortex neurons demonstrated both *Arc* and *Homer1a* mRNA expression in home cage controls. Rats exposed to the novel

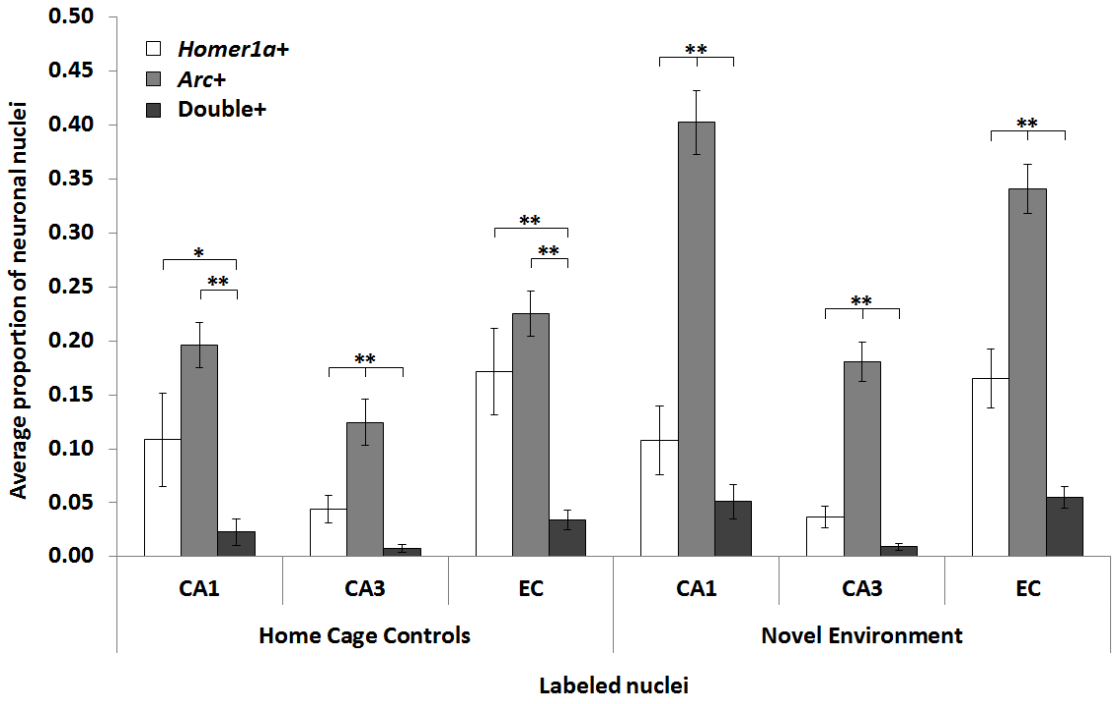

Figure 7: Average proportions of single *Arc*-labeled (*Arc*+), single *Homer1a*-labeled (*Homer1a*+) and double *Arc/Homer1a*-labeled (Double+) nuclei in CA1, CA3 and dorsolateral entorhinal cortex (EC) of home cage (HC) controls and rats that explored a novel environment (NE) after a period of home cage rest. Home cage control animals, on average, did not show a significant difference in the proportion of nuclei exhibiting IEG foci between epochs of home cage rest in CA1 nor in dorsolateral entorhinal cortex (CA1, $p = 0.06$; EC, $p = 0.09$). However, there was a significant increase in the proportion of nuclei exhibiting *Arc* foci (corresponding to the second epoch of home cage rest) relative to that exhibiting *Homer1a* foci (corresponding to the first epoch of home cage rest) observed in CA3 ($p < 0.01$). Rats that explored a novel environment during the second behavioural epoch demonstrated a significant increase in the proportion of nuclei exhibiting *Arc* foci (corresponding to exploration of the novel environment) relative to *Homer1a* foci (corresponding to home cage rest) in CA1, CA3 and dorsolateral entorhinal cortex (CA1, $p < 0.0001$; CA3 & EC, $p < 0.001$). In all animals, the average proportion of double-labeled cells was significantly lower than that of *Homer1a*-labeled nuclei (CA1, $p < 0.05$; CA3 & EC, $p < 0.01$) and *Arc*-labeled nuclei (HC CA1 & CA3, $p < 0.001$; HC EC, $p < 0.01$; NE CA1, $p < 0.00001$; NE CA3 & EC, $p < 0.0001$). Error bars indicate standard error.

environment during the second epoch had approximately 5% ± 4% of CA1 neurons, 0.9% ± 0.5% of CA3 neurons and 6% ± 3% of neurons in the entorhinal cortex that were double *Arc/Homer1a*-labeled. There was no statistically significant difference between the observed proportions of double-labeled cells in home cage controls versus experimental rats in all regions analyzed (Figure 7; Appendix B).

Observed pattern overlap was equivalent to that expected by random chance

On average across animals, the observed proportion of double *Arc/Homer1a*-labeled nuclei was not significantly higher than that expected by the uniform random sample with replacement model in CA1, CA3 nor in dorsolateral entorhinal cortex after exploration of a novel environment (CA1, $p = 0.08$; CA3, $p = 0.09$; EC, $p = 0.33$). There was also no statistically significant difference between the observed and random chance overlap of IEG expression patterns in all regions analyzed in home cage control animals (CA1, $p = 0.25$; CA3, $p = 0.12$; EC, $p = 0.17$; Figure 8; Appendix B).

Equalization of home cage proportions of *Arc*- and *Homer1a*-labeled nuclei

Previous studies have demonstrated statistically equivalent proportions of nuclei exhibiting IEG expression during repeat exposure to the same environment (for example, Vazdarjanova et al., 2002). Thus, the average red pixel intensity threshold was increased from 40 to 60 to approximately equalize home cage proportions of *Arc*- and *Homer1a*-labeled nuclei in control rats (refer to Figure 7). After this increase, home cage control animals, on average, did not show a significant difference in the proportion of nuclei exhibiting IEG foci during the second epoch of home cage activity relative to the first in

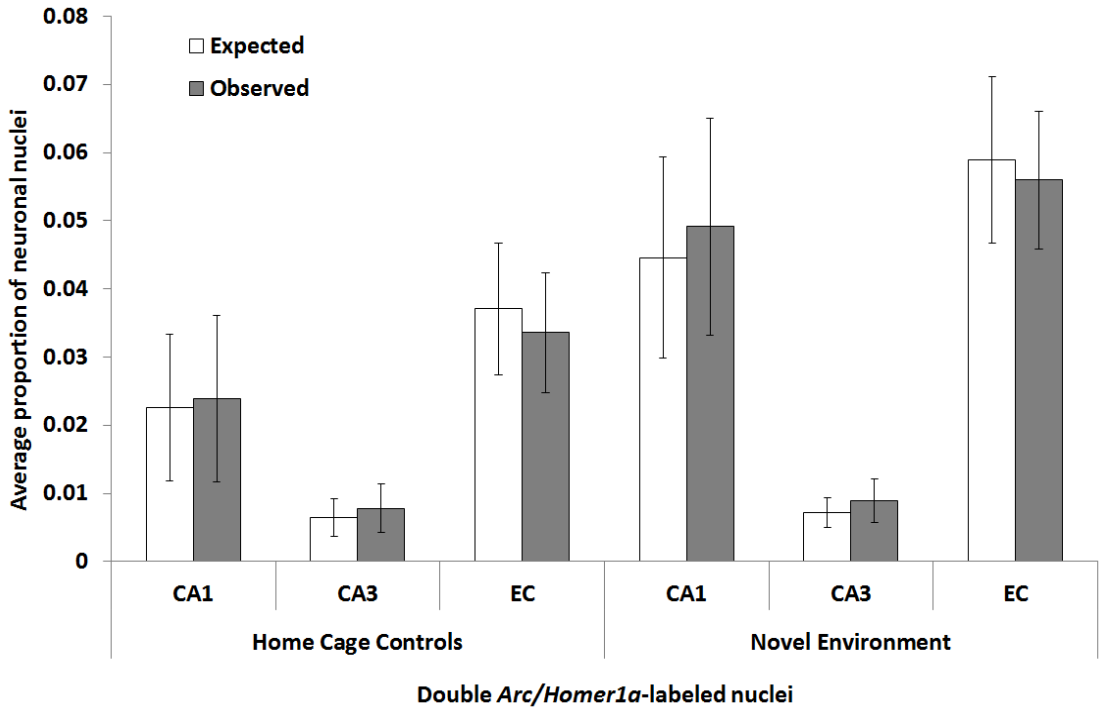

Figure 8: Average observed proportions and proportions expected based on the uniform random sample replacement model of *Arc/Homer1a* double-labeled nuclei in CA1, CA3 and the dorsolateral entorhinal (EC) cortex of home cage controls and rats that explored a novel environment after a period of home cage rest. Expected overlap was determined by calculating the product of the proportion of *Homer1a*-labeled nuclei and the proportion of *Arc*-labeled nuclei. On average across animals, the observed proportion of double *Arc/Homer1a*-labeled nuclei was not significantly higher than that expected by random chance in CA1, CA3 nor in the entorhinal cortex after exploration of a novel environment (CA1, $p = 0.08$; CA3, $p = 0.09$; EC, $p = 0.33$). There was also no statistically significant difference between the observed and expected overlap of IEG expression patterns in all regions analyzed in home cage control animals (CA1, $p = 0.25$; CA3, $p = 0.12$; EC, $p = 0.17$). Error bars indicate standard error. Large variability in the proportions of neural populations expressing IEGs was evident between animals, which may account for the large error bars (Appendix B).

CA1, CA3 nor in dorsolateral entorhinal cortex (CA1, $p = 0.57$; CA3, $p = 0.07$; EC, $p = 0.32$; Figure 9; Appendix B).

Rats that explored a novel environment during the second epoch of activity still demonstrated a significant increase in the observed proportion of nuclei exhibiting *Arc* foci (corresponding to novel environment exploration) relative to that exhibiting *Homer1a* foci (corresponding to home cage rest) in CA1 and CA3 (CA1 & CA3, $p < 0.001$) but not in dorsolateral entorhinal cortex (EC, $p = 0.10$). Based on an unpaired, two-tailed *t*-test, the proportion of *Homer1a*-labeled nuclei observed during home cage rest in experimental animals was not significantly different from that observed during the first behavioural epoch in home cage controls (in all analyzed regions). Compared to the second epoch of home cage rest in control animals, the proportion of *Arc*-labeled cells was significantly elevated in experimental rats after exploration of a novel environment in CA1, CA3 and dorsolateral entorhinal cortex (CA1, $p < 0.001$; CA3, $p < 0.05$; EC, $p < 0.01$; Figure 9; Appendix B).

In all animals, the average proportion of double-labeled cells was significantly lower than that of *Homer1a*-labeled nuclei (HC CA1, HC CA3, HC EC, & NE CA1, $p < 0.05$; NE CA3 & NE EC, $p < 0.01$) and *Arc*-labeled nuclei (HC CA1, HC CA3, & NE CA1, $p < 0.01$; HC EC, $p < 0.05$; NE CA3 & NE EC, $p < 0.001$). There was no statistically significant difference between the observed proportions of double-labeled cells in home cage controls versus experimental rats in neither CA1 nor CA3 but there was a significantly higher proportion of double-labeled nuclei in dorsolateral entorhinal cortex after exploration of a novel environment relative to home cage controls ($p < 0.05$; Figure 9; Appendix B).

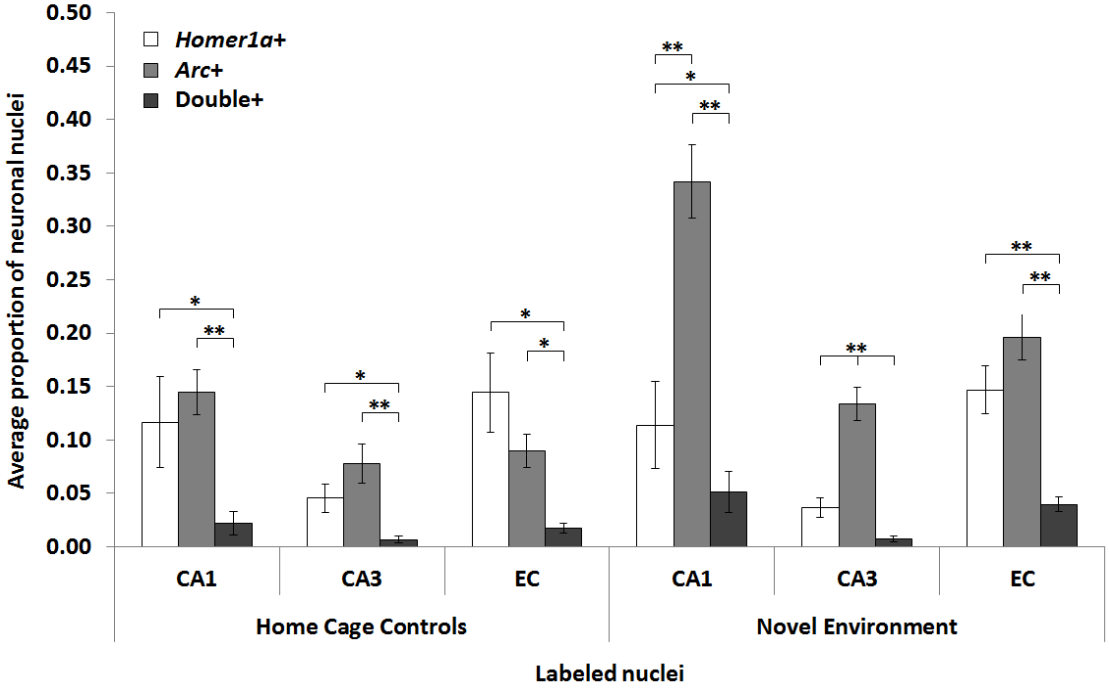

Figure 9: Normalized average proportions of single *Arc*-labeled (*Arc*+), single *Homer1a*-labeled (*Homer1a*+) and double *Arc/Homer1a*-labeled (Double+) nuclei in CA1, CA3 and dorsolateral entorhinal cortex (EC) of home cage (HC) controls and rats that explored a novel environment (NE) after a period of home cage rest. The average red pixel intensity threshold was increased to approximately equalize home cage proportions of *Arc*- and *Homer1a*-labeled nuclei in control rats (refer to Figure 7). Home cage control animals, on average, did not show a significant difference in the proportion of nuclei exhibiting IEG foci during the second epoch of home cage activity relative to the first in CA1, CA3 nor in dorsolateral entorhinal cortex (CA1, $p = 0.57$; CA3, $p = 0.07$; EC, $p = 0.32$). Rats that explored a novel environment during the second epoch of activity still demonstrated a significant increase in the proportion of nuclei exhibiting *Arc* foci (corresponding to exploration of the novel environment) relative to that exhibiting *Homer1a* foci (corresponding to home cage rest) observed in CA1 and CA3 (CA1 & CA3, $p < 0.001$) but not in dorsolateral entorhinal cortex ($p = 0.10$). In all animals, the average proportion of double-labeled cells was significantly lower than that of *Homer1a*-labeled nuclei (HC CA1, HC CA3, HC EC, & NE CA1, $p < 0.05$; NE CA3 & NE EC, $p < 0.01$) and *Arc*-labeled nuclei (HC CA1, HC CA3, & NE CA1, $p < 0.01$; HC EC, $p < 0.05$; NE CA3 & NE EC, $p < 0.001$). Error bars indicate standard error.

On average across animals, observed overlap between *Arc* and *Homer1a* mRNA expression patterns was not significantly higher than that expected by the uniform random sample with replacement model in CA1 and CA3 in home cage controls (CA1, $p = 0.09$; CA3, $p = 0.09$) nor in CA3 and dorsolateral entorhinal cortex of experimental animals (CA3, $p = 0.09$; EC, $p = 0.05$). However, the dorsolateral entorhinal cortex of home cage animals and CA1 of rats that explored a novel environment during the second epoch of activity showed a significantly higher proportion of double-labeled nuclei than expected by random chance (HC EC & NE EC, $p < 0.05$; Figure 10; Appendix B).

Long-tailed, highly skewed distribution of focus volumes

The mean *Arc* and/or *Homer1a* focus volume was calculated for each labeled nuclei. A comparison of the cumulative percentages of average focus volumes revealed both an increase in the number of nuclei exhibiting *Arc* foci and an obvious shift towards increased mean *Arc* focus volumes after exploration of a novel environment during the second behavioural epoch (relative to that of home cage controls). In comparison, the number of nuclei expressing *Homer1a* and the mean *Homer1a* focus volume were very comparable between treatment groups during the first behavioural epoch (home cage rest) (Figure 11). The frequency distributions of average focus volumes were highly skewed with long tails towards higher volumes in all regions, behavioural epochs and treatment groups (Figure 12). These distributions were approximately log-normal, though threshold restrictions during foci detection truncate the left portions of the curves (Figure 13).

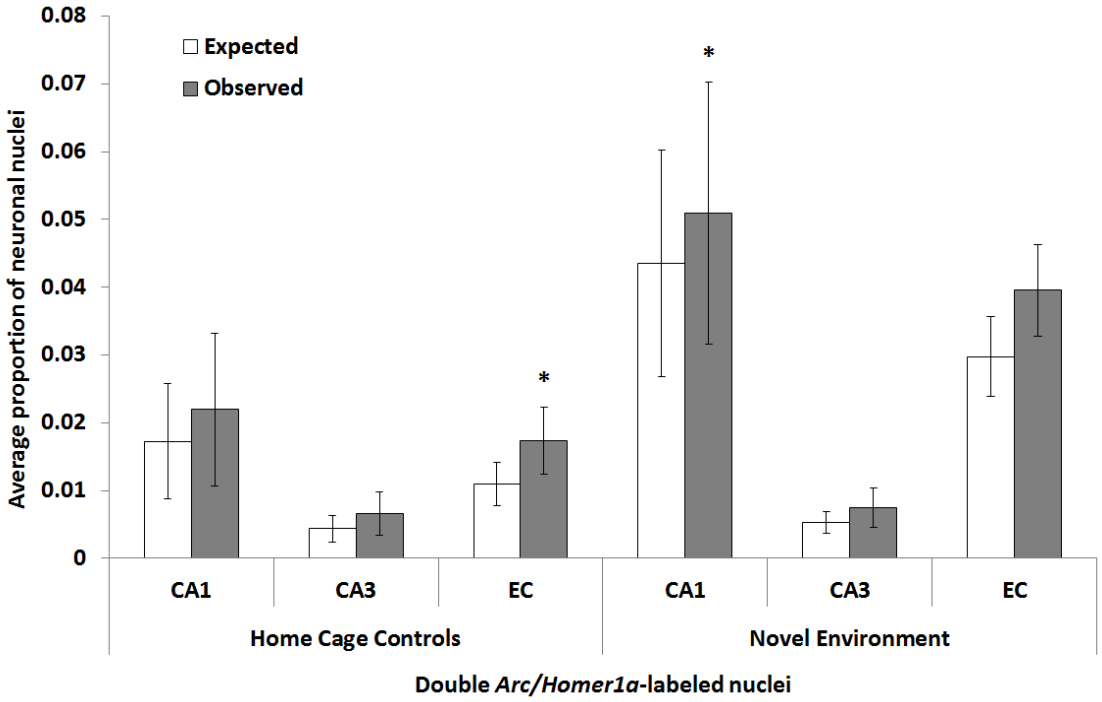

Figure 10: Normalized average observed proportions and proportions expected based on the uniform random sample replacement model of *Arc/Homer1a* double-labeled nuclei in CA1, CA3 and the dorsolateral entorhinal (EC) cortex of home cage (HC) controls and rats that explored a novel environment (NE) after a period of home cage rest. The average red pixel intensity threshold was increased to approximately equalize home cage proportions of *Arc*- and *Homer1a*-labeled nuclei in control rats. Expected overlap was determined by calculating the product of the proportion of *Homer1a*-labeled nuclei and the proportion of *Arc*-labeled nuclei. On average across animals, observed overlap between *Arc* and *Homer1a* mRNA expression patterns was not significantly higher than that expected by random chance in CA1 and CA3 in home cage controls (CA1, $p = 0.09$; CA3, $p = 0.09$) nor in CA3 and dorsolateral entorhinal cortex of experimental animals (CA3, $p = 0.09$; EC, $p = 0.05$). The dorsolateral entorhinal cortex of home cage animals and CA1 of rats that explored a novel environment during the second epoch of activity showed a significantly higher proportion of double-labeled nuclei than expected by random chance (HC EC & NE CA1, $p < 0.05$). Error bars indicate standard error. Large variability in the proportions of neural populations expressing IEGs was evident between animals, which may account for the large error bars (Appendix B). Note: after application of the Bonferroni correction (the most conservative method of addressing Type I errors associated with multiple comparisons), there was no significant difference evident between expected and observed pattern overlap in any region.

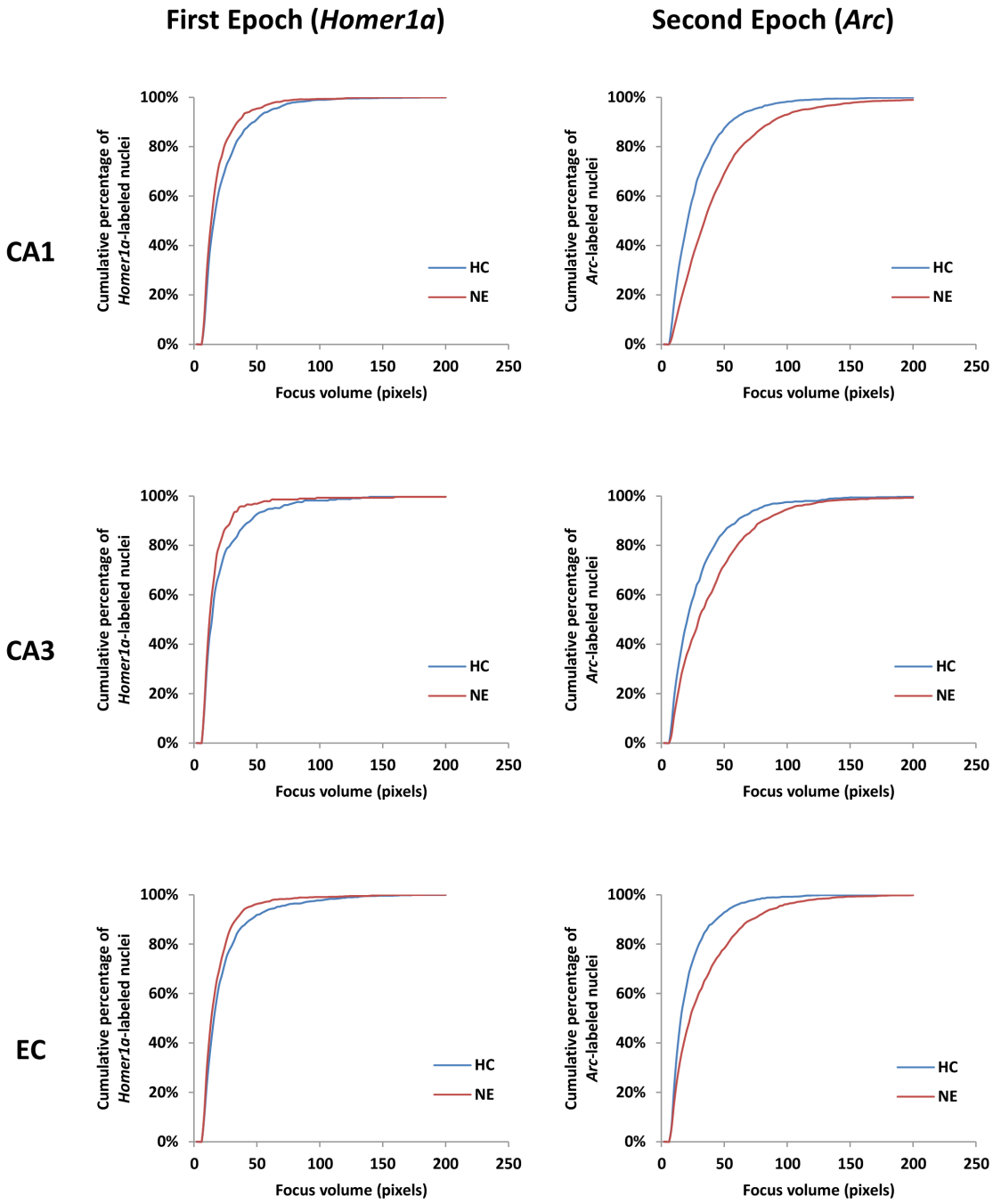

Figure 11: Cumulative percentages of average *Homer1a* and *Arc* focus volumes in CA1, CA3 and dorsolateral entorhinal cortex (EC) of home cage (HC) controls and rats that explored a novel environment (NE) after a period of home cage rest. The number of nuclei expressing *Homer1a* and the mean *Homer1a* focus volume were very comparable between treatment groups during the first epoch of home cage rest. In comparison, there was both an increase in the number of nuclei exhibiting *Arc* foci and an obvious shift towards increased mean *Arc* focus volumes after exploration of a novel environment during the second behavioural epoch (relative to home cage controls).

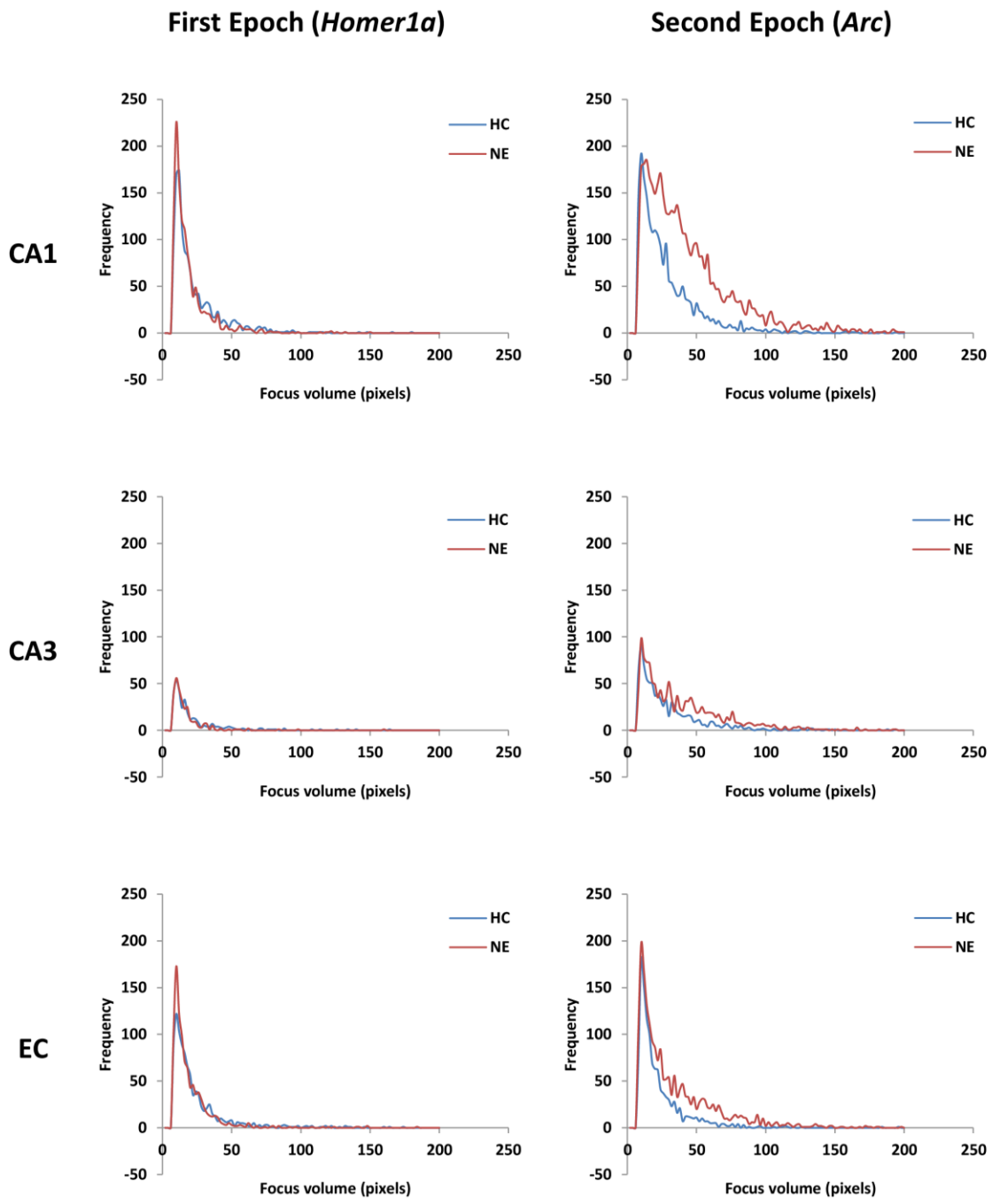

Figure 12: Average *Homer1a* and *Arc* focus volume frequency distributions (linear scale) in CA1, CA3 and dorsolateral entorhinal cortex (EC) of home cage (HC) controls and rats that explored a novel environment (NE) after a period of home cage rest. The frequency distributions of average focus volumes were highly skewed with long tails towards higher volumes in all regions, behavioural epochs and treatment groups.

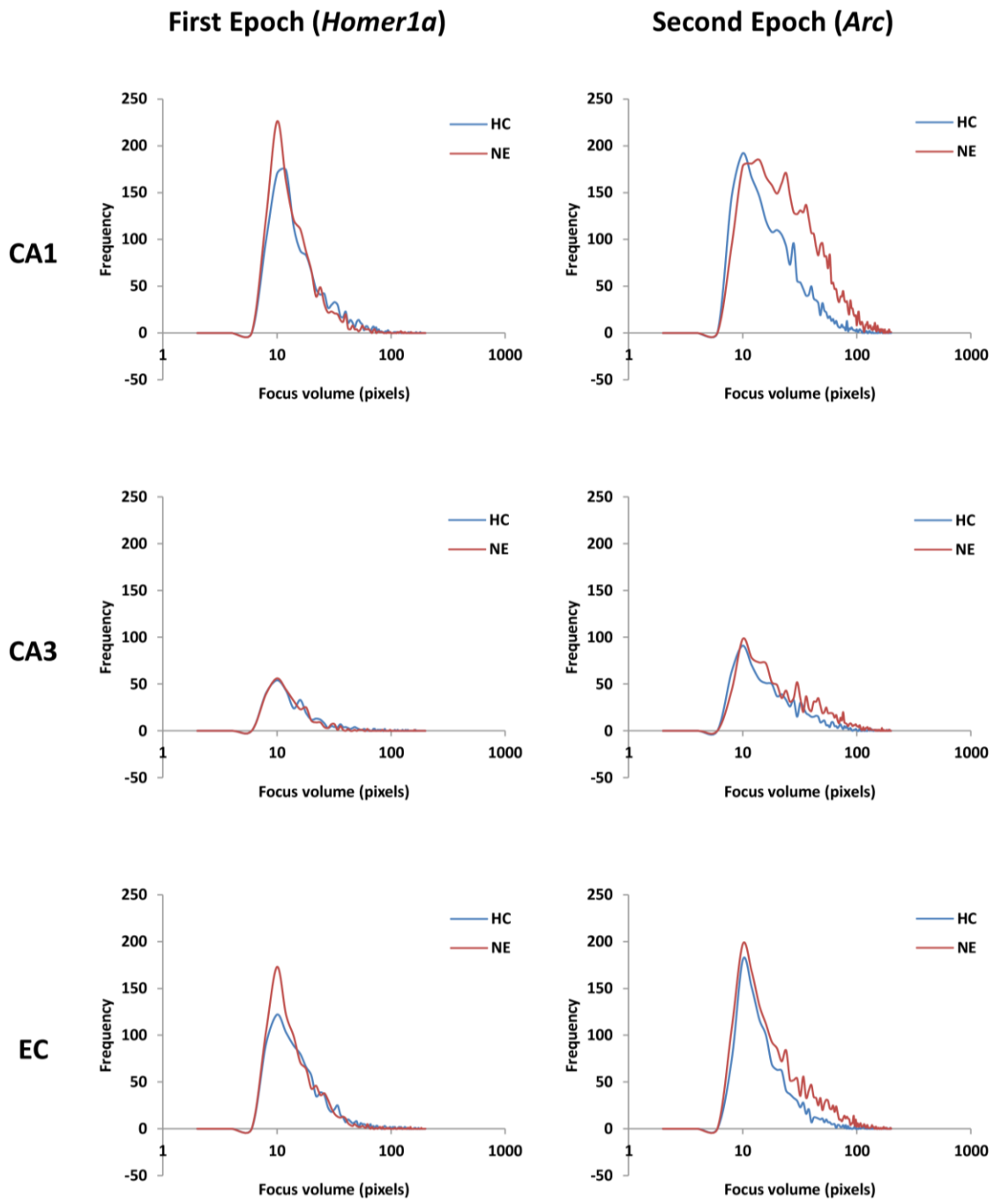

Figure 13: Average *Homer1a* and *Arc* focus volume frequency distributions (logarithmic scale) in CA1, CA3 and dorsolateral entorhinal cortex (EC) of home cage (HC) controls and of rats that explored a novel environment (NE) after a period of home cage rest. The frequency distributions of average focus volumes were approximately log-normal in all regions, behavioural epochs and treatment groups, though threshold restrictions during foci detection truncate the left portions of the curves.

Nuclei containing IEG foci of above average volume demonstrated greater pattern overlap than the total active population

As a consequence of manual cell counting methods and the use of imaging thresholds that largely eliminated the "baseline level" of home cage IEG expression in previous studies, nuclear IEG detection tended to be biased towards larger, brighter foci (for example, Vazdarjanova & Guzowski, 2004), which likely denotes increased transcriptional activity (Miyashita, Kubik, Haghighi, Steward, & Guzowski, 2009; W.L. Witharana, personal communication, August, 2013). Similarly, spike detection is also often methodologically biased towards more frequently firing cells. Accordingly, to bias the current results towards nuclei with presumably higher firing rates, analysis was restricted to nuclei containing at least one focus demonstrating greater than average volume (for double-labeled cells, at least one *Arc* and one *Homer1a* focus of greater than average volume were required to meet these criteria). For analysis of mRNA expression during the novel environment epoch, the average *Arc* foci volume exhibited in home cage controls was used as the threshold.

Across regions, the average volume of *Arc* foci in home cage controls was not significantly different from that of *Homer1a* foci in both home cage controls ($p = 0.42$) and rats that explored a novel environment after a period of home cage rest ($p = 0.12$). However, the average volume of *Homer1a* foci in home cage controls was significantly larger than that of rats that explored a novel environment during the second behavioural epoch ($p < 0.01$). *Arc* foci that arose during exploration of a novel environment were, on average, significantly larger in volume than *Homer1a* foci that arose during the preceding home cage rest ($p < 0.05$) and *Arc* foci in home cage controls ($p < 0.05$; Table 1).

Table 1: Average volumes of *Homer1a* and *Arc* foci from CA1, CA3 and dorsolateral entorhinal cortex (EC) of home cage (HC) controls and rats that explored a novel environment (NE) after a period of home cage rest. Across regions, the average volume of *Arc* foci in home cage controls was not significantly different from that of *Homer1a* foci in both home cage controls ($p = 0.42$) and rats that explored a novel environment after a period of home cage rest ($p = 0.12$). However, the average volume of *Homer1a* foci in home cage controls was significantly larger than that of rats that explored a novel environment during the second behavioural epoch ($p < 0.01$). *Arc* foci that arose during exploration of a novel environment were, on average, significantly larger in volume than *Homer1a* foci that arose during the preceding home cage rest ($p < 0.05$) and *Arc* foci in home cage controls ($p < 0.05$).

Treatment Group	Region	Average volume of *Homer1a* foci (pixels ± standard error)	Average volume of *Arc* foci (pixels ± standard error)
Home cage controls	**CA1**	25 ± 9	29 ± 10
	CA3	24 ± 11	32 ± 12
	EC	26 ± 12	23 ± 9
Novel environment	**CA1**	20 ± 8	46 ± 16
	CA3	18 ± 8	43 ± 15
	EC	21 ± 8	37 ± 14

As expected, the proportions of total nuclei considered *Arc*-, *Homer1a*- or double-labeled were greatly reduced by restricting analysis to only those that contained at least one focus of above average volume (Figure 14; refer to Figure 7 and Figure 9; Appendix B). However, most of the IEG expression pattern trends evident in the total population of sampled nuclei persisted after this restriction. Home cage control animals, on average, still demonstrated a significant increase in the observed proportion of nuclei exhibiting *Arc* foci (corresponding to the second epoch of home cage rest) relative to that exhibiting *Homer1a* foci (corresponding to the first epoch of home cage rest) in CA3 ($p < 0.05$) but not in CA1 nor in dorsolateral entorhinal cortex (CA1, $p = 0.23$; EC, $p = 0.34$). In experimental animals, the significant increase in the observed proportion of nuclei exhibiting *Arc* foci (corresponding to novel environment exploration) relative to that exhibiting *Homer1a* foci (corresponding to home cage rest) in CA1, CA3, and dorsolateral entorhinal cortex was also still evident (CA1 & CA3, $p < 0.01$; EC, $p < 0.05$). In most cases, the average proportion of double-labeled cells was still significantly lower than that of either *Homer1a*-labeled nuclei (HC EC, NE CA1 & NE CA3, $p < 0.05$; NE EC, $p < 0.01$) or *Arc*-labeled nuclei (HC CA1 & HC CA3, $p < 0.05$; HC EC, NE CA1, NE CA3 & NE EC, $p < 0.01$). Based on an unpaired, two-tailed *t*-test, the proportion of *Homer1a*-labeled nuclei observed during home cage rest in experimental animals was not significantly different from that during the first epoch in home cage controls (in all analyzed regions). Compared to the second epoch of home cage rest in control animals, the proportion of *Arc*-labeled cells was significantly elevated after exploration of a novel environment in CA1 and dorsolateral entorhinal cortex (CA1 & EC, $p < 0.05$) but not in CA3 ($p = 0.15$). There was no statistically significant difference

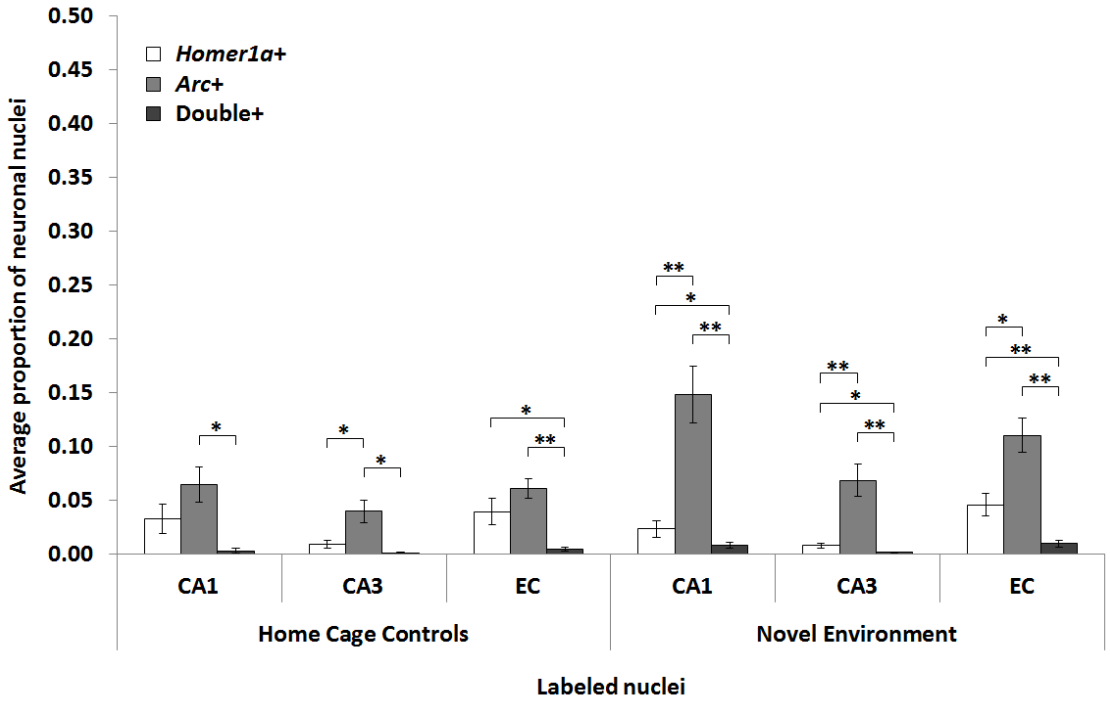

Figure 14: Average proportions of single *Arc*-labeled (*Arc*+), single *Homer1a*-labeled (*Homer1a*+) and double *Arc/Homer1a*-labeled (Double+) nuclei with at least one *Arc* and/or one *Homer1a* focus of above average volume in CA1, CA3 and dorsolateral entorhinal cortex (EC) of home cage (HC) controls and rats that explored a novel environment (NE) after a period of home cage rest. To bias the current results towards nuclei with presumably higher firing rates, analysis was restricted to nuclei containing at least one IEG focus of greater than average volume (for double-labeled cells, at least one *Arc* and one *Homer1a* focus of greater than average volume were required to meet these criteria). Home cage control animals, on average, did not show a significant difference in the proportion of nuclei exhibiting IEG foci during the second epoch of home cage activity relative to the first in CA1 nor in dorsolateral entorhinal cortex. However, there was a significant increase observed in CA3 ($p < 0.05$). Rats that explored the novel environment during the second epoch demonstrated a significant increase in the proportion of nuclei exhibiting IEG foci relative to the home cage epoch in CA1, CA3 and dorsolateral entorhinal cortex (CA1 & CA3, $p < 0.01$; EC, $p < 0.05$). In most cases, the average proportion of double-labeled cells was significantly lower than that of either *Homer1a*-labeled nuclei (HC EC, NE CA1 & NE CA3, $p < 0.05$; NE EC, $p < 0.01$) or *Arc*-labeled nuclei (HC CA1 & HC CA3, $p < 0.05$; HC EC, NE CA1, NE CA3 & NE EC, $p < 0.01$). Error bars indicate standard error.

between the observed proportions of double-labeled cells in home cage controls versus experimental rats in all regions analyzed (Figure 14; Appendix B).

In all treatment groups and across all regions, the observed IEG expression pattern overlap increased relative to the expected overlap though this trend was only significant for CA3 in home cage controls ($p < 0.01$), and CA1 and CA3 in experimental rats ($p < 0.05$). In all cases, the observed overlap was approximately double that expected by the uniform random sample with replacement model (Figure 15; Appendix B).

Average nuclear *Homer1a* and *Arc* pixel intensities were moderately correlated

Since IEG foci-based analysis utilizes pixel intensity thresholds to identify foci or "blobs" of labeling (and thus potentially excludes very weak or diffuse areas of labeling that could be fundamentally relevant), a "blobless" analysis was conducted to determine *Arc* and *Homer1a* labeling characteristics within entire nuclei without threshold restrictions. Although a large proportion of glia was excluded based on nuclear volume in the blobless analyses, the ranges of glial and neuronal nuclear volumes overlapped and no combination of nuclear blue (DAPI) pixel measures was found that could be used to unequivocally exclude glia from the total sampled population (data not shown). Hence, some glial nuclei were undoubtedly included in the following correlation analyses.

Among the total population of sampled nuclei (including both labeled and unlabeled nuclei classified based on the IEG foci analysis) within one standard deviation of the mean nuclear volume (including glial nuclei that fell within that range), there was a moderate average correlation between the average nuclear red (*Arc*-labeled) pixel intensity and average nuclear green (*Homer1a*-labeled) pixel intensity in home cage

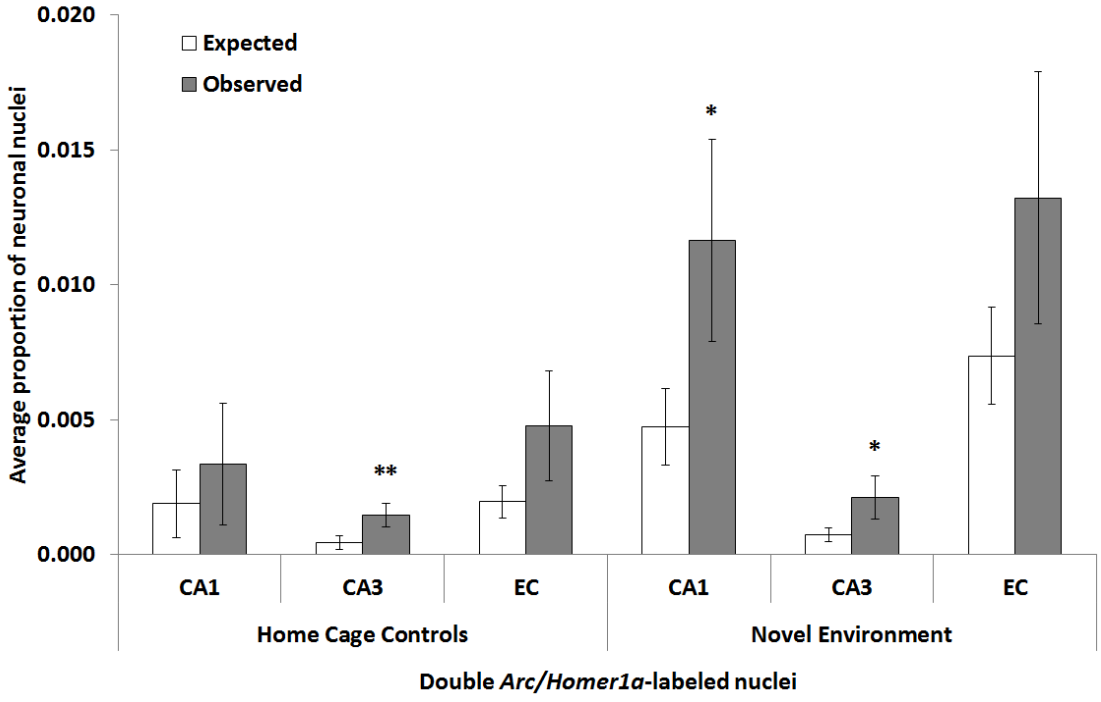

Figure 15: Average observed proportions and proportions expected based on the uniform random sample replacement model of *Arc/Homer1a* double-labeled nuclei with at least one *Arc* and one *Homer1a* focus of above average volume in CA1, CA3 and the dorsolateral entorhinal (EC) cortex of home cage controls and rats that explored a novel environment after a period of home cage rest. Analysis was restricted to nuclei containing at least one focus each of *Arc* and *Homer1a* mRNA of above average volume. Expected overlap was determined by calculating the product of the proportion of *Homer1a*-labeled nuclei and the proportion of *Arc*-labeled nuclei. On average across animals, observed overlap between *Arc* and *Homer1a* mRNA expression patterns was significantly higher than that expected by random chance in CA1 and CA3 after exploration of a novel environment (CA1, $p < 0.05$; CA3, $p < 0.05$) and in CA3 in home cage controls (CA3, $p < 0.01$). There was no statistically significant difference between the observed and random chance overlap of IEG expression patterns in CA1 or dorsolateral entorhinal cortex in home cage control animals (CA1, $p = 0.11$; EC, $p = 0.06$) nor in cortex of experimental animals (EC, $p = 0.08$). Error bars indicate standard error. Large variability in the proportions of neural populations expressing IEGs was evident between animals, which may account for the large error bars (Appendix B). Note: after application of the Bonferroni correction (the most conservative method of addressing Type I errors associated with multiple comparisons), there was no significant difference evident between expected and observed pattern overlap in any region.

controls (CA1, r = 0.6086; CA3, r = 0.7129; EC, r = 0.6978; Figure 16) and in experimental animals (CA1, r = 0.5271; CA3, r = 0.7178; EC, r = 0.6486; Figure 17).

Populations of nuclei that expressed *Arc* only or *Homer1a* only (based on the results of the foci-based analysis) that fell within one standard deviation of the mean nuclear volume clustered in largely non-overlapping populations that were, similar to the total population of sampled nuclei, moderately correlated with regards to the average nuclear red and green pixel intensities. In home cage controls, the average correlations observed within the population of *Arc*-labeled nuclei (CA1, r = 0.5124; CA3, r = 0.6332; EC, r = 0.5180) were not significantly different from those observed among *Homer1a*-labeled nuclei (CA1, r = 0.4897; CA3, r = 0.5179; EC, r = 0.4906; Figure 16). Similarly, the average correlations observed within the population of *Arc*-labeled nuclei in experimental animals (CA1, r = 0.4658; CA3, r = 0.5598; EC, r = 0.4908) were not significantly different from those observed among *Homer1a*-labeled nuclei (CA1, r = 0.5890; CA3, r = 0.7210; EC, r = 0.5502; Figure 17).

Considering only double-labeled nuclei (that is, nuclei that exhibited both *Arc* and *Homer1a* foci), there was a low to moderate average correlation observed between the average nuclear red and green pixel intensities in both home cage controls (CA1, r = 0.4559; CA3, r = 0.1714; EC, r = 0.5163; Figure 16) and experimental rats (CA1, r = 0.2750; CA3, r = 0.3341; EC, r = 0.5465; Figure 17). The correlations observed among populations of double-labeled nuclei in each region were not significantly different from those observed among single *Arc*- or *Homer1a*-labeled nuclei.

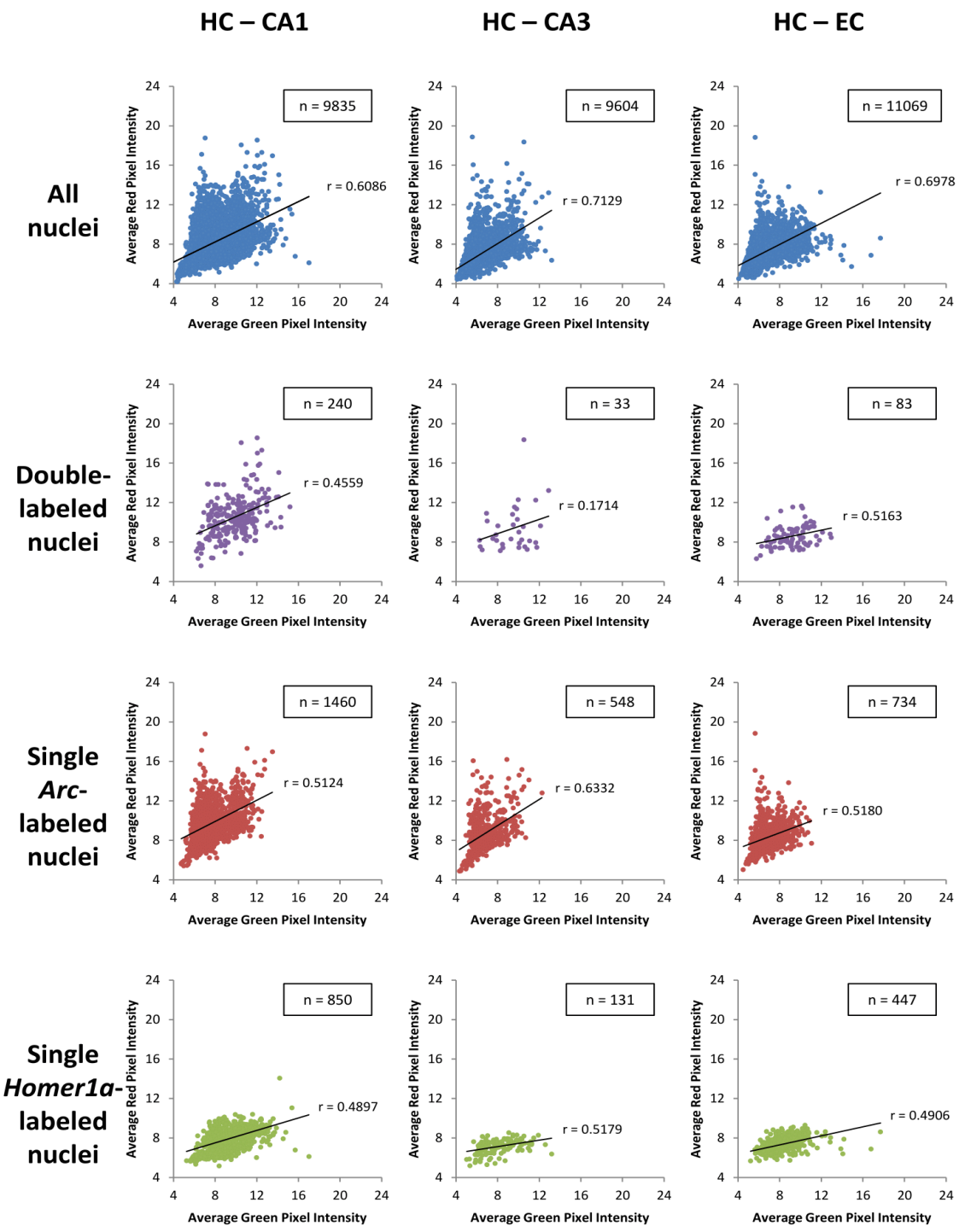

Figure 16: Average correlations between nuclear average red and average green pixel intensities among all nuclei (both labeled and unlabeled), double-labeled nuclei, single *Arc*-labeled nuclei and single *Homer1a*-labeled nuclei in home cage (HC) controls. All regions and subgroups of labeled nuclei (classified based on the foci analysis) demonstrated moderate correlations (*r*) between nuclear average red and green pixel intensities (n = number of nuclei). The clustering can be attributed to differences between animals (Appendix B).

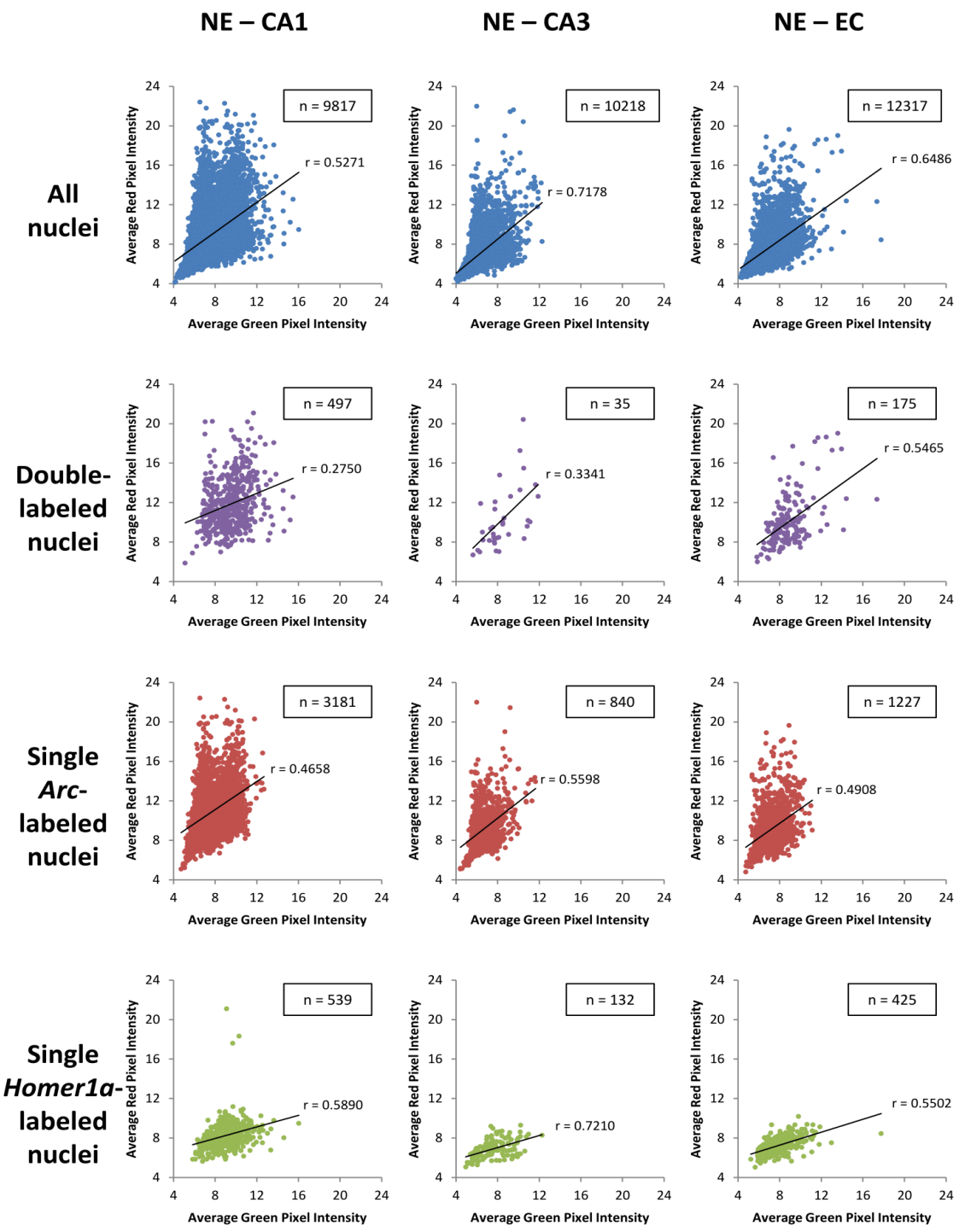

Figure 17: Average correlations between nuclear average red and average green pixel intensities among all nuclei (both labeled and unlabeled), double-labeled nuclei, single *Arc*-labeled nuclei and single *Homer1a*-labeled nuclei in rats that explored a novel environment (NE) after a period of home cage rest. All regions and subgroups of labeled nuclei (classified based on the foci analysis) demonstrated moderate correlations (*r*) between nuclear average red and green pixel intensities (n = number of nuclei). The clustering can be attributed to differences between animals (Appendix B).

DISCUSSION

Molecular memory representations did not exhibit significant preplay following a single exposure to a novel environment

Dragoi and Tonegawa (2011) argued that the failure of previous electrophysiological studies to demonstrate preplay was likely due to inadequate population sampling (for example, Lee & Wilson, 2002) or because the use of pairwise correlations is an insufficiently sensitive method of detection (for example, Kudrimoti et al., 1999; Skaggs & McNaughton, 1996; Wilson & McNaughton, 1994). Consistent with this argument, previous IEG-based work that similarly failed to demonstrate preplay (Marrone et al., 2008) was published prior to the recent advances in automated analysis that now allow for sampling of a far larger population of neurons. The present study was designed to address these issues and to determine if molecular memory representations in the hippocampus are orthogonal and conform to the uniform random sample with replacement model or if hippocampal neurons do, in fact, demonstrate experience-independent patterns of IEG expression. Specifically, this study utilized double-label *Arc/Homer1a* fluorescent *in situ* hybridization and FARSIGHT automated nuclear segmentation coupled with automated foci detection to analyze an irrefutably extensive population of neurons. Unlike previous studies that focused on preplay in the CA1 subregion of the hippocampus specifically (Dragoi & Tonegawa, 2011; Marrone et al., 2008), this study investigated CA1 as well as CA3 and the dorsolateral entorhinal cortex.

Based on the overall mRNA expression patterns of the IEGs *Arc* and *Homer1a*, the current results support that statistically discrete patterns of activity-regulated IEG

expression arise in the CA1 and CA3 regions of the hippocampus and in the dorsolateral entorhinal cortex during rest or sleep in a familiar environment and after a subsequent single exposure to a novel environment. The evidence supporting the orthogonal nature of IEG expression patterns becomes even more compelling when comparing tissue sections within individual animals rather than within treatment groups (Appendix B). Indeed, disparities in neural recruitment between rats appear to contribute largely to the considerable standard error evident in this study, which would likely be reduced by replications of this study with additional animals and a more stringent correction for glial nuclei (see "Future directions" section of Discussion). Furthermore, there was no statistically significant difference within analyzed regions among the correlations of average red (*Arc*) and average green (*Homer1a*) nuclear pixel intensities between single *Arc*-labeled nuclei, single *Homer1a*-labeled nuclei, and double-labeled nuclei, which supports that elevated nuclear *Arc* or *Homer1a* mRNA levels do not necessarily predict subsequent reactivation. It should be noted, though, that it is possible the moderate correlations observed in all groups may have been largely influenced by "background" fluorescent labeling (or "noise") and thus may not be an accurate reflection of the relationship between diffuse nuclear *Arc* and *Homer1a* mRNA, which (combined with the necessary inclusion of glia in the analysis) limits the utility of the blobless analysis.

Altogether, there is an apparent lack of correlation between the hippocampal and cortical neuronal populations active during rest or sleep in the home cage environment and those active during the subsequent exploration of a remote novel environment, which supports that hippocampal neurons (and at least a portion of cortical neurons) conform to the uniform random sample with replacement model. In consideration of these results, a

possible explanation for previous neural ensemble recording data (Dragoi & Tonegawa, 2011; Dragoi & Tonegawa, 2013) might be that the sleep episode occurred near the apparatus used for recording during wakefulness. The continuous attractor neural network model for place field generation (for example, Samsonovich & McNaughton, 1997) predicts that if the "activity bump" (a stable attractor state balanced by local excitation and global inhibition) is allowed to move randomly around the location where it was when the rat went to sleep, it might visit states that will subsequently be observed when the rat visits nearby locations. Dragoi and Tonegawa (2013) state that this "mental traveling" was prevented in more recent studies by housing the rats in an opaque, high-walled sleep box before introduction of the novel linear tracks to the room. However, the spatial code described by Samsonovich and McNaughton (1997) appears immediately on entering an environment for the first time (which, in this case, likely included the testing room outside of the sleep box), and does not normally undergo subsequent topographical modifications after exploration or changes in environmental stimuli. Alternatively, considering the inherent bias in electrophysiological studies towards more highly active cells (that is, those that exhibit higher firing rates), it is possible that only a small framework of neurons exhibit preselection and this minority might be masked by a much larger population of less active cells in IEG studies.

Highly active minority of neurons could exhibit preselection

IEG foci volume and average pixel intensity have been demonstrated to be non-Boolean and likely reflect differences in transcriptional activity between cells (Miyashita et al., 2009; W.L. Witharana, personal communication, August, 2013). Correspondingly,

not only did the proportion of active cells in this study increase following exploration of a novel environment, but the average volume of foci also increased relative to home cage levels, confirming a multidimensional elevation in activity-regulated IEG expression. Interestingly, there was also a significant difference between the average *Homer1a* focus volumes of home cage controls and rats that eventually explored a novel environment (despite the fact that *Homer1a* expression was representative of home cage activity in both treatment groups), which could also reflect the *cessation* of previously initiated transcription due to either the presentation of a sufficiently novel context or simply as a result of the transition from "offline" to "online" hippocampal activity. Furthermore, consistent with the skewed firing rates observed by Mizuseki and Buzsáki (2013) and the gamma-Poisson rate of field formation in place cells suggested by Rich et al. (2014), the distributions of foci volumes were highly skewed with long tails towards higher volumes in all regions and treatment groups, which could indicate a highly active minority population of neurons. Since spike detection is often methodologically biased towards highly active cells and silent cells are omitted entirely, the observation of preplay in CA1 (Dragoi & Tonegawa, 2011) could be a result of this prejudice. Consistent with this inference, when the current data are biased towards presumably more highly active neural populations by restricting the analysis to nuclei containing foci of above average volume, there is a significantly higher overlap of IEG expression patterns in CA1 and CA3 of experimental rats and in CA3 of home cage controls than predicted by the uniform sample with replacement model. Hence it appears that the preplay of neural activity patterns may be a consequence of a highly skewed neural excitability distribution and is,

therefore, restricted to a marginal subset of highly active neurons that are masked by the greater population of less active neurons in IEG studies.

This trend towards sustained IEG expression among a minority of highly active cells suggests that the activation propensity of place cells may be at least partially predetermined during rest or sleep. It has been previously suggested that pre-existing differences in place cell firing rate and field propensity may arise from intrinsic variations in cellular excitability and/or from network inputs (Maurer et al., 2006; Rich et al., 2014). On one hand, for instance, Epsztein et al. (2011) suggested that future place cells "could possess dendritic segments with greater excitability (Frick, Magee & Johnston, 2004; Losonczy, Makara & Magee, 2008), organized such that a spatially-uniform set of synaptic inputs is converted into a spatially-tuned input as seen by the soma (Jia, Rochefort, Chen & Konnerth, 2010)". Alternatively, the merely moderate correlation between average red and average green nuclear pixel intensities in double-labeled nuclei in this study suggests that, although that subset of neurons was collectively active during both epochs of activity, the individual firing rates of each place cell may have been adjusted, which suggests modulation at the network level. The continuous attractor neural network model proposed by Samsonovich and McNaughton (1997) predicts a multichart architecture for place cell assembly where "a given place cell has meaning only in the context of the ensemble of other cells that are active with it at a given location on a given chart". The dynamic changeability between multiple network states (across multiple charts) suggested by this model could not only account for variations in the burst propensity of a single place cell in different environments but also for the preplay of sequential patterns of activity (which was demonstrated

computationally by Azizi, Wiskott & Cheng, 2013). Furthermore, because of its recurrent connections, CA3 was proposed as a possible location for this multichart architecture. The significantly higher overlap of IEG mRNA expression patterns (relative to random chance) apparent in CA3 (of both control and experimental animals) after restriction of analyses to presumably more active neurons does, in fact, afford additional credibility to this theory. For instance, if the highly active minority of cells in CA3 is assumed to represent the collective ensemble of mutually excited neurons that constitute a stable point attractor, the elevated pattern overlap observed in home cage controls (that is, during "offline" rest or sleep) could reflect the continuous movement between a limited number of these stable network states. The similarly elevated activity pattern overlap among the highly active minority in CA3 after exploration of a novel environment could then be presumed to represent reactivation of one of these "preselected" ensembles (designated now as the framework to encode a new spatial map). It follows, then, that the significantly higher overlap also observed in CA1 in these animals could reflect the propagation of sequential patterns of activity in the feedforward connections between the CA3 and CA1 neural networks as part of the integration of spatial and non-spatial information during the memory encoding process (Azizi et al., 2013).

Support for both the uniform random sample with replacement and preselection models of hippocampal pattern separation

The results of this study may, in fact, bridge the seemingly contradictory results of early IEG studies that exhibit patterns of neural activity that conform to the uniform random sample with replacement model (Guzowski et al., 1999; Vazdarjanova &

Guzowski, 2004) with those of more recent IEG studies that failed to demonstrate the proportionate increase in neuron recruitment predicted to accompany exploration of multiple or larger environments (Alme et al., 2010; unpublished data, Chawla et al., 2013; unpublished data, Witharana et al., 2013). Perhaps a subset of intrinsically predisposed future place cells allotted to a single novel experience is sufficiently small such that neural activation *appears* random when comparing only two epochs of activity but pattern overlap becomes increasingly necessary (and apparent) with the introduction of multiple novel environments or experiences of more magnitude. Accordingly, only 5% ± 4% of *all* CA1 neurons (regardless of activity state) were active in both home cage and a single novel environment in this study whereas Dragoi and Tonegawa (2013) demonstrated preplay in an average 6-7% of *active* CA1 neurons per introduced track. Therefore, it is certainly plausible that a significant overlap of IEG expression patterns was undetectable after the introduction of only one novel environment but could summate above random chance levels after exploration of multiple environments.

Non-overlapping molecular memory representations during home cage rest

Previous research indicates that repeat exposure to the same environment generates highly overlapping molecular memory representations (Guzowski et al., 1999; Vazdarjanova & Guzowski 2004; Vazdarjanova et al., 2002) and, more specifically, Marrone et al. (2008) demonstrated that IEG expression occurs repeatedly in the same cells in home cage animals. However, home cage controls in this study demonstrated pattern overlap between *Arc* and *Homer1a* mRNA expression equivalent to random chance. The caged controls in some IEG-based studies (Guzowski et al., 1999;

Vazdarjanova & Guzowski 2004) appear to demonstrate similarly lower proportions of double-labeled nuclei than expected after repeat exposure to the home cage environment but the reasons behind this occurrence are not discussed. Pertaining to this study, it is possible that, because the animals were taken for sacrifice during their sleep cycle, the rats were not actively processing their home cage environment but rather episodes of replay and/or preplay. As previously discussed, replay of recent experience predominantly occurs within thirty minutes of the initiation of the sleep or rest period but can be observed intermittently up to 24 hours later (Kudrimoti et al., 1999) and preplay has similarly been demonstrated to coincide with high frequency "ripple" oscillations that occur during periods of quiet wakefulness and slow-wave sleep (Dragoi & Tonegawa, 2011). Consequently, it is plausible that there are short cycles of replay and/or preplay of different, non-overlapping activity patterns during sleep and thus the pattern separation observed between epochs of home cage rest or sleep may reflect two separate replay and/or preplay events. Alternatively, although state variation was not measured in this study, if control rats that were asleep during the first home cage epoch were awake long enough prior to sacrifice (that is, at least five minutes prior to perfusion), *Homer1a* mRNA expression may reflect replay and/or preplay events during sleep while *Arc* mRNA expression may reflect the attentive state within the home cage environment. It is also plausible, then, that differences in wake or sleep state during home cage rest also contributed to the variation in neural recruitment evident between individual rats and between epochs of home cage rest in controls.

Proportions of active neurons were elevated in home cage epochs relative to literature

Considering the prominent role of IEGs in hippocampal synaptic plasticity, it is unsurprising that resting IEG expression is lower than that induced by exploration of a novel environment. The proportion of active neurons observed during home cage epochs in this study, however, is considerably higher than previously reported (for example, Vazdarjanova & Guzowski, 2004). Previous IEG studies often regarded home cage animals as a form of negative control and, accordingly, imaging parameters and cell counting methods were optimized largely to eliminate this "baseline level" of presumably behaviourally-uncorrelated expression. The methodological differences between the present study and previous work may account for the artificial inflation of the apparent difference between home cage and exploration-induced IEG expression observed in some prior studies.

Consistent with previous literature, approximately 40% of CA1 neurons and 20% of CA3 neurons demonstrated IEG mRNA upregulation during spatial exploration (Guzowski et al., 1999; Vazdarjanova & Guzowski, 2004; Vazdarjanova et al., 2002). Unexpectedly, however, there was a significant difference in CA3 neuron recruitment observed between home cage epochs in control animals such that the proportion of neurons demonstrating *Arc* mRNA expression during the second epoch was significantly higher than that expressing *Homer1a* during the first epoch of home cage activity. A similar effect was observed for CA1 and cortical neurons, though the differences were not statistically significant. While these discrepancies do not discredit these probability-based analyses, they suggest that either *Arc* and *Homer1a* are differentially expressed

during rest or that the current method of *Homer1a* mRNA detection (one-step amplification) is insufficiently sensitive compared with that of *Arc* mRNA detection (two-step amplification). Though the latter seems unlikely as there was no significant difference in average focus volume between *Arc* and *Homer1a* foci in home cage controls, this theory was nevertheless examined by increasing the average red pixel intensity threshold to approximately equalize average home cage proportions of *Arc*- and *Homer1a*-labeled nuclei (consistent with results of previous IEG studies; for example, Vazdarjanova et al., 2002). Though most regions (in both treatment groups) still showed no difference between the observed expression pattern overlap and that expected by the uniform random sample with replacement model, dorsolateral entorhinal cortex in home cage controls and CA1 in experimental rats demonstrated statistically higher proportions of double-labeled cells than expected by random chance. It should be noted, though, that the neural population removed during restriction by average pixel intensity (total intensity/volume) may not be comparable to that eliminated during restriction by focus volume alone. Focus volume and total intensity were highly correlated (data not shown) and thus restricting by average intensity involves a complicated interaction of these two measures, which could explain the discrepancy in the identity of regions where observed pattern overlap was significantly higher than expected. Regardless, the data were still presumably partially restricted to more active nuclei by increasing the threshold for detection, which gives further credence to the theory that some neurons have a higher propensity for activation but are masked by the larger population of less active cells in IEG studies that do not take into account the magnitude of activation at the cellular level. This trend is also consistent with an underrepresentation of less active *Homer1a*-labeled

nuclei, the inclusion of which (via enhanced amplification) under the original equivalent red and green pixel thresholds would theoretically produce the opposite effect: a further *dilution* of the highly active minority. Considering that this is not an ideal method of normalizing *Arc* and *Homer1a* expression, however, further analyses of expression patterns where *Arc* and *Homer1a* mRNA are labeled with opposite amplification and detection procedures (or where *Homer1a* riboprobe and/or antibody concentrations are increased) are required to elaborate on these results.

Future research

Despite the exceptional capacity of automated analysis for processing extensive populations of neurons in substantially less time than manual counting methods, the high density of granule cells in the dentate gyrus of the hippocampus still considerably hinders the accuracy of automated nuclear segmentation (hence the dentate gyrus was excluded from this study). However, there is recent molecular evidence that, although memory representations from two environments differing in size by a magnitude of four are largely orthogonal in CA1 and CA3, patterns of IEG expression exhibited in the dentate gyrus were more overlapping in adult rats than predicted by the uniform random sample with replacement model (J.Y. Xie, personal communication, September, 2013). Furthermore, dentate gyrus cells show no obvious increase in *Arc* expression following exploration of a novel environment (Guzowski et al., 1999). Considering these findings, further analysis of the tissue processed in this study is required to determine if the dentate gyrus conforms to the uniform random sample with replacement model or, rather, exhibits preconfiguration to some extent.

In addition to the limitations of automated nuclear segmentation, the automated classification of neuronal and glial nuclei was similarly inadequate (Appendix B) and the application of a general glial correction factor could potentially be a source of bias. For instance, actual proportions of glia and neurons undoubtedly differ between animals and a general glial correction may be too modest for an individual rat. This could lead to false positive effects where IEG expression pattern overlap appears statistically significant due to the inflated total "neuronal" population. In this study, however, the proportions of glial nuclei observed based on manual classification were very comparable between specific regions of the two animals analyzed and thus bias was likely not substantial. Ultimately, the development of a technique for simultaneously labeling principle neurons and/or glia during the fluorescent *in situ* hybridization process is necessary to eliminate the error associated with current automated classification methods and the bias associated with using a generalized glial correction factor.

Finally, if small preconfigured subsets of neurons are designated for activation prior to an experience (such that activity pattern overlap appears random between only two environments but increases with the inclusion of additional temporally-related experiences), can an increase in neural activity pattern overlap be detected after the introduction of multiple environments? *In vivo* two-photon fluorometric calcium imaging or *in vivo* two-photon imaging of transgenic IEG reporter mice (for example, Arc-EGFP mice) could provide such insight into changes in orthogonalization over more extensive periods of time than permitted by IEG mRNA detection methods.

Conclusion

Based on the overall mRNA expression patterns of the IEGs *Arc* and *Homer1a*, the active CA1, CA3 and dorsolateral entorhinal cortex neuronal populations during rest or sleep in a familiar environment and during the subsequent exploration of a novel environment were only weakly correlated and the observed pattern overlap could statistically be attributed to random chance (as dictated by the uniform random sample with replacement model). However, when analysis was restricted to presumably more active neurons, the observed overlap between IEG expression patterns became significantly higher than that expected by random chance in both CA1 and CA3 hippocampal subregions after exploration of a novel environment (as predicted by the preselection model). Altogether, it appears that a minority of hippocampal cells have a higher propensity for activation but are masked by the immense population of less active cells in IEG studies that do not take into account the magnitude of activation at the cellular level. Hence, this study unites the uniform random sample with replacement and preselection models of hippocampal pattern separation and emphasizes the necessity of taking into account the highly skewed nature of activity distributions when assessing neural ensemble representations.

REFERENCES

Alme, C.B., Buzzetti, R.A., Marrone, D.F., Leutgeb, J.K., Chawla, M.K., Schaner, M.J., Bohanick, J.D., Khoboko, T., Leutgeb, S., Moser, E.I., Moser, M.-B., McNaughton, B.L., & Barnes, C.A. (2010). Hippocampal granule cells opt for early retirement. *Hippocampus, 20,* 1109-1123.

Azizi, A.H., Wiskott, L., & Cheng, S. (2013). A computational model for preplay in the hippocampus. *Frontiers in Computational Neuroscience, 7,* 1-15.

Barnes, C.A., McNaughton, B.L., Mizumori, S.J., Leonard, B.W., & Lin, L.H. (1990). Comparison of spatial and temporal characteristics of neuronal activity in sequential stages of hippocampal processing. *Progress in Brain Research, 83,* 287-300.

Bjornsson, C.S., Lin, G., Al-Kofahi, Y., Narayanaswamy, A., Smith, K.L., Shain, W., & Roysam, B. (2008). Associative image analysis: A method for automated quantification of 3D multi-parameter images of brain tissue. *Journal of Neuroscience Methods, 170,* 165-178.

Brakeman, P.R., Lanahan, A.A., O'Brien, R., Roche, K., Barnes, C.A., Huganir, R.L., & Worley, P.F. (1997). Homer: a protein that selectively binds metabotropic glutamate receptors. *Nature, 386,* 284-288.

Chawla, M.K., Sekhadia, N., Olson, K., Alme, C.B., Moser, E.I., Moser, M.-B., McNaughton, B.L., & Barnes, C.A. (2013, November). *Massed trial induced underexpression of* Arc *mRNA in rat hippocampal neurons.* Poster presented at the Society for Neuroscience Annual International Meeting, San Diego, CA.

Davidson, T.J., Kloosterman, F., & Wilson, M.A. (2009). Hippocampal replay of extended experience. *Neuron, 63,* 497–507.

Dragoi, G. & Tonegawa, S. (2013). Distinct preplay of multiple novel spatial experiences in the rat. *Proceedings of the National Academy of Sciences, 110,* 9100-9105.

Dragoi, G. & Tonegawa, S. (2011). Preplay of future place cell sequences by hippocampal cellular assemblies. *Nature, 469,* 397-401.

Du, G., Drexler, G.A., Friedland, W., Greubel, C., Hable, V., Kugler, A., Krücken, R., Tonelli, L., Friedl, A., & Dollinger, G. (2011). Spatial dynamics of DNA damage response protein foci along the ion trajectory of high-LET particles. *Radiation Research, 176,* 706-715.

Epsztein, J., Brecht, M., & Lee, A.K. (2011). Intracellular determinants of hippocampal CA1 place and silent cell activity in a novel environment. *Neuron, 70,* 109-120.

Fenton, A.A., Kao, H.Y., Neymotin, S.A., Olypher, A., Vayntrub, Y., Lytton, W.W., & Ludvig, N. (2008). Unmasking the CA1 ensemble place code by exposures to small and large environments: more place cells and multiple, irregularly arranged, and expanded place fields in the larger space. *The Journal of Neuroscience, 28,* 11250–11262.

Foster, D.J. & Wilson, M.A. (2006). Reverse replay of behavioral sequences in hippocampal place cells during the awake state. *Nature, 440,* 680-683.

Frick, A., Magee, J., & Johnston, D. (2004). LTP is accompanied by an enhanced local excitability of pyramidal neuron dendrites. *Nature Neuroscience, 7,* 126-135.

Guzowski, J.F. (2002). Insights into immediate-early gene function in hippocampal memory consolidation using antisense oligonucleotide and fluorescent imaging approaches. *Hippocampus, 12,* 86-104.

Guzowski, J.F., McNaughton, B.L., Barnes, C.A., & Worley, P.F. (1999). Environment-specific expression of the immediate-early gene *Arc* in hippocampal neuronal ensembles. *Nature Neuroscience, 2,* 1120-1124.

Guzowski, J.F., Timlin, J.A., Roysam, B., McNaughton, B.L., Worley, P.F., & Barnes, C.A. (2005). Mapping behaviorally relevant neural circuits with immediate-early gene expression. *Current Opinion in Neurobiology, 15,* 599-606.

Hafting, T., Fyhn, M., Molden, S., Moser, M.-B., & Moser, E.I. (2005). Microstructure of a spatial map in the entorhinal cortex. *Nature, 436,* 801-806.

Hargreaves, E.L., Rao, G., Lee, I., & Knierim, J.J. (2005). Major dissociation between medial and lateral entorhinal input to dorsal hippocampus. *Science, 308,* 1792-1794.

Jia, H. Rochefort, N.L., Chen, X., & Konnerth, A. (2010). Dendritic organization of sensory input to cortical neurons in vivo. *Nature, 464,* 1307-1312.

Knierim, J.J., Lee, I., & Hargreaves, E.L. (2006). Hippocampal place cells: parallel input streams, subregional processing, and implications for episodic memory. *Hippocampus, 16,* 755-764.

Kudrimoti, H.S., Barnes, C.A., & McNaughton, B.L. (1999). Reactivation of hippocampal cell assemblies: Effects of behavioral state, experience and EEG dynamics. *The Journal of Neuroscience, 19,* 4090-4101.

Lee, A.K. & Wilson, M.A. (2002). Memory of sequential experience in the hippocampus during slow wave sleep. *Neuron, 36,* 1183-1194.

Leutgeb, J.K., Leutgeb, S., Moser, M.-B., & Moser, E.I. (2007). Pattern separation in the dentate gyrus and CA3 of the hippocampus. *Science, 315,* 961-966.

Leutgeb, S., Leutgeb, J.K., Treves, A., Moser, M.-B., & Moser, E.I. (2004). Distinct ensemble codes in hippocampal areas CA3 and CA1. *Science, 305,* 1295-1298.

Link, W., Konietzko, U., Kauselmann, G., Krug, M., Schwanke, B., Frey, U., & Kuhl, D. (1995). Somatodendritic expression of an immediate early gene is regulated by synaptic activity. *Proceedings of the National Academy of Sciences of the United States of America, 92,* 5734-5738.

Losonczy, A., Makara, J.K., & Magee, J.C. (2008). Compartmentalized dendritic plasticity and input feature storage in neurons. *Nature, 452,* 436-441.

Lyford, G. L., Yamagata, K., Kaufmann, W. E., Barnes, C. A., Sanders, L. K., Copeland, N. G., Gilbert, D. J., Jenkins, N. A., Lanahan, A. A., & Worley, P. F. (1995). *Arc,* a growth factor and activity-regulated gene, encodes a novel cytoskeleton-associated protein that is enriched in neuronal dendrites. *Neuron, 14,* 433-445.

Maurer, A.P., Cowen, S.L., Burke, S.N., Barnes, C.A., & McNaughton, B.L. (2006). Organization of hippocampal cell assemblies based on theta phase precession. *Hippocampus, 16,* 785-794.

McClelland, J.L., McNaughton, B.L., & O'Reilly, R.C. (1995). Why there are complementary learning systems in the hippocampus and neocortex: insights from the successes and failures of connectionist models of learning and memory. *Psychological Review, 102,* 419-457.

McNaughton, B.L., Barnes, C.A., Gerrard, J.L., Gothard, K., Jung, M.W., Knierim, J.J., Kudrimoti, H., Qin, Y., Skaggs, W.E., Suster, M., & Weaver, K.L. (1996). Deciphering the hippocampal polyglot: the hippocampus as a path integration system. *The Journal of Experimental Biology, 199,* 173-185.

McNaughton, B.L. & Nadel, L. (1990). Hebb-Marr networks and the neurobiological representation of action space. In M.A. Gluck & D.E. Rumelhart (Eds.), *Neuroscience and Connectionist Theory* (pp. 1-63). Hillsdale, NJ: Lawrence Erlbaum Associates.

Marr, D. (1971). Simple memory: a theory of archicortex. *Philosophical Transactions of the Royal Society of London B, 262,* 23-81.

Marrone, D.F., Schaner, M.J., McNaughton, B.L., Worley, P.F., & Barnes, C.A. (2008). Immediate-early gene expression at rest recapitulates recent experience. *The Journal of Neuroscience, 28,* 1030-1033.

McNaughton, B.L. & Morris, R.G.M. (1987). Hippocampal synaptic enhancement and information storage within a distributed memory system. *Trends in Neuroscience, 10,* 408-415.

Mizuseki, K. & Buzsáki, G. (2013). Preconfigured, skewed distribution of firing rates in the hippocampus and entorhinal cortex. *Cell Reports, 4,* 1010-1021.

Montes-Rodríguez, C.J., Lapointe, V., Trivedi, V., Lu, Q., Demchuk, A.M., & McNaughton, B.L. (2013). Postnatal development of *Homer1a* in the rat hippocampus. *Hippocampus, 23,* 890-902.

Muller, R.U. & Kubie, J.L. (1987). The effects of changes in the environment on the spatial firing of hippocampal complex-spike cells. *The Journal of Neuroscience, 7,* 1951-1968.

Miyashita, T., Kubik, S., Haghighi, N., Steward, O., & Guzowski, J.F. (2009). Rapid activation of plasticity-associated gene transcription in hippocampal neurons provides a mechanism for encoding of one-trial experience. *The Journal of Neuroscience, 29,* 898-906.

O'Keefe, J. & Dostrovsky, J. (1971). The hippocampus as a spatial map. Preliminary evidence from unit activity in the freely-moving rat. *Brain Research, 34,* 171-175.

O'Keefe, J. & Nadel, L. (1978). *The hippocampus as a cognitive map.* Oxford: Oxford University Press.

O'Neill, J., Senior, T., & Csicvari, J. (2006). Place selective firing of CA1 pyramidal cells during sharp wave/ripple network patterns in exploratory behavior. *Neuron, 49,* 143-155.

Pavlides, C. & Winson, J. (1989). Influences of hippocampal place cell firing in the awake state on the activity of these cells during subsequent sleep episodes. *The Journal of Neuroscience, 9,* 2907-2918.

Paxinos, G. & Watson, C. (1997). *The rat brain in stereotaxic coordinates* (3rd ed.). San Diego, CA: Academic Press, Inc.

Rich, P.D., Liaw, H.-P., & Lee, A.K. (2014). Place cells. Large environments reveal the statistical structure governing hippocampal representations. *Science, 345,* 814-817.

Samsonovich, A. & McNaughton, B.L. (1997). Path integration and cognitive mapping in a continuous attractor neural network model. *The Journal of Neuroscience, 17,* 5900-5920.

Scoville, W.B. & Milner, B. (1957). Loss of recent memory after bilateral hippocampal lesions. *Journal of Neurology, Neurosurgery and Psychiatry, 20,* 11-21.

Skaggs, W.E. & McNaughton, B.L. (1996). Replay of neuronal firing sequences in rat hippocampus during sleep following spatial experience. *Science, 271,* 1870-1873.

Squire, L.R. & Alvarez, P. (1995). Retrograde amnesia and memory consolidation: a neurobiological perspective. *Current Opinion in Neurobiology, 5,* 169-177.

Sutherland, G.R. & McNaughton, B.L. (2000). Memory trace reactivation in hippocampal and neocortical neuronal ensembles. *Current Opinion in Neurobiology, 10,* 180-186.

Thompson, L.T. & Best, P.J. (1989). Place cells and silent cells in the hippocampus of freely-behaving rats. *The Journal of Neuroscience, 9,* 2382–2390.

Vazdarjanova, A. & Guzowski, J.F. (2004). Differences in hippocampal neuronal population responses to modifications of an environmental context: evidence for distinct, yet complementary, functions of CA3 and CA1 ensembles. *The Journal of Neuroscience, 24,* 6489-6496.

Vazdarjanova, A., McNaughton, B.L., Barnes, C.A., Worley, P.F., & Guzowski, J.F. (2002). Experience-dependent coincident expression of the effector immediate-early genes *Arc* and *Homer 1a* in hippocampal and neocortical neuronal networks. *The Journal of Neuroscience, 22,* 10067-10071.

Wilson, M.A. & McNaughton, B.L. (1993). Dynamics of the hippocampal ensemble code for space. *Science, 261,* 1055-1058.

Wilson, M.A. & McNaughton, B.L. (1994). Reactivation of hippocampal ensemble memories during sleep. *Science, 265,* 676-679.

Witharana, W.K., Xie, J.Y., Cardiff, J., Lapointe, V., Demchuk, A., Sutherland, R.J., & McNaughton, B.L. (2013, November). *How the hippocampus allocates cells to places: random draw with replacement?* Poster presented at the Society for Neuroscience Annual International Meeting, San Diego, CA.

Witter, M.P., Wouterlood, F.G., Naber, P.A., & Van Haeften, T. (2000). Anatomical organization of the parahippocampal-hippocampal network. *Annals of the New York Academy of Sciences, 911,* 1-24.

APPENDICES

A. Supplementary Materials and Methods

IEG foci-based analysis software

Images of *z* optical planes were processed for automated 3D intranuclear foci (INF) quantification using software plug-ins developed in Java for ImageJ as previously described (Montes-Rodríguez et al., 2013). Briefly, the software's core algorithm assumed that each INF had a single local maximum represented by a pixel or a group of connected pixels with an intensity greater than the user defined threshold value and background value in 3D space (Du et al., 2011). After discovering the local maxima, the INF object was expanded in 3D space recursively using N-connected pixels. All of the connected pixels with an intensity greater than or equal to both the threshold and background value were included as INF objects. During the final stage, discovered INF objects were validated as per various user defined parameters such as size, peak deflection, etc. These criteria were crucial to filter out noisy INF objects and provide a level of user control over the automated detection algorithm.

NeuN-based automated FARSIGHT classification of nuclei

Although manual counts of NeuN-positive cells (neurons) and NeuN-negative cells (glia) were used to determine a glial correction factor for this study (refer to Materials and Methods), Matlab and FARSIGHT were also employed to automatically classify these cell types (in an attempt to bypass manual analysis) based on DAPI saturation within segmented nuclei and the integrated intensity of surrounding extranuclear NeuN staining. NeuN-stained slides were re-imaged as previously described but with the added correction of high voltage (HV; or "sensitivity") values in the *z*-plane to reduce the gradient of DAPI and NeuN staining observed with increasing tissue depth. Images were automatically segmented and edited (to exclude nuclei outside of CA1 and CA3 as well as to correct obvious under-segmentation errors) as previously described (refer to Materials and Methods). In Matlab, the blue (DAPI) channel of each FARSIGHT segmented nucleus was analyzed for volume, average pixel intensity, integrated intensity, fano factor, tail, skew, and sparsity. Subsequently, each nucleus was individually excised and dilated and the same measures were computed for the red (NeuN) channel within the extracted region. If any given nucleus exhibited labeling that was both higher than the threshold for DAPI saturation (average percent saturated pixels) and below the threshold for NeuN staining (average intensity – 0.5 standard deviations), the nucleus was automatically classified as a glial cell (see below for Matlab script). Automated classification results were subsequently manually corrected using the FARSIGHT Nucleus Editing Tool.

Matlab script for FARSIGHT automated nuclear segmentation

batch_FarsightSegmentation.m

```
% Written by: Dr. Ben Clark

% This is the main script for FARSIGHT segmentation

path = '\\huxley.resrch.uleth.ca\IMG\backup\Aubrey -
Preplay\Preplay TIFs\C1-s36\nuc';

inParam = FindFiles('ProjectDef_seg.xml', 'StartingDirectory',
'C:\Users\aubrey.demchuk\Documents\MATLAB');

% FindFiles is a MClust3.1 Util

fldr_list = dir(path);

for i = 1:length(fldr_list);
    if fldr_list(i).isdir && fldr_list(i).name(1) ~= '.'
        cd([path filesep fldr_list(i).name]);
        foldername = [path '\' fldr_list(i).name];
        createInputImageXML_seg(foldername);
        inImg = FindFiles('Input_Image_Seg.xml');
        resTIF = 'Results_Image_nuc.tif';
        resTXT = 'Results_table_nuc.txt';
        c = ['projproc ' inImg{1} ' ' resTIF ' ' resTXT ' '
inParam{1}];
        [status] = dos(['projproc Input_Image_Seg.xml'  ' '
resTIF ' ' resTXT ' ' inParam{1}], '-echo');
    end
end

cd(path);
```

createInputImageXML_seg.m

```
% Written by: Lilia Mesina, April 18, 2013

function createInputImageXML_seg(dn)

cd(dn);
fileList = dir('*_BG.tif');
if length(fileList)~= 3
    disp(['Error: Input image file missing/tooMany in folder '
dn]);
    return
end

docNode = com.mathworks.xml.XMLUtils.createDocument('Image');
docRootNode = docNode.getDocumentElement;
for i1 = 1:length(fileList)
    fileName = fileList(i1);
    if strfind(fileName.name, 'blue')
```

```
            thisElement = docNode.createElement('file');
            thisElement.setAttribute('chname','Nuclei');
            thisElement.setAttribute('r','0');
            thisElement.setAttribute('g','0');
            thisElement.setAttribute('b','255');
            thisElement.appendChild(docNode.createTextNode([dn '\'
fileName.name]));
            docRootNode.appendChild(thisElement);
        end
    end
    xmlFileName = [dn '\Input_Image_Seg.xml'];
    disp(['Create XML file ' xmlFileName])
    xmlwrite(xmlFileName,docNode);
```

Matlab script to overlay FARSIGHT segmentation results and IEG foci analysis results

ieg_analyze.m

```
% This is the main script for overlaying segmentation
% results from FARSIGHT and IEG foci results from
% Vivek Trivedi's ImageJ plugin (Original author unknown)

function ieg_analyze()

fblob = dir('results_arc*tif');
fblob = [fblob dir('results_homer*tif')];
fblob = {fblob(:).name};
resim = 'results_image_nuc.tif';
restab = 'results_table_nuc.txt';

[nuc,nuctype,orphan_hom,orphan_arc] =
ieg_classify_nuc_byimg(resim,restab,fblob,0);
[gnuc,gnuctype] = guard_zones(nuc,nuctype,30,7);

ncell = size(gnuc,1);
nhom = length(find(gnuc(:,2)==1));
narc = length(find(gnuc(:,2)==2));
ndub = length(find(gnuc(:,2)==3));

fprintf('\nHomer only: %.2d\n', nhom);
fprintf('Arc only: %.2d\n', narc);
fprintf('Double: %.2d\n', ndub);
fprintf('Number of cells: %d\n', ncell);
```

ieg_classify_nuc_byimg.m

```
% Written by: Dr. Michael Eckert

function [nuc,nuctype,orphan_hom,orphan_arc] =
ieg_classify_nuc_byimg(fname_nuc,fname_seg,fname_blob,gz)
```

```
% nuctype = ieg_classify_nuc(fname_nuc,fname_seg, fname_blobxml)
% Classifies nuclei defined by farsight as single, double labeled
% fname_nuc = results image filename from farsight
% fname_seg = results table filename from farsight
% fname_blob = cell array of blob image filenames
%
% Returns 'nuctype', a matrix with the nuclei ids and types
% type 0 = no label
% type 1 = homer
% type 2 = arc
% type 3 = double
%
% Also returns the IDs of blobs not claimed by nuclei (possible
% hanging blobs)

orphan_arc = [];
orphan_hom = [];
if nargin < 4
    gz = 0;
end
fname_blob = sortnames(fname_blob);

imnuc = read_multitiff(fname_nuc,'int');
if isempty(imnuc)
    fprintf('Could not open nuclei image\n');
    return
end
if gz; imnuc = guard_zone(imnuc); end

nuc = farsight_read_table(fname_seg);
if isempty(nuc)
    fprintf('Could not read segmentation results\n');
    return
end
idnuc = uint16(nuc(:,1));
nuctype = struct_init(idnuc);

blobim = read_multitiff(fname_blob{1},'int');
if gz; blobim = guard_zone(blobim); end
[nblob,b,orphan_hom] = get_blob_parents(blobim,imnuc,idnuc);
ix = find(~cellfun('isempty',b));
for i = 1:length(ix)
    j = ix(i);
    nuctype(j).class = 1;
    nuctype(j).idhom = b{j};
end
nunc = length(orphan_hom);
fprintf('Claimed homer blobs %d  %.1f %%\n',nblob-nunc,(nblob-
nunc)/nblob*100);
fprintf('Unclaimed homer blobs %d  %.1f
%%\n',nunc,nunc/nblob*100);

if length(fname_blob) == 2
    blobim = read_multitiff(fname_blob{2},'int');
    if gz; blobim = guard_zone(blobim); end
    [nblob,b,orphan_arc] = get_blob_parents(blobim,imnuc,idnuc);
    ix = find(~cellfun('isempty',b));
```

```
    for i = 1:length(ix)
        j = ix(i);
        nuctype(j).class = nuctype(j).class + 2;
        nuctype(j).idarc = b{j};
    end
    nunc = length(orphan_arc);
    fprintf('Claimed arc blobs %d  %.1f %%\n',nblob-nunc,(nblob-
nunc)/nblob*100);
    fprintf('Unclaimed arc blobs %d  %.1f
%%\n',nunc,nunc/nblob*100);
end

c = [nuctype(:).class]';
c = double(c);
nuc = [nuc(:,1) c nuc(:,2:4)];
return

% Functions used in main script %

function fsort = sortnames(f)
if length(f) == 1
    fsort = f;
    return
end
a = f{1}; b = f{2};
if isempty(strfind(lower(a),'homer'))
    fsort = {b; a};
else
    fsort = f;
end
return

function unc = get_unclaimed(idclaimed,blobid)
for i = 1:length(idclaimed)
    ix = blobid == idclaimed(i);
    blobid(ix) = 0;
end
unc = blobid(blobid>0);
return

function [nblob,b,orphan] = get_blob_parents(blobim,imnuc,idnuc)
blobid = farsight_get_id_from_image(blobim);
nblob = length(blobid);
blobimb = logical(blobim);
imnucb = logical(imnuc);
blobsinnuc = imnucb & blobimb;
blobs = blobim(blobsinnuc);
nucs = imnuc(blobsinnuc);
b = cell(size(idnuc));
u = unique(blobs);
for i = 1:length(u)
    blob = u(i);
    ix = blobs==blob;
    nuc = nucs(ix);
    nuc = nuc(1);
    ix = idnuc==nuc;
    b{ix}(end+1) = blob;
```

```
end

%check for unclaimed blobs
blobsinnuc = blobim(blobsinnuc);
idclaimed = farsight_get_id_from_image(blobsinnuc);
nc = length(idclaimed);
if nc ~= nblob
    orphan = get_unclaimed(idclaimed,blobid);
else
    orphan = [];
end
return

function nuctype = struct_init(id)
nuctype = struct('idnuc',{},'class',{},'idarc',{},'idhom',{});
a = zeros(1,'uint8');
for i = 1:length(id)
    nuctype(i).idnuc = id(i);
    nuctype(i).class = a;
end
return

function imgz = guard_zone(im)
gx = 20 + 1;
gz = 5 + 1;
[h,w,z] = size(im);
imgz = im(gx:h-gx, gx:w-gx, gz:z-gz);
return
```

read_multitiff.m

```
% Written by: Dr. Michael Eckert, January 2013

function im = read_multitiff(fname,imtype)

% function im = read_multitiff(fname,imtype)
%
% Reads a tiff image that contains multiple slices or a folder
% with multiple tiff files and puts them into a stack.  Works on
% a single colour channel.
%
% 'fname' is the name of a multi-page tiff file or it can be one
% of 'r' 'g' 'b' if you are in a folder that contains multiple
% tiff files that make up a stack.  r,g,b, determines which
% channel is read from the tiff files.
%
% 'imtype' is a string specifying data type to return, it can be:
% 'short', 'uint8' both return byte images [0 255]
% 'int', 'uint16' both return uint images [0 65535]
% If not specified, default is 'uint8'
% The farsight results image is 'int'

im = [];
if nargin < 2
    imtype = 'uint8';
```

```
elseif strcmp(imtype,'short')
    imtype = 'uint8';
elseif strcmp(imtype,'int')
    imtype = 'uint16';
end

if strcmp(fname,'r') || strcmp(fname,'g') || strcmp(fname,'b')
    isadir = 1;
    ch = find('rgb'==fname);
    dlist = dir('*.tif');
    fnames = {dlist(:).name};
    fname = fnames{1};
else
    isadir = 0;
end

info = imfinfo(fname);
info = info(1);
w = info.Width;
h = info.Height;

z = 0;
if isadir
    z = length(fnames);
else
    if isfield(info,'PageNumber')
        z = info.PageNumber(2);
    elseif isfield(info,'ImageDescription')
        s = info.ImageDescription;
        ix = strfind(s,'slices');
        if ix
            s = s(ix+7:end);
            ix = find(s==10,1,'first');
            z = str2double(s(1:ix));
        end
    end
end
if ~z
    fprintf('Could not determine number of z-slices\n');
    return
end

im = zeros(h,w,z,imtype);

for i = 1:z
    if isadir
        tmp = imread(fnames{i});
        im(:,:,i) = tmp(:,:,ch);
    else
        im(:,:,i) = imread(fname,'Index',i);
    end
end
```

farsight_read_table.m

```
% Written by: Dr. Michael Eckert

function dat = farsight_read_table(fname,colname)
% dat = farsight_read_table(fname)
%
% Reads in data from the farsight results table
% Optional 'colname' specifies the name of the column to read
% If omitted, the first 4 columns are read (id,x,y,z)

dat = [];
fid = fopen(fname,'r');
if fid < 0
    fprintf('Could not open file\n');
    return
end

if nargin < 2
    fmt = '%f %f %f %f %*[^\n]';
    C = textscan(fid,fmt,'HeaderLines',1);
    fclose(fid);
    dat = [C{1} C{2} C{3} C{4}];
    return
end

hdr = fgetl(fid);
H = textscan(hdr,'%s');
H = H{1};
ix = find(strcmp(colname,H));
if isempty(ix)
    fprintf('Could not find column name: %s\n',colname);
    fclose(fid);
    return
end

pos = ftell(fid);
n = 0;
s = fgetl(fid);
while ischar(s)
    if ~isspace(s(1))
        n = n + 1;
    end
    s = fgetl(fid);
end
fseek(fid,pos,'bof');
dat = zeros(n,1);
for i = 1:n
    s = fgetl(fid);
    if ~isspace(s(1))
        S = textscan(s,'%f');
        dat(i) = S{1}(ix);
    end
end
fclose(fid);
return
```

farsight_get_id_from_image.m

```
% Written by: Dr. Michael Eckert

function id = farsight_get_id_from_image(im)
%
% id = farsight_get_id_from_image(im)
%
% Retrieves cell IDs from the farsight results image 'im'
%

a = im(im>0);
a = sort(a);
ix = find(diff(a));
id = [a(ix); a(end)];
```

guard_zones.m

```
% Written by: Dr. Michael Eckert

function [gnuc,gnuctype] = guard_zones(nuc,nuctype,gxy,gz)
%
% [gnuc,gnuctype] = guard_zones(nuc,nuctype,gxy,gz)
%
% Applies guard zones to nuclei and returns the restricted output
%
% nuc is matrix of nuclei ID and coordinates and nuctype is the
% corresponding structure array with blob contents for each cell.
% gxy specifies distance in xy direction and gz specifies the
% distance in z direction.

im = read_multitiff('results_image_nuc.tif','int');
[sxy,~,sz] = size(im);

nuc = nuc + 1;
ixx = (nuc(:,3) < gxy) | (nuc(:,3) > sxy-gxy);
ixy = (nuc(:,4) < gxy) | (nuc(:,4) > sxy-gxy);
ixz = (nuc(:,5) < gz) | (nuc(:,5) > sz-gz);
ix = ixx | ixy | ixz;
nuc = nuc - 1;
gnuc = nuc(~ix,:);
gnuctype = nuctype(~ix);
```

Matlab script for blobless analysis

batch_merge_measures.m

```
% Written by: Dr. Michael Eckert

% This is the main script for blobless analysis (batch)
```

```
function batch_merge_measures

dlist = dir('C*');
dlist = {dlist(:).name};

for iroot = 1:length(dlist)
    cd(dlist{iroot})
    cd('nuc')
    flist = dir('*processed');
    flist = {flist(:).name};

    for istack = 1:length(flist)
        cd(flist{istack})
        farsight_merge_measures;
        cd ..
    end
    cd ..
end
```

farsight_merge_measures.m

```
% Written by: Dr. Michael Eckert

% This is the main script for blobless analysis (single file)

function farsight_merge_measures
% this gets run in the blobless folder

% blobless section
fid = fopen('blobless_green.txt','r');
c = textscan(fid,'%f %f %f %f %f %f %f %f','headerlines',1);
fclose(fid);
g = [c{1} c{2} c{3} c{4} c{5} c{6} c{7} c{8}];

fid = fopen('blobless_red.txt','r');
c = textscan(fid,'%f %f %f %f %f %f %f %f','headerlines',1);
fclose(fid);
r = [c{1} c{2} c{3} c{4} c{5} c{6} c{7} c{8}];

res = farsight_read_table('results_table_nuc.txt');

fblue = dir('*blue_raw.tif');
fblue = fblue(1).name;
imblue = read_multitiff(fblue,'uint8');
imres = read_multitiff('results_image_nuc.tif','uint16');
[avg,total,fano,tail,skew,spars] =
farsight_compute_measures(imres, imblue, res(:,1));

nres = size(res,1);
nguard = size(g,1);
ix = false(nres,1);
for i = 1:nguard
    ix = ix | (g(i,1)==res(:,1));
end
res = res(ix,:);
```

```
avg = avg(ix);
total = total(ix);
fano = fano(ix);
tail = tail(ix);
skew = skew(ix);
spars = spars(ix);

% blob section
curdir = pwd;
[d,stack] = pathsplit(curdir);
[d,~] = pathsplit(d);
ip = strfind(stack,'processed') - 2;
stack = stack(1:ip);
ip = strfind(stack,'.tif') - 1;
dblob = [d '\foci\' stack '\' stack(1:ip) '_blobs'];
cd(dblob)

farc = dir('results_arc*txt');
fid = fopen(farc(1).name,'r');
c = textscan(fid,'%f %f %f %f %f %f %f %f %f %f
%f','headerlines',1);
fclose(fid);
arc = [c{1} c{2} c{3} c{4} c{5} c{6} c{10}];
farc = dir('results_arc*tif');
imarc = read_multitiff(farc(1).name,'uint16');

fhom = dir('results_hom*txt');
fid = fopen(fhom(1).name,'r');
c = textscan(fid,'%f %f %f %f %f %f %f %f %f %f
%f','headerlines',1);
fclose(fid);
hom = [c{1} c{2} c{3} c{4} c{5} c{6} c{10}];
fhom = dir('results_hom*tif');
imhom = read_multitiff(fhom(1).name,'uint16');

arcout = zeros(nguard,6);
homout = zeros(nguard,6);
for i = 1:size(arc,1)
    id = arc(i,1);
    ix = (imarc==id) & imres;
    idnuc = imres(ix);
    if any(idnuc)
        idnuc = mode(idnuc);
        j = find(g(:,1) == idnuc);
        if any(j)
            if arcout(j,1)
                arcout(j,4:6) = arc(i,5:7);
            else
                arcout(j,1:3) = arc(i,5:7);
            end
        end
    end
end
for i = 1:size(hom,1)
    id = hom(i,1);
    ix = (imhom==id) & imres;
    idnuc = imres(ix);
```

```
        if any(idnuc)
            idnuc = mode(idnuc);
            j = find(g(:,1) == idnuc);
            if any(j)
                if homout(j,1)
                    homout(j,4:6) = hom(i,5:7);
                else
                    homout(j,1:3) = hom(i,5:7);
                end
            end
        end
    end

    % output everything
    cd(curdir)
    out = [res g(:,end) avg total fano tail skew spars g(:,2:end-1)
    homout r(:,2:end-1) arcout];
    ishom = out(:,18) > 0;
    isarc = (out(:,30) > 0) * 2;
    label = ishom + isarc;
    out = [out label];

    fid = fopen('results_all.txt','w');
    if fid < 0
        fprintf('Saving output failed in folder: %s\n', curdir);
    else
        %fprintf(fid,'\t\t\t\t\tnuc\t\t\t\t\t\thom\t\t\t\t\t\tblob
    1\t\t\tblob 2\t\t\tarc\t\t\t\t\t\tblob 1\t\t\tblob 2\n');

    %fprintf(fid,'id\tx\ty\tz\tvolume\taverage\ttotal\tfano\ttail\tsk
    ew\tspars\taverage\ttotal\tfano\ttail\tskew\tspars\tvolume\tavera
    ge\ttotal\tvolume\taverage\ttotal\taverage\ttotal\tfano\ttail\tsk
    ew\tspars\tvolume\taverage\ttotal\tvolume\taverage\ttotal\n');

    fprintf(fid,'nuc_ID\tX\tY\tZ\tvolume\tnuc_average\tnuc_total\tnuc
    _fano\tnuc_tail\tnuc_skew\tnuc_sparsity\t');

    fprintf(fid,'hom_average\thom_total\thom_fano\thom_tail\thom_skew
    \thom_sparsity\t');

    fprintf(fid,'homB1_volume\thomB1_average\thomB1_total\thomB2_volu
    me\thomB2_average\thomB2_total\t');

    fprintf(fid,'arc_average\tarc_total\tarc_fano\tarc_tail\tarc_skew
    \tarc_sparsity\t');

    fprintf(fid,'arcB1_volume\tarcB1_average\tarcB1_total\tarcB2_volu
    me\tarcB2_average\tarcB2_total\t');
        fprintf(fid,'label\r\n');
        for i = 1:nguard

    fprintf(fid,'%d\t%d\t%d\t%d\t%d\t%f\t%f\t%f\t%f\t%f\t%f\t%f\t%f\t
    %f\t%f\t%f\t%f\t%f\t%f\t%f\t%f\t%f\t%f\t%f\t%f\t%f\t%f\t%f\t%f\t%
    f\t%f\t%f\t%f\t%f\t%f\t%d\r\n',out(i,:));
        end
        fclose(fid);
    end
```

farsight_compute_measures.m

```
% Written by: Dr. Michael Eckert, January 2013
% Dr. Ben Clark added sparsity, total, and avg measures - January
2013

function [avg,total,fano,tail,skew,spars,vol] =
farsight_compute_measures(imres, imblob, id)
%
% [avg,total,fano,tail,skew,spars] =
farsight_compute_measures(imres, imblob, id)
%
% Calculates the following measures of IEG expression within
% nuclei:
%     total = sum of pixel intensities in nuclei
%     avg = average pixel intensity
%     fano = Fano factor = var/mean
%     tail = mean intensity value of top 0.1% of histogram
%     skew = skewness of histogram
%     sparsity = measure of how diffuse the intensity is in the
%     nucleus (larger values indicate intensity is diffuse)
%
% 'imres' is the farsight results image stack
% 'imblob' is image stack of the channel to be measured
% 'id' is the optional list of cell IDs.  If not given,
% they are determined from the results image.

tic
if nargin < 3
    fprintf('\nGetting cell IDs from results image\n');
    id = farsight_get_id_from_image(imres);
    fprintf('Got IDs\n');
end
n = length(id);
fprintf('There are %d cells\n',n);
fano = zeros(n,1);
tail = zeros(n,1);
skew = zeros(n,1);
total = zeros(n,1);
avg = zeros(n,1);
spars = zeros(n,1);
vol = zeros(n,1);

fprintf('\nComputing IEG expression measurements...\n');
for i = 1:n
    ix = (imres == id(i));
    x = double(imblob(ix));
    avg(i) = mean(x);
    total(i) = sum(x);
    fano(i) = var(x)/avg(i);
    tail(i) = tail_mean(x);
    skew(i) = skewness(x);
    spars(i) = farsight_sparsity(x);
    vol(i) = numel(x);
end
fprintf('Done.  Took %d sec.\n', round(toc));
```

tail_mean.m

```
% Written by: Dr. Michael Eckert, January 2013

function tail = tail_mean(x,p)
%
% tail = tail_mean(x,p)
%
% For farsight IEG detection
% Calculates the mean value of histogram tail of the variable 'x'
% The amount of tail to include can be given by 'p'
% If omitted, p = 0.001
% Higher mean values mean IEG is expressed.

if nargin < 2
    p = .001;
end
bins = 0:255;
h = hist(x,bins);
h = h/sum(h);

i = 256;
s = 0;
tail = 0;
while s < p
    tail = tail + h(i)*bins(i);
    s = s + h(i);
    i = i - 1;
end
tail = tail / s;
```

farsight_sparsity.m

```
% Written by: Dr. Ben Clark, 2013

function [spars] = farsight_sparsity(x)

% For farsight IEG detection
% Calculates the sparsity of variable 'x'
% Sparsity is a measure of how diffuse intensity values are
% throughout the nucleus.
% Larger values indicate more diffuse intensity;
% lower values indicate compact intensity
%
% based on Jung et al 1994 J Neuro
%
% patched together from tail_mean.m and sparsity.m (NMSA code)

bins = 0:255;
h = hist(x,bins);
h = h/sum(h);
spars = sum(h).^2./(256*sum(h.^2));
```

pathjoin.m

```
% Written by: Dr. Michael Eckert

function s = pathjoin(head,tail,nix)

if nargin < 3
    if head(end) ~= filesep
        head(end+1) = filesep;
    end
else
    if nix
        if head(end) == '\'
            head(end) = '/';
        elseif head(end) ~= '/'
            head(end+1) = '/';
        end
    else
        if head(end) == '/'
            head(end) = '\';
        elseif head(end) ~= '\'
            head(end+1) = '\';
        end
    end
end
s = [head tail];
```

blobless_clean.m

```
% Written by: Dr. Bruce L. McNaughton, January 2014
% Modified by: Aubrey Demchuk, April 2014

% Note: Below script is for home cage CA3 data only but
% script was modified (not shown) for data from CA1,
% CA3 and EC of both home cage and experimental groups

% Extract the nuclear segmentation and pixel data from the
% xlsx file and plot

% hc_xCA3 = home cage CA3 data, x = rats 1-6

hc_1CA3= xlsread('G:\Aubrey\THE ONE Preplay Foci & Blobless
Datasheet TO RULE THEM ALL','HC CA3','A2:AP2195');
hc_2CA3= xlsread('G:\Aubrey\THE ONE Preplay Foci & Blobless
Datasheet TO RULE THEM ALL','HC CA3','A2196:AP4329');
hc_3CA3= xlsread('G:\Aubrey\THE ONE Preplay Foci & Blobless
Datasheet TO RULE THEM ALL','HC CA3','A4330:AP6711');
hc_4CA3= xlsread('G:\Aubrey\THE ONE Preplay Foci & Blobless
Datasheet TO RULE THEM ALL','HC CA3','A6712:AP9002');
hc_5CA3= xlsread('G:\Aubrey\THE ONE Preplay Foci & Blobless
Datasheet TO RULE THEM ALL','HC CA3','A9003:AP11425');
hc_6CA3= xlsread('G:\Aubrey\THE ONE Preplay Foci & Blobless
Datasheet TO RULE THEM ALL','HC CA3','A11426:AP13426');
```

```
% Plot histogram of all nuclei
allvol=([ hc_1CA3(:,11); hc_2CA3(:,11); hc_3CA3(:,11);
hc_4CA3(:,11); hc_5CA3(:,11);hc_6CA3(:,11)]);
hx=[0:16000./64:16000];
figure (25); n=hist(allvol,hx);
n=n./length(allvol); bar(hx, n);axis([0 16000 0 0.15]); shg
meanvol= mean(allvol)
stdvol= std(allvol)
kurtvol=kurtosis(allvol)

% The data deviates substantially from normal due to
% undersegmentation of nuclei and inclusion of glia.
% Thus we should restrict the analysis to data
% falling within 1 standard deviation of the mean volume

hicut=meanvol+stdvol;
locut=meanvol-stdvol;

% "Clean" data

% find the row indices of the volume outliers
hc_1CA3_cut=find((hc_1CA3(:,11)<locut) | (hc_1CA3(:,11)>hicut));
% copy raw data to new array
hc_1CA3_clean=hc_1CA3;
% get rid of rows with outlier nuclei
hc_1CA3_clean(hc_1CA3_cut,:)=[];

hc_2CA3_cut=find((hc_2CA3(:,11)<locut) | (hc_2CA3(:,11)>hicut));
hc_2CA3_clean=hc_2CA3;
hc_2CA3_clean(hc_2CA3_cut,:)=[];

hc_3CA3_cut=find((hc_3CA3(:,11)<locut) | (hc_3CA3(:,11)>hicut));
hc_3CA3_clean=hc_3CA3;
hc_3CA3_clean(hc_3CA3_cut,:)=[];

hc_4CA3_cut=find((hc_4CA3(:,11)<locut) | (hc_4CA3(:,11)>hicut));
hc_4CA3_clean=hc_4CA3;
hc_4CA3_clean(hc_4CA3_cut,:)=[];

hc_5CA3_cut=find((hc_5CA3(:,11)<locut) | (hc_5CA3(:,11)>hicut));
hc_5CA3_clean=hc_5CA3;
hc_5CA3_clean(hc_5CA3_cut,:)=[];

hc_6CA3_cut=find((hc_6CA3(:,11)<locut) | (hc_6CA3(:,11)>hicut));
hc_6CA3_clean=hc_6CA3;
hc_6CA3_clean(hc_6CA3_cut,:)=[];

% Write to Excel spreadsheet
xlswrite('G:\Aubrey\Blobless Clean', hc_1CA3_clean, 'HC CA3 1')
xlswrite('G:\Aubrey\Blobless Clean', hc_2CA3_clean, 'HC CA3 2')
xlswrite('G:\Aubrey\Blobless Clean', hc_3CA3_clean, 'HC CA3 3')
xlswrite('G:\Aubrey\Blobless Clean', hc_4CA3_clean, 'HC CA3 4')
xlswrite('G:\Aubrey\Blobless Clean', hc_5CA3_clean, 'HC CA3 5')
xlswrite('G:\Aubrey\Blobless Clean', hc_6CA3_clean, 'HC CA3 6')
```

Matlab script for NeuN-based automated FARSIGHT classification of nuclei

ng_class.m

```
% Written by: Dr. Michael Eckert

% This is the main script for FARSIGHT classification of neurons
% based on both saturation in the blue channel within a nucleus
% (there is often DAPI saturation in glia) and average intensity
% of red NeuN labeling surrounding a nucleus (extranuclear NeuN
% staining indicates a neuron; glia are not labeled).

function ng_class

d = dir('*blue_BG.tif');
imb = read_multitiff(d(1).name,'uint8');
d = dir('*red_RAW.tif');
imr = read_multitiff(d(1).name,'uint8');
%imrcor = grad_cor(imr);
imnuc = read_multitiff('results_image_nuc.tif','uint16');

[bavg,btot,bfano,btail,bskew,bspar,blone,bsat] =
farsight_compute_measures(imnuc, imb);
[ravg,rtot,rfano,rtail,rskew,rspar,rlone,rsat] =
compute_with_dilate(imnuc, imr);

ix = ravg < (mean(ravg)-std(ravg)/2);
ix = ix & bsat>mean(bsat);
grp = ix+1;
cols = {'bsat'; 'rtot'; 'prediction_active_ng'};
farsight_results_append('results_table_nuc.txt',cols,[bsat ravg
grp]);

d = pwd;
fid = fopen('Input_Image_Seg.xml','w');
if fid < 0
    fprintf('Could not create xml file in: %s\n',d);
    return
end
d = [d '\'];
db = dir('*blue_RAW.tif');
dg = dir('*green_RAW.tif');
dr = dir('*red_RAW.tif');
fprintf(fid,'<?xml version="1.0" encoding="utf-8"?>\n');
fprintf(fid,'<Image>\n');
fprintf(fid,'    <file chname="blue" b="255" g="0" r="0">');
fprintf(fid,'%s%s</file>\n',d,db(1).name);
fprintf(fid,'    <file chname="green" b="0" g="255" r="0">');
fprintf(fid,'%s%s</file>\n',d,dg(1).name);
fprintf(fid,'    <file chname="red" b="0" g="0" r="255">');
fprintf(fid,'%s%s</file>\n',d,dr(1).name);
fprintf(fid,'</Image>');
fclose(fid);
```

compute_with_dilate.m

```
% Written by: Dr. Michael Eckert

function [avg,total,fano,tail,skew,spars,lone,psat] =
compute_with_dilate(imres, imblob, id)

tic
if nargin < 3
    fprintf('\nGetting cell IDs from results image\n');
    id = farsight_get_id_from_image(imres);
    fprintf('Got IDs\n');
end
n = length(id);
bins = 0:255;
fprintf('\nThere are %d cells\n',n);
fano = zeros(n,1);
tail = zeros(n,1);
skew = zeros(n,1);
total = zeros(n,1);
avg = zeros(n,1);
spars = zeros(n,1);
lone = zeros(n,1);
psat = zeros(n,1);

fprintf('Computing IEG expression measurements...\n');
for i = 1:n
    dres = farsight_result_nuc_dilate(imres,5,id(i));
    ix = dres>0;
    x = double(imblob(ix));
    h = hist(x,bins);
    h = h / sum(h);
    avg(i) = mean(x);
    total(i) = sum(x);
    if avg(i) == 0
        fano(i) = 0;
    else
        fano(i) = var(x)/avg(i);
    end
    tail(i) = tail_mean(x);
    skew(i) = skewness(x);
    spars(i) = farsight_sparsity(x);
    lone(i) = sum(find(h)-1);
    ix = x==255;
    psat(i) = length(find(ix)) / length(x);
end
fprintf('Done.  Took %d sec.\n', round(toc));
```

farsight_results_append.m

```
% Written by: Dr. Michael Eckert, January 2013

function farsight_results_append(fname,colname,c)

% farsight_append_table(fname,colname,c)
%
% Appends columns of data to the farsight results table
%
% 'fname' is the name of the results table.
% A new file is created for the new table with 'edit' appended to
% 'fname'
%
% 'colname' is the text name for the column.
% If the number of columns is more than 1, colname must be a cell
% array otherwise colname can be cell array of 1 or a
% regular string
%
% 'c' is the data to append and should be in columns
% (ncell x nmeasure)

ncol = size(c,2);
if ischar(colname)
    if ncol > 1
        fprintf('colname must be cell array\n');
        return
    else
        colname = {colname};
    end
else
    if length(colname) ~= ncol
        fprintf('number of columns and number of names dont
match\n');
        return
    end
end

i = strfind(fname,'.txt');
if isempty(i)
    fntmp = [fname '_cm_BG.txt'];
else
    fntmp = [fname(1:i-1) '_cm_BG.txt'];
end
fid = fopen(fname,'r');
if fid < 0
    fprintf('Could not open results table\n');
    return
end

fgetl(fid);
n = 0;
while ischar(fgetl(fid))
    n = n + 1;
end
if n ~= size(c,1)
```

```
        fprintf('Data to append differs in length from file\n');
        fprintf('File has %d measures, data has %d\n',n,length(c));
        fclose(fid);
        return
    end

    ftmp = fopen(fntmp,'w');
    if ftmp < 0
        fprintf('Could not creat new file, try deleting the file
    %s\n',fntmp);
        fclose(fid);
        return
    end

    fseek(fid,0,'bof');
    s = fgetl(fid);
    if s(end) == sprintf('\t')
        t = '';
    else
        t = '\t';
    end
    scol = sprintf('%s\t',colname{:});
    fprintf(ftmp,['%s' t '%s\r\n'], s, scol);

    f = [];
    for i = 1:ncol
        if mean(c(:,i)) > 10
            f = [f '%.2f\t'];
        else
            f = [f '%.4f\t'];
        end
    end

    for i = 1:n
        s = fgetl(fid);
        fprintf(ftmp,['%s' t f '\r\n'],s,c(i,:));
    end
    fclose(fid);
    fclose(ftmp);
```

farsight_result_nuc_dilate.m

```
    % Written by: Dr. Michael Eckert, February 2013

    function d = farsight_result_nuc_dilate(res,r,id)
    %
    % e = farsight_result_nuc_erode(res, r, id)
    %
    % Dilates the size of a single nuclei
    % res - farsight results image
    % id - ID of the nuclei to dilate
    % r - size in pixels to dilate by (must be integer)
    %     (r/2 is used for z dimension)
    % returns d, a results image that contains only the single
    % dilated nucleus
```

```
% Requires image processing toolbox

gx = 20;
gz = 10;

H = size(res,1)+gx;
W = size(res,2)+gx;
Z = size(res,3)+gz;
d = zeros(size(res),'uint16');
e = zeros(H,W,Z,'uint16'); % expanded stack to hold dilated nuc
rr = r/2;
se = strel('ball',r,rr,0);

% find extent of nucleus in each dimension
ix = res==id;
xy = max(ix,[],3);
h = max(xy,[],2);
w = max(xy);
wz = squeeze(max(ix));
z = max(wz);

% get indices of nuc and fill any gaps (due to bad segmentation)
fh = find(h); fh = fh(1):fh(end); h(fh) = 1;
fw = find(w); fw = fw(1):fw(end); w(fw) = 1;
fz = find(z); fz = fz(1):fz(end); z(fz) = 1;

% make a container stack to hold the nucleus
dx = gx/2;
dz = gz/2;
hl = length(fh) + gx;
wl = length(fw) + gx;
zl = length(fz) + gz;
v = false(hl,wl,zl);
c = zeros(hl,wl,zl,'uint8');

% put the nucleus in the container and dilate
v(dx+1:hl-dx, dx+1:wl-dx, dz+1:zl-dz) = ix(h,w,z);
c(v) = 200;
ce = imdilate(c,se);
ce(ce<100) = 0;

% put the dilated nuc into the expanded stack, then crop and
return
nh = h;
nh(fh(1):fh(end)+gx) = 1;
nw = w;
nw(fw(1):fw(end)+gx) = 1;
nz = z;
nz(fz(1):fz(end)+gz) = 1;
tmp = e(nh,nw,nz);
tmp = uint16(tmp | ce);
tmp(tmp>0) = id;
e(nh,nw,nz) = tmp;
d = e(dx+1:end-dx, dx+1:end-dx, dz+1:end-dz);
```

farsight_nuc_outline.m

```
% Written by: Dr. Michael Eckert

function farsight_nuc_outline %(fname_im, fname_res)

%im = read_multitiff_rgb(fname_im);
%res = read_multitiff(fname_res,'int');

res = read_multitiff('results_image_nuc.tif','uint16');
d = dir('*RAW.tif');
if length(d) ~= 3
    error('wrong number of image files');
end
imb = read_multitiff(d(1).name,'uint8');
img = read_multitiff(d(2).name,'uint8');
imr = read_multitiff(d(3).name,'uint8');
[h,w,z] = size(imr);
im = zeros(h,w,3,z,'uint8');
im(:,:,1,:) = imr;
im(:,:,2,:) = img;
im(:,:,3,:) = imb;
imr=[]; img=[]; imb=[];

for k = 1:z
    for i = 2:h-1
        for j = 2:w-1
            v = res(i,j,k);
            if v
                v1 = res(i+1,j,k);
                v2 = res(i-1,j,k);
                v3 = res(i,j+1,k);
                v4 = res(i,j-1,k);
                if v~=v1 || v~=v2 || v~=v3 || v~=v4
                    im(i,j,1,k) = 255;
                    im(i,j,2,k) = 255;
                    im(i,j,3,k) = 255;
                end
            end
        end
    end
end
ix = strfind(d(1).name,'.tif');
fout = [d(1).name(1:ix-1) '_outline'];
write_multitiff(im,fout)
```

B. Supplementary Results

NeuN-based automated classification of nuclei was inadequate

FARSIGHT classification of nuclei produced a very modest representation of the total glial population and, consequently, an over-representation of the total neuronal population. Though all automatically classified glial cells were correctly categorized, a considerable proportion of glial cells were incorrectly classified as neurons. The proportion of total nuclei classified as glia by the automated program was 12.9 ± 0.6% for CA1, 33.3 ± 0.2% for CA3 and 34.0 ± 2.6% for entorhinal cortex. After manual correction, these proportions increased to 16.5 ± 1.8% in CA1, 55.5 ± 3.2% in CA3 and 59.1 ± 2.6% in cortex (Figure 18). Based on a paired one-tailed *t*-test, automated estimations of glial populations were significantly lower than the populations determined following manual correction (CA1, $p < 0.05$; CA3 & EC, $p < 0.01$). Due to these discrepancies, manual (rather than automated) nuclei counts were used to determine a glial correction factor for this study.

Extent of novel environment exploration was similar between experimental rats

Experimental rats completed an average of 2.25 ± 0.59 laps in the clockwise direction and 1.92 ± 1.08 laps in the counterclockwise direction during unassisted exploration of the novel track. On average, 4.17 ± 1.25 laps were completed (including both clockwise and counterclockwise directions; Table 2).

Proportion of IEG-labeled nuclei increased after exploration of a novel environment and observed pattern overlap was equivalent to that expected by random chance

See Table 3.

Equalization of home cage proportions of *Arc*- and *Homer1a*-labeled nuclei

See Table 4.

Nuclei containing IEG foci of above average volume demonstrated greater pattern overlap than the total active population

See Table 5.

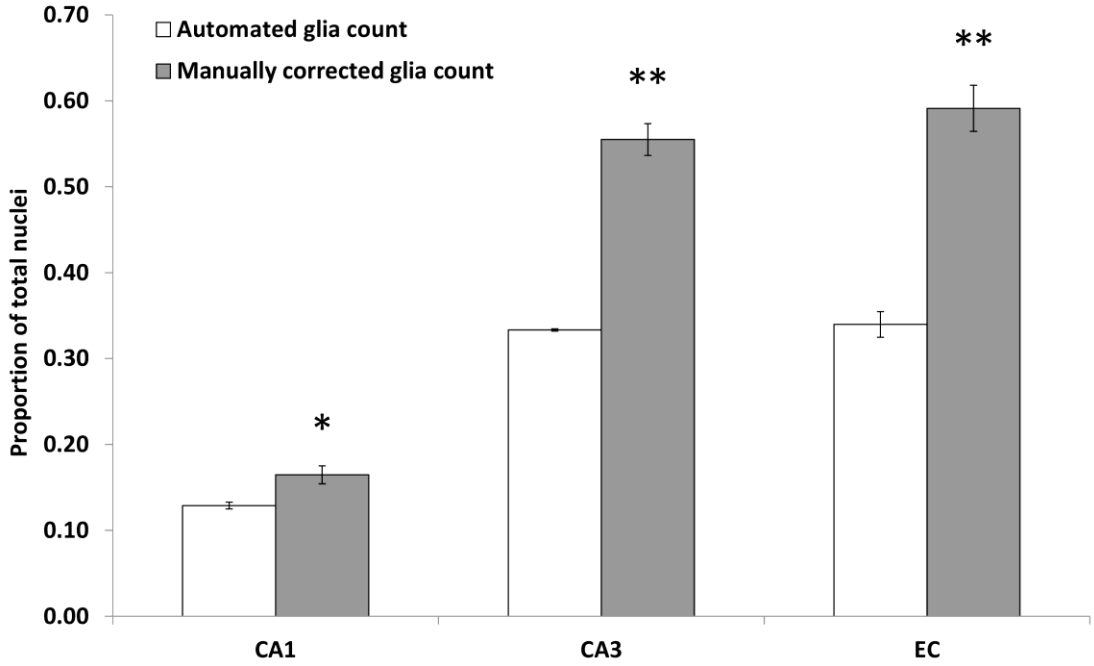

Figure 18: Proportion of total nuclei classified as glia in CA1, CA3 and dorsolateral entorhinal cortex (EC) by FARSIGHT automated classification compared to manual visual classification based on NeuN and DAPI staining. Automated estimations of glial populations were significantly lower than the populations determined following manual correction in all regions analyzed (CA1, $p < 0.05$; CA3 & EC, $p < 0.01$).

Table 2: Number of laps completed by each experimental rat during exploration of the novel circular track. "Total laps" refers to the sum of both clockwise and counterclockwise laps. The extent of novel environment exploration was comparable between individual experimental rats.

Rat	Clockwise Laps	Counterclockwise Laps	Total Laps
NE-1	2.50	2.00	4.50
NE-2	2.25	0.25	2.50
NE-3	2.00	2.50	4.50
NE-4	1.50	3.00	4.50
NE-5	3.25	2.75	6.00
NE-6	2.00	1.00	3.00
Average (± Standard Deviation)	2.25 ± 0.59	1.92 ± 1.08	4.17 ± 1.25

Table 3: Average proportions of *Arc*-labeled (*Arc*+) nuclei, *Homer1a*-labeled (*Homer1a*+) nuclei, observed double-labeled (Double+) nuclei, and double-labeled nuclei expected by the uniform random sample with replacement model. Expected overlap was determined by calculating the product of the proportion of *Homer1a*-labeled nuclei and the proportion of *Arc*-labeled nuclei. *p*-values were obtained from paired, one-tailed *t*-tests comparing the expected and observed proportions of double-labeled nuclei across animals within treatment groups. Standard error (SE) is shown. Refer to Figures 7-8.

Treatment	Region	*Homer1a*+ (± SE)	*Arc*+ (± SE)	Observed Double+ (± SE)	Expected Double+ (± SE)	*p*-value
Home Cage Controls	CA1	0.111 ± 0.043	0.197 ± 0.021	0.024 ± 0.012	0.023 ± 0.011	0.253
	CA3	0.044 ± 0.013	0.124 ± 0.021	0.008 ± 0.004	0.006 ± 0.003	0.117
	EC	0.161 ± 0.040	0.237 ± 0.021	0.034 ± 0.009	0.037 ± 0.010	0.166
Novel Environment	CA1	0.104 ± 0.032	0.397 ± 0.030	0.049 ± 0.016	0.045 ± 0.015	0.076
	CA3	0.037 ± 0.010	0.182 ± 0.018	0.009 ± 0.003	0.007 ± 0.002	0.089
	EC	0.167 ± 0.028	0.341 ± 0.023	0.056 ± 0.010	0.059 ± 0.012	0.331

Table 4: Normalized average proportions of *Arc*-labeled (*Arc*+) nuclei, *Homer1a*-labeled (*Homer1a*+) nuclei, observed double-labeled (Double+) nuclei, and double-labeled nuclei expected by the uniform random sample with replacement model in CA1, CA3 and dorsolateral entorhinal cortex (EC) of home cage controls and rats that explored a novel environment after a period of home cage rest. The average red pixel intensity threshold was increased to approximately equalize home cage proportions of *Arc*- and *Homer1a*-labeled nuclei in control rats. Expected overlap was determined by calculating the product of the proportion of *Homer1a*-labeled nuclei and the proportion of *Arc*-labeled nuclei. *p*-values were obtained from paired, one-tailed *t*-tests comparing the expected and observed proportions of double-labeled nuclei across animals within treatment groups. Standard error (SE) is shown. Refer to Figures 9-10.

Treatment	Region	*Homer1a*+ (± SE)	*Arc*+ (± SE)	Observed Double+ (± SE)	Expected Double+ (± SE)	*p*-value
Home Cage Controls	**CA1**	0.117 ± 0.43	0.144 ± 0.021	0.022 ± 0.011	0.017 ± 0.009	0.094
	CA3	0.045 ± 0.014	0.078 ± 0.018	0.007 ± 0.003	0.004 ± 0.002	0.094
	EC	0.145 ± 0.037	0.090 ± 0.015	0.017 ± 0.005	0.011 ± 0.003	0.048
Novel Environment	**CA1**	0.114 ± 0.041	0.342 ± 0.034	0.051 ± 0.019	0.044 ± 0.016	0.037
	CA3	0.037 ± 0.009	0.134 ± 0.016	0.007 ± 0.003	0.005 ± 0.002	0.093
	EC	0.147 ± 0.022	0.196 ± 0.022	0.040 ± 0.007	0.030 ± 0.006	0.053

Table 5: Average proportions of *Arc*-labeled (*Arc*+), *Homer1a*-labeled (*Homer1a*+), and observed double-labeled (Double+) nuclei containing at least one *Arc* and/or one *Homer1a* focus of above average volume, and the average proportions of double-labeled nuclei expected by the uniform random sample with replacement model in CA1, CA3 and dorsolateral entorhinal cortex (EC) of home cage controls and rats that explored a novel environment after a period of home cage rest. Analysis was restricted to nuclei containing at least one focus of *Arc* or *Homer1a* mRNA (or one of each in the case of double-labeled nuclei) of above average volume. Expected overlap was determined by calculating the product of the proportion of *Homer1a*-labeled nuclei and the proportion of *Arc*-labeled nuclei. *p*-values were obtained from paired, one-tailed *t*-tests comparing the expected and observed proportions of double-labeled nuclei across animals within treatment groups. Standard error (SE) is shown. Refer to Figures 14-15.

Treatment	Region	*Homer1a*+ (± SE)	*Arc*+ (± SE)	Observed Double+ (± SE)	Expected Double+ (± SE)	*p*-value
Home Cage Controls	CA1	0.036 ± 0.014	0.070 ± 0.016	0.004 ± 0.002	0.002 ± 0.001	0.107
	CA3	0.010 ± 0.004	0.044 ± 0.012	0.0016 ± 0.0004	0.0005 ± 0.0002	0.009
	EC	0.040 ± 0.012	0.069 ± 0.015	0.005 ± 0.002	0.002 ± 0.001	0.064
Novel Environment	CA1	0.028 ± 0.011	0.211 ± 0.024	0.013 ± 0.005	0.006 ± 0.003	0.016
	CA3	0.008 ± 0.002	0.093 ± 0.015	0.002 ± 0.001	0.0008 ± 0.0002	0.040
	EC	0.045 ± 0.010	0.153 ± 0.017	0.013 ± 0.005	0.007 ± 0.002	0.085

Large variability in proportions of nuclei expressing IEGs was evident between animals within treatment groups

There was large variation in the observed proportions of *Arc*-labeled nuclei relative to that of *Homer1a*-labeled nuclei between individual rats. In CA1, half of the home cage animals demonstrated a significantly higher proportion of *Arc*-labeled nuclei than *Homer1a*-labeled nuclei (HC-2, $p < 0.001$; HC-3, $p < 0.01$; HC-5, $p < 0.05$) whereas this significant increase was observed in five of six experimental animals (NE-1 & NE-6, $p < 0.05$; NE-2, $p < 0.01$; NE-3 & NE-5, $p < 0.001$). Similarly, four home cage controls and five experimental animals demonstrated this trend in CA3 (HC-2 & HC-3, $p < 0.01$; HC-5 & HC-6, $p < 0.05$; NE-1 & NE-6, $p < 0.05$; NE-2, NE-3 & NE-5, $p < 0.01$). Of all home cage controls and experimental animals, only one experimental rat demonstrated a significantly higher proportion of *Arc*-labeled nuclei relative to *Homer1a*-labeled nuclei in dorsolateral entorhinal cortex (NE-2, $p < 0.05$). Similarly, there was variation among individual rats in the proportion of double-labeled cells relative to *Homer1a*-labeled nuclei or *Arc*-labeled nuclei. Relative to the proportion of nuclei expressing *Arc* or *Homer1a* foci, there was a significantly lower proportion of double-labeled nuclei in three home cage controls and two experimental rats in CA1 (HC-2, HC-4, NE-1 & NE-3, $p < 0.05$; HC-5, $p < 0.001$), three home cage controls and one experimental animal in CA3 (HC-3, HC-6 & NE-3, $p < 0.05$; HC-5, $p < 0.01$), and one home cage control in the dorsolateral entorhinal cortex (HC-5, $p < 0.05$; Table 6 and Table 7).

Individual rats demonstrated pattern overlap equivalent to random chance

Considering the large variability in IEG expression evident across animals and to rule out the possibility that uncontrollable environmental disturbances or variations in wakefulness or sleep states during the epochs of home cage rest could contribute differently to the observed patterns of hippocampal activity, the overlap expected by the uniform random sample with replacement model was compared to the observed overlap of IEG expression patterns within individual rats. All regions across all animals excluding two from both home cage and experimental treatment groups showed no statistically significant difference between the observed and expected proportions of double *Arc/Homer1*-labeled nuclei. One home cage animal and one experimental animal actually demonstrated a significantly *lower* proportion of double-labeled nuclei than expected by random chance (HC-6, $p < 0.05$; NE-3, $p < 0.01$; Table 6 and Table 7).

Large variability in correlations between nuclear *Arc* and *Homer1a* pixel intensities between animals within treatment groups

Among the total population of sampled nuclei (both labeled and unlabeled based on the foci-based analysis) within one standard deviation of the mean nuclear volume (including glial nuclei that fell within that range), there was a moderate average correlation between the average nuclear red (*Arc*-labeled) pixel intensity and average nuclear green (*Homer1a*-labeled) pixel intensity in home cage controls and in

Table 6: Proportions of *Arc*-labeled (*Arc*+) nuclei, *Homer1a*-labeled (*Homer1a*+) nuclei, observed double-labeled (Double+) nuclei, and double-labeled nuclei expected by the uniform random sample with replacement model in CA1, CA3 and dorsolateral entorhinal cortex (EC) of home cage (HC) controls. Expected overlap was determined by calculating the product of the proportion of *Homer1a*-labeled nuclei and the proportion of *Arc*-labeled nuclei. *p*-values were obtained from paired, one-tailed *t*-tests comparing the expected and observed proportions of double-labeled nuclei across sections within each animal. Large variability between individual rats is evident. Standard error (SE) is shown. Note: statistical analyses were not applicable to the EC of HC-1 because of damage to some of the tissue sections (the sample size was too small).

Region	Animal	*Homer1a*+ (± SE)	*Arc*+ (± SE)	Observed Double+ (± SE)	Expected Double+ (± SE)	*p*-value
CA1	HC-1	0.118 ± 0.068	0.214 ± 0.071	0.027 ± 0.024	0.025 ± 0.021	0.254
	HC-2	0.016 ± 0.002	0.221 ± 0.008	0.006 ± 0.003	0.0035 ± 0.0004	0.286
	HC-3	0.021 ± 0.012	0.229 ± 0.015	0.007 ± 0.004	0.005 ± 0.003	0.148
	HC-4	0.166 ± 0.017	0.116 ± 0.049	0.016 ± 0.010	0.018 ± 0.008	0.253
	HC-5	0.291 ± 0.015	0.251 ± 0.022	0.082 ± 0.016	0.074 ± 0.010	0.193
	HC-6	0.064 ± 0.045	0.148 ± 0.011	0.006 ± 0.006	0.009 ± 0.006	0.020
CA3	HC-1	0.060 ± 0.047	0.159 ± 0.050	0.009 ± 0.009	0.012 ± 0.011	0.123
	HC-2	0.027 ± 0.007	0.146 ± 0.017	0.004 ± 0.001	0.004 ± 0.002	0.500
	HC-3	0.009 ± 0.002	0.080 ± 0.007	0.002 ± 0.001	0.0007 ± 0.0001	0.171
	HC-4	0.051 ± 0.020	0.069 ± 0.020	0.004 ± 0.002	0.0028 ± 0.0004	0.335
	HC-5	0.091 ± 0.007	0.198 ± 0.020	0.024 ± 0.004	0.018 ± 0.001	0.107
	HC-6	0.017 ± 0.005	0.085 ± 0.019	0.003 ± 0.002	0.0013 ± 0.0003	0.170
EC	HC-1	0.008	0.269	0.005	0.002	N/A
	HC-2	0.243 ± 0.107	0.193 ± 0.017	0.038 ± 0.017	0.045 ± 0.019	0.245
	HC-3	0.073 ± 0.049	0.202 ± 0.022	0.016 ± 0.009	0.013 ± 0.008	0.084
	HC-4	0.241 ± 0.122	0.179 ± 0.011	0.029 ± 0.018	0.045 ± 0.024	0.123
	HC-5	0.188 ± 0.036	0.298 ± 0.009	0.061 ± 0.020	0.056 ± 0.012	0.316
	HC-6	0.219 ± 0.083	0.279 ± 0.044	0.053 ± 0.017	0.057 ± 0.013	0.192

Table 7: Proportions of *Arc*-labeled (*Arc*+) nuclei, *Homer1a*-labeled (*Homer1a*+) nuclei, observed double-labeled (Double+) nuclei, and double-labeled nuclei expected by the uniform random sample with replacement model in CA1, CA3 and dorsolateral entorhinal cortex (EC) of rats that explored a novel environment (NE) after a period of home cage rest. Expected overlap was determined by calculating the product of the proportion of *Homer1a*-labeled nuclei and the proportion of *Arc*-labeled nuclei. *p*-values were obtained from paired, one-tailed *t*-tests comparing the expected and observed proportions of double-labeled nuclei across sections within each animal. Large variability between individual rats is evident. Standard error (SE) is shown.

Region	Animal	*Homer1a*+ (± SE)	*Arc*+ (± SE)	Observed Double+ (± SE)	Expected Double+ (± SE)	*p*-value
CA1	NE-1	0.168 ± 0.044	0.504 ± 0.037	0.083 ± 0.018	0.082 ± 0.017	0.113
	NE-2	0.013 ± 0.006	0.282 ± 0.019	0.004 ± 0.002	0.004 ± 0.002	0.493
	NE-3	0.015 ± 0.005	0.377 ± 0.008	0.004 ± 0.002	0.006 ± 0.002	0.005
	NE-4	0.137 ± 0.067	0.377 ± 0.075	0.059 ± 0.033	0.053 ± 0.033	0.268
	NE-5	0.083 ± 0.039	0.424 ± 0.037	0.047 ± 0.026	0.038 ± 0.021	0.125
	NE-6	0.193 ± 0.097	0.423 ± 0.025	0.093 ± 0.047	0.086 ± 0.043	0.143
CA3	NE-1	0.060 ± 0.035	0.236 ± 0.012	0.021 ± 0.013	0.014 ± 0.009	0.156
	NE-2	0.014 ± 0.005	0.115 ± 0.013	0.0021 ± 0.0002	0.002 ± 0.001	0.349
	NE-3	0.010 ± 0.001	0.157 ± 0.017	0.002 ± 0.001	0.0015 ± 0.0002	0.481
	NE-4	0.070 ± 0.030	0.168 ± 0.012	0.014 ± 0.005	0.011 ± 0.005	0.054
	NE-5	0.036 ± 0.015	0.179 ± 0.053	0.008 ± 0.004	0.007 ± 0.004	0.195
	NE-6	0.026 ± 0.010	0.226 ± 0.027	0.006 ± 0.001	0.006 ± 0.002	0.425
EC	NE-1	0.097 ± 0.076	0.375 ± 0.030	0.022 ± 0.016	0.035 ± 0.027	0.220
	NE-2	0.128 ± 0.080	0.349 ± 0.024	0.052 ± 0.030	0.048 ± 0.033	0.311
	NE-3	0.191 ± 0.105	0.336 ± 0.022	0.048 ± 0.025	0.067 ± 0.040	0.185
	NE-4	0.103 ± 0.043	0.224 ± 0.112	0.041 ± 0.030	0.028 ± 0.021	0.196
	NE-5	0.197 ± 0.087	0.366 ± 0.002	0.079 ± 0.046	0.072 ± 0.032	0.353
	NE-6	0.283 ± 0.031	0.392 ± 0.009	0.091 ± 0.007	0.110 ± 0.010	0.225

experimental animals (refer to Figures 16 and 17). The correlations observed among individual home cage animals ranged from r = 0.4317-0.7351 in CA1, r = 0.4836-0.8789 in CA3, and r = 0.5227-0.7877 in dorsolateral entorhinal cortex (Figures 19-24). Similarly, the correlations observed among individual experimental animals ranged from r = 0.3519-0.6787 in CA1, r = 0.6198-0.8119 in CA3, and r = 0.5366-0.7281 in entorhinal cortex (Figures 25-30).

Populations of nuclei in both home cage and experimental rats that expressed *Arc* only or *Homer1a* only (based on the results of the foci-based analysis) that fell within one standard deviation of the mean nuclear volume clustered in largely non-overlapping populations that were, on average, moderately correlated with regards to the average nuclear red and green pixel intensities (refer to Figures 16 and 17). The correlations observed among individual home cage controls, however, ranged from r = 0.2965-0.7024 in CA1, r = 0.3561-0.7491 in CA3, and r = 0.1640-0.7506 in dorsolateral entorhinal cortex for single *Arc*-labeled nuclei and r = 0.0583-0.7957 in CA1, r = 0.0781-0.7912 in CA3, and r = 0.3404-0.6259 in cortex for single *Homer1a*-labeled nuclei (Figures 19-24). Similarly, the correlations observed among experimental rats ranged from r = 0.1565-0.6540 in CA1, r = 0.2796-0.8016 in CA3, and r = 0.1349-0.6596 in dorsolateral entorhinal cortex for single *Arc*-labeled nuclei and r = 0.2737-0.8406 in CA1, r = 0.5516-0.9369 in CA3, and r = 0.3960-0.7250 in entorhinal cortex for single *Homer1a*-labeled nuclei (Figures 25-30).

When considering only double-labeled nuclei (that is, nuclei that exhibited both *Arc* and *Homer1a* foci), there was a low to moderate average correlation observed between the average nuclear red and green pixel intensities in both home cage controls and experimental rats (refer to Figures 16 and 17). The correlations observed among individual home cage controls, however, ranged from r = 0.1849-0.6528 in CA1, r = 0.1265-0.2163 in CA3, and r = 0.2876-0.8734 in dorsolateral entorhinal cortex (Figures 19-24). Similarly, the correlations observed among individual experimental animals ranged from r = -0.3259-0.6898 in CA1, r = -0.5253-0.7361 in CA3, and r = 0.1349-0.6596 in entorhinal cortex (Figures 25-30).

It should be noted that an animal was only included in these ranges (and in the overall averaged correlations) if three or more nuclei demonstrated the applicable foci within that region. The large variations in correlations observed among single and double-labeled nuclei across individual rats can likely be largely attributed to variations in the proportions of active nuclei observed between animals (refer to Table 6 and Table 7).

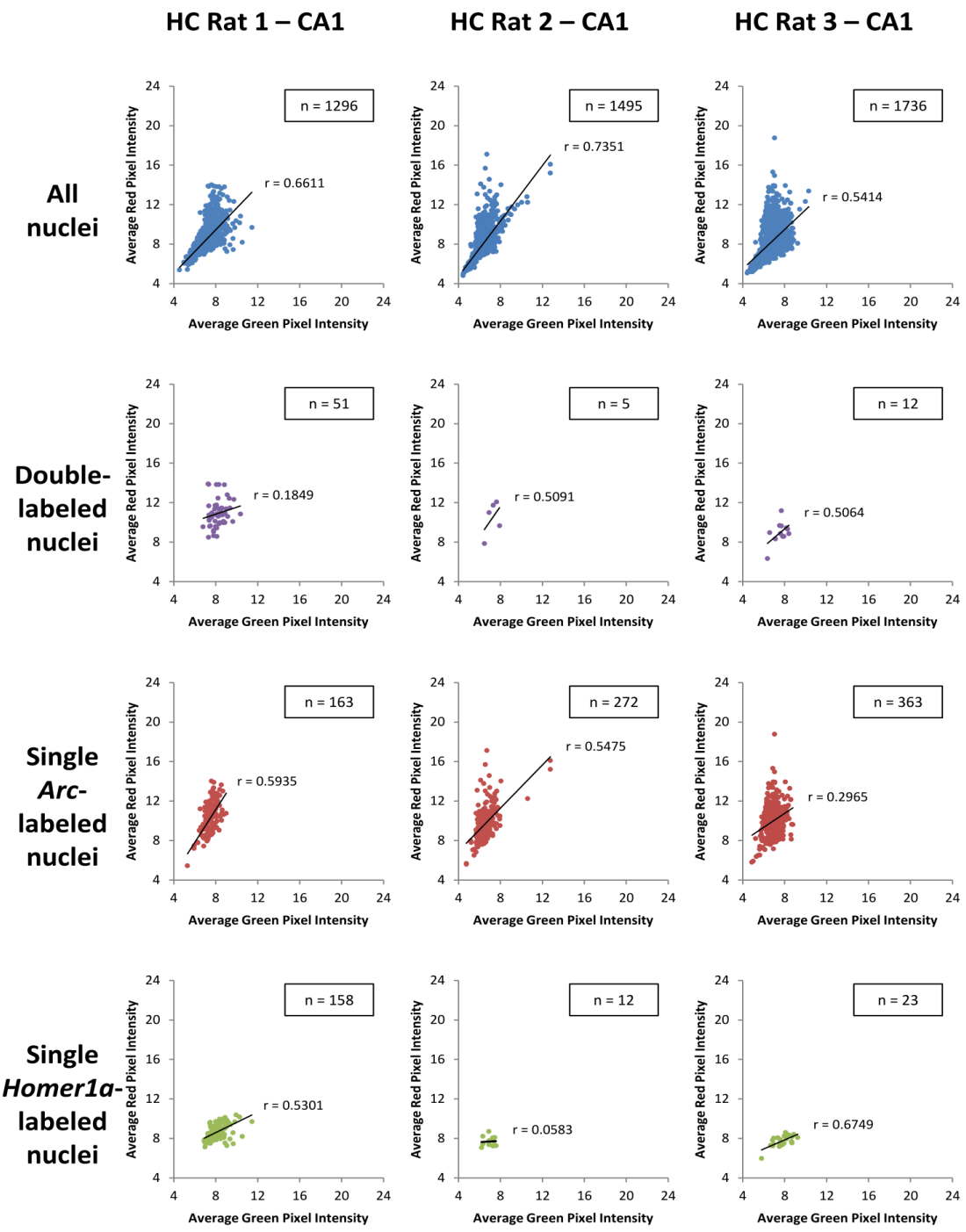

Figure 19: Correlations between nuclear average red and average green pixel intensities among all nuclei (both labeled and unlabeled), double-labeled nuclei, single *Arc*-labeled nuclei and single *Homer1a*-labeled nuclei in CA1 of the first cohort (Rats 1-3) of home cage (HC) controls. Individuals rats demonstrated a range of low to moderate correlations (*r*) between nuclear average red and green pixel intensities among subgroups of labeled nuclei (classified based on the foci analysis; n = number of nuclei).

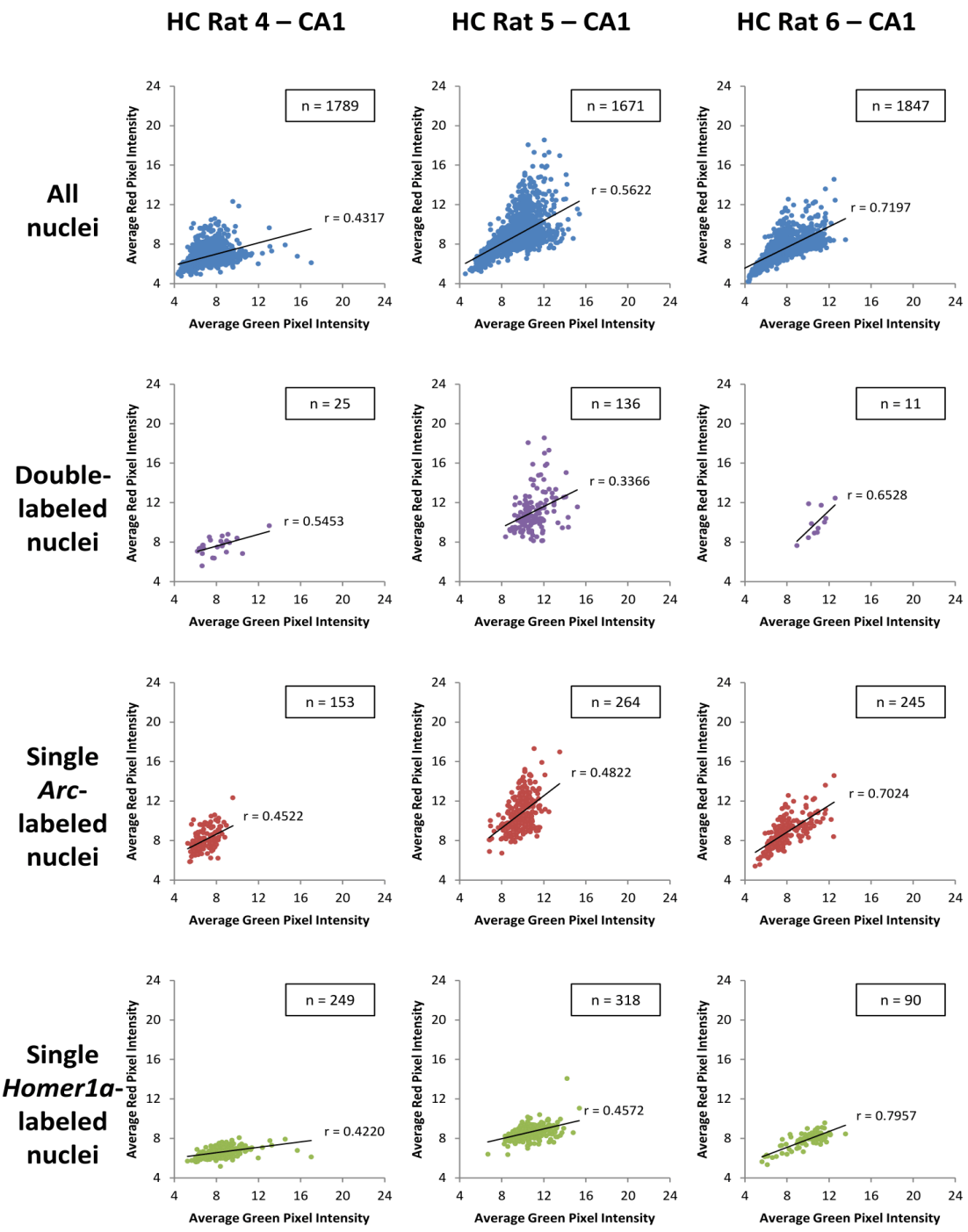

Figure 20: Correlations between nuclear average red and average green pixel intensities among all nuclei (both labeled and unlabeled), double-labeled nuclei, single *Arc*-labeled nuclei and single *Homer1a*-labeled nuclei in CA1 of the second cohort (Rats 4-6) of home cage (HC) controls. Individuals rats demonstrated a range of moderate to high correlations (*r*) between nuclear average red and green pixel intensities among subgroups of labeled nuclei (classified based on the foci analysis; n = number of nuclei).

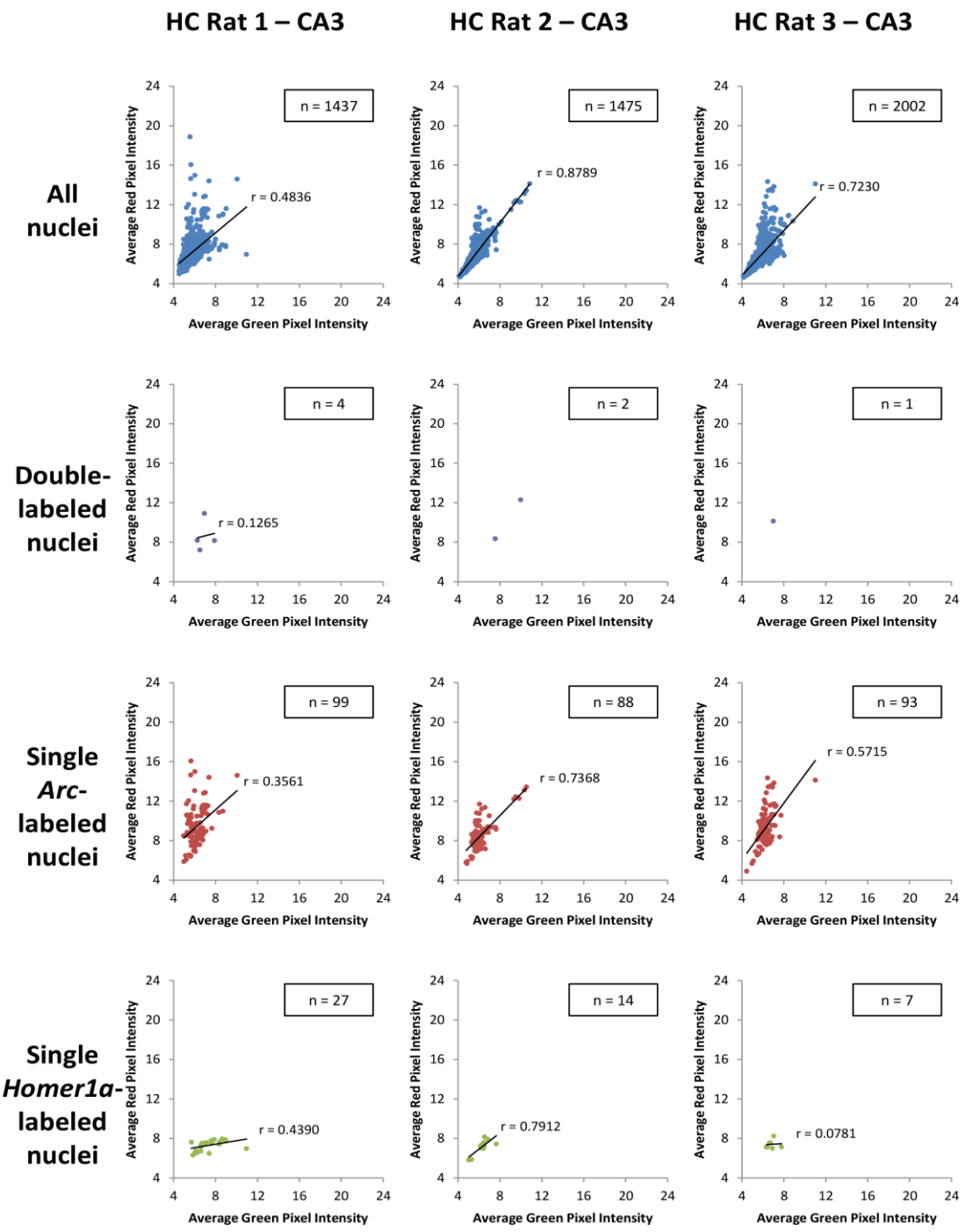

Figure 21: Correlations between nuclear average red and average green pixel intensities among all nuclei (both labeled and unlabeled), double-labeled nuclei, single *Arc*-labeled nuclei and single *Homer1a*-labeled nuclei in CA3 of the first cohort (Rats 1-3) of home cage (HC) controls. Individuals rats demonstrated a range of low to high correlations (*r*) between nuclear average red and green pixel intensities among subgroups of labeled nuclei (classified based on the foci analysis; n = number of nuclei).

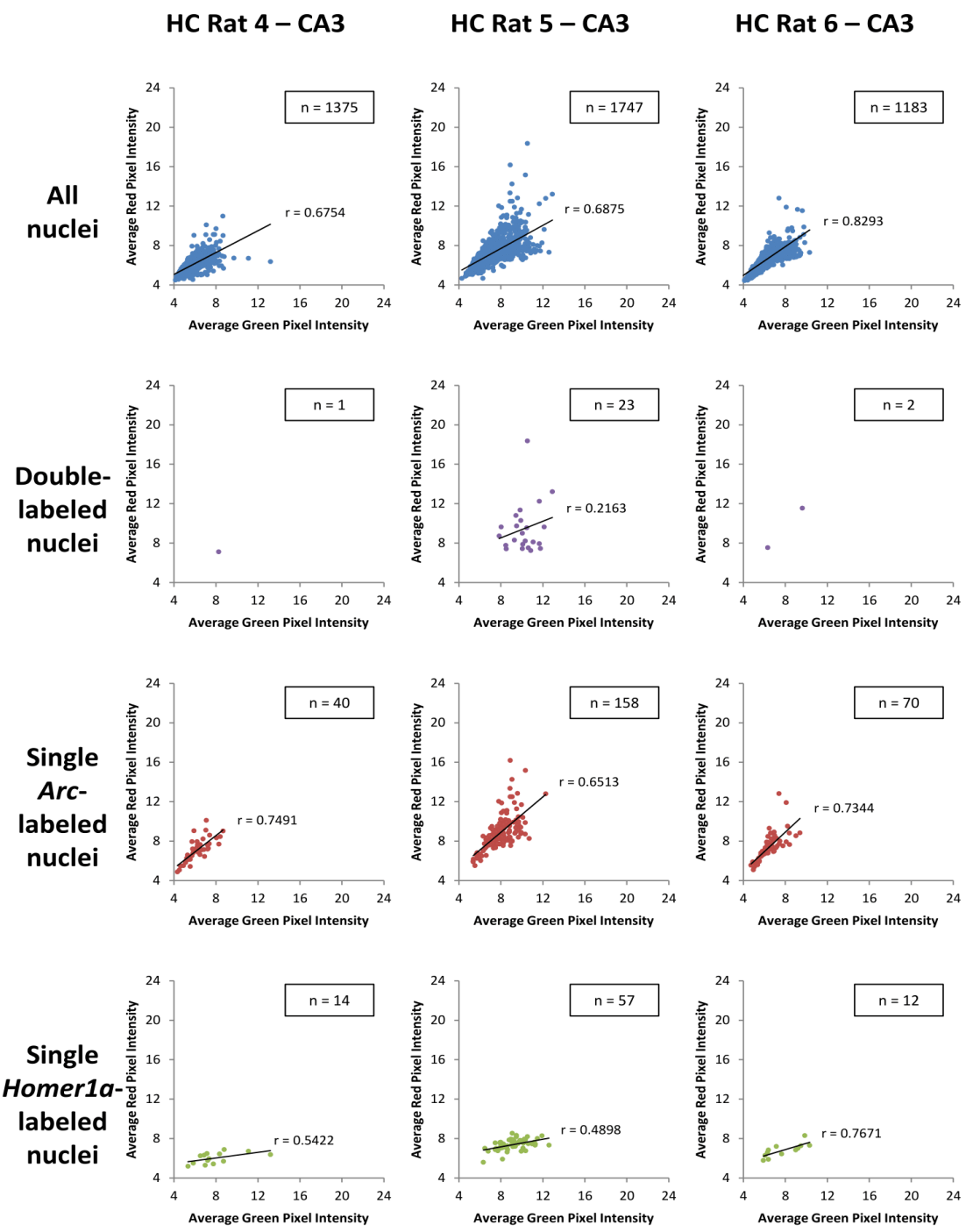

Figure 22: Correlations between nuclear average red and average green pixel intensities among all nuclei (both labeled and unlabeled), double-labeled nuclei, single *Arc*-labeled nuclei and single *Homer1a*-labeled nuclei in CA3 of the second cohort (Rats 4-6) of home cage (HC) controls. Individuals rats demonstrated a range of low to high correlations (*r*) between nuclear average red and green pixel intensities among subgroups of labeled nuclei (classified based on the foci analysis; n = number of nuclei).

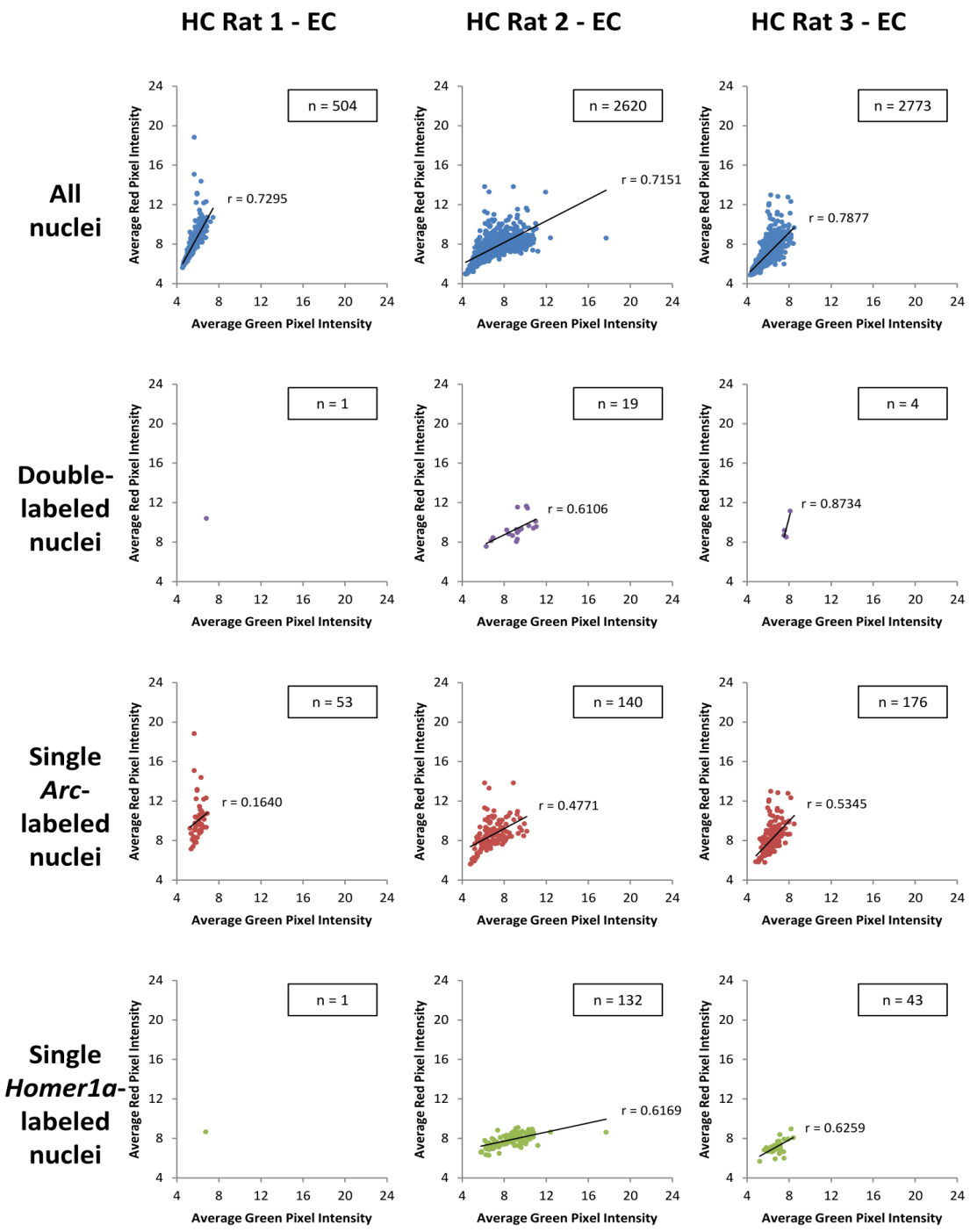

Figure 23: Correlations between nuclear average red and average green pixel intensities among all nuclei (both labeled and unlabeled), double-labeled nuclei, single *Arc*-labeled nuclei and single *Homer1a*-labeled nuclei in dorsolateral entorhinal cortex (EC) of the first cohort (Rats 1-3) of home cage (HC) controls. Individuals rats demonstrated a range of low to high correlations (*r*) between nuclear average red and green pixel intensities among subgroups of labeled nuclei (classified based on the foci analysis; n = number of nuclei).

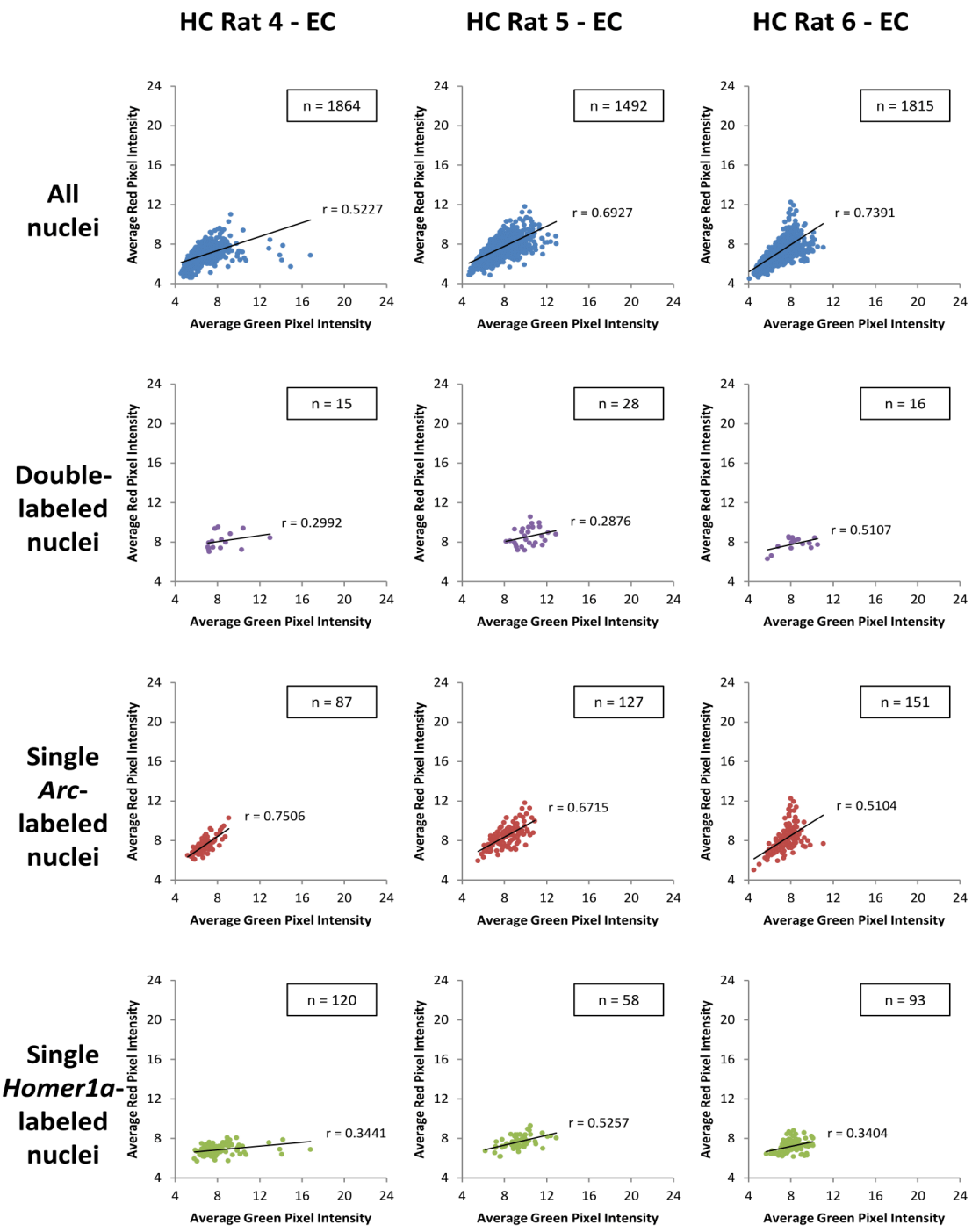

Figure 24: Correlations between nuclear average red and average green pixel intensities among all nuclei (both labeled and unlabeled), double-labeled nuclei, single *Arc*-labeled nuclei and single *Homer1a*-labeled nuclei in dorsolateral entorhinal cortex (EC) of the second cohort (Rats 4-6) of home cage (HC) controls. Individuals rats demonstrated moderate correlations (*r*) between nuclear average red and green pixel intensities among subgroups of labeled nuclei (classified based on the foci analysis; n = number of nuclei).

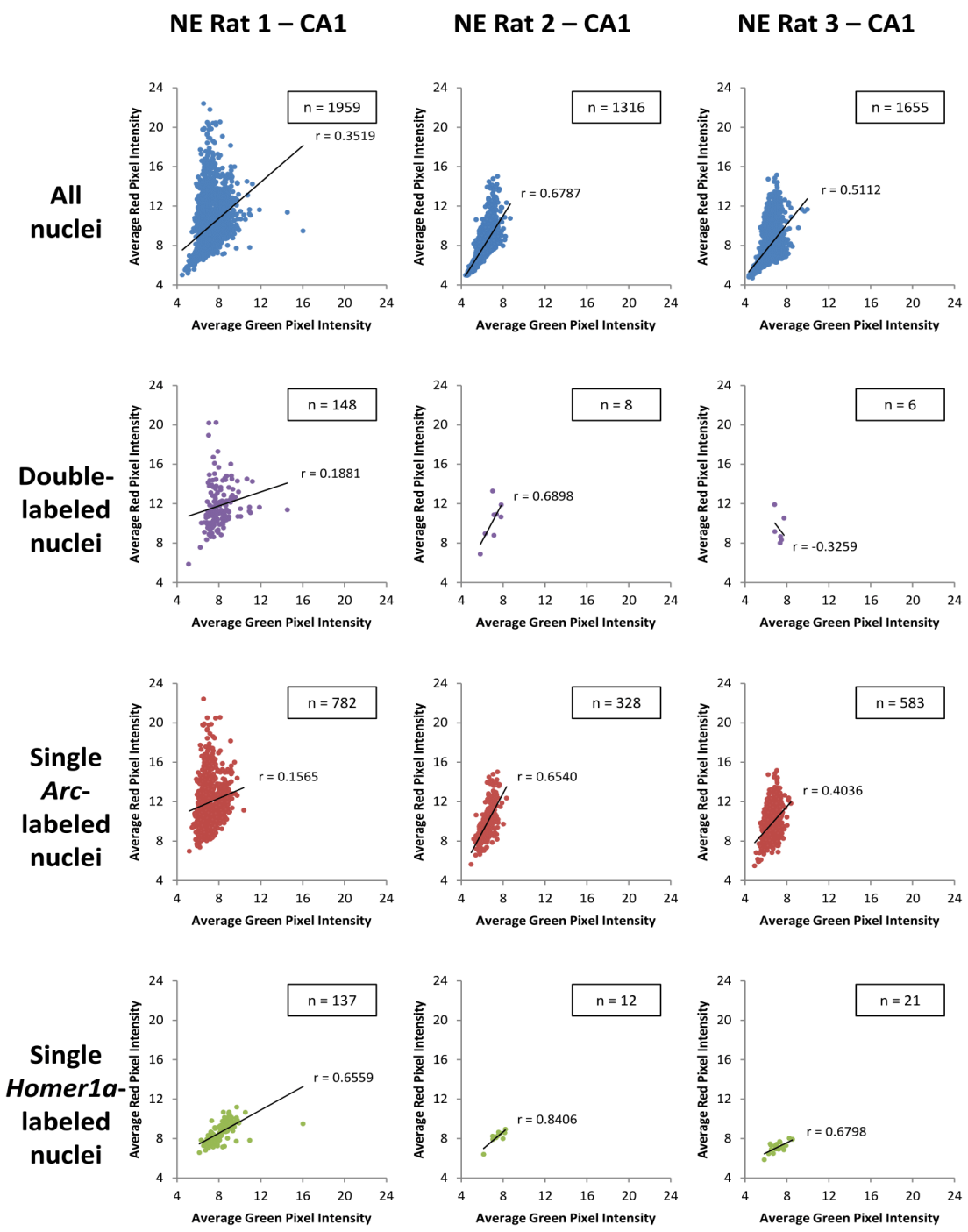

Figure 25: Correlations between nuclear average red and average green pixel intensities among all nuclei (both labeled and unlabeled), double-labeled nuclei, single *Arc*-labeled nuclei and single *Homer1a*-labeled nuclei in CA1 of the first cohort (Rats 1-3) of rats that explored a novel environment (NE) after a period of home cage rest. Individuals rats demonstrated a range of low to high correlations (*r*) between nuclear average red and green pixel intensities among subgroups of labeled nuclei (classified based on the foci analysis; n = number of nuclei).

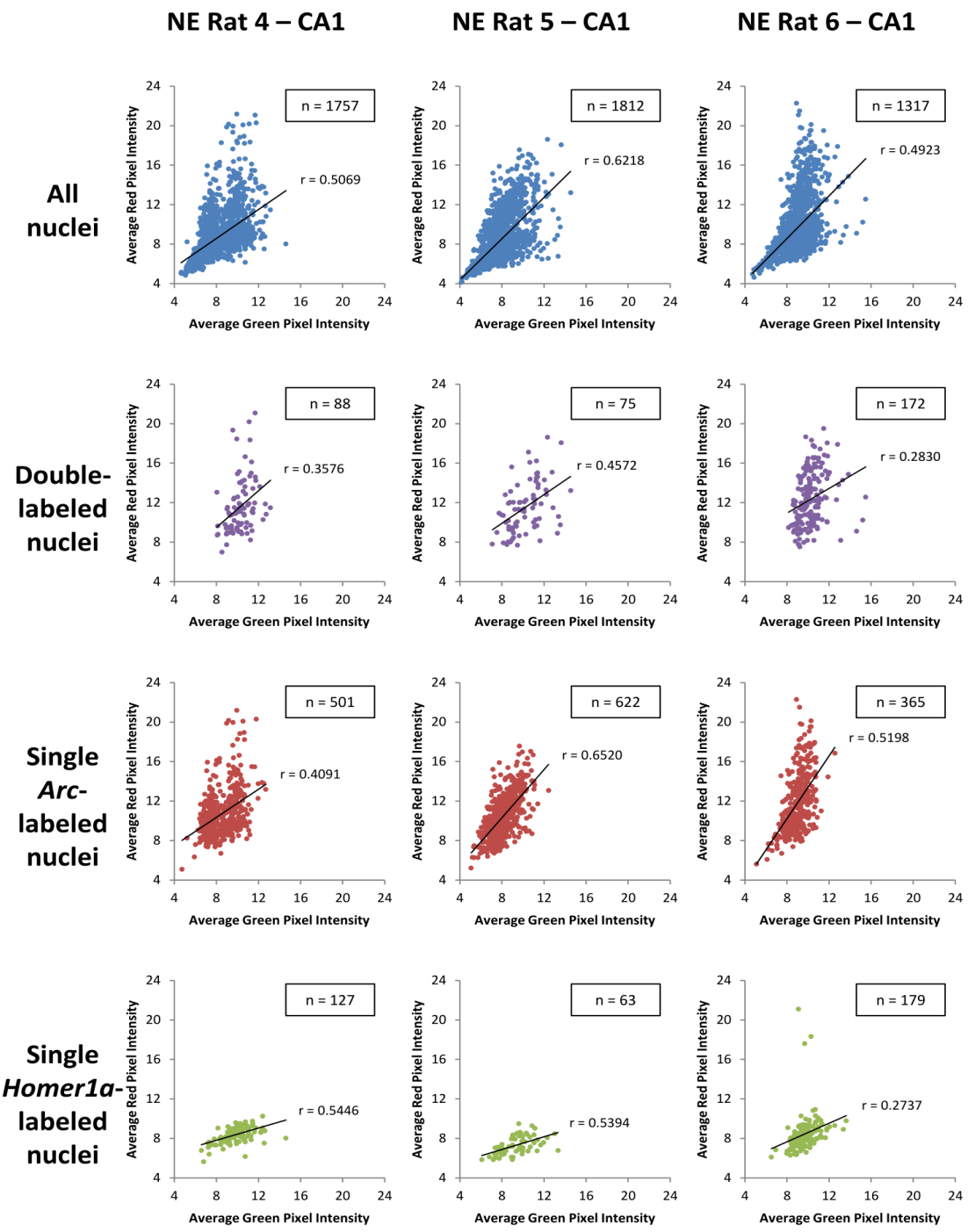

Figure 26: Correlations between nuclear average red and average green pixel intensities among all nuclei (both labeled and unlabeled), double-labeled nuclei, single *Arc*-labeled nuclei and single *Homer1a*-labeled nuclei in CA1 of the second cohort (Rats 4-6) of rats that explored a novel environment (NE) after a period of home cage rest. Individuals rats demonstrated moderate correlations (*r*) between nuclear average red and green pixel intensities among subgroups of labeled nuclei (classified based on the foci analysis; n = number of nuclei).

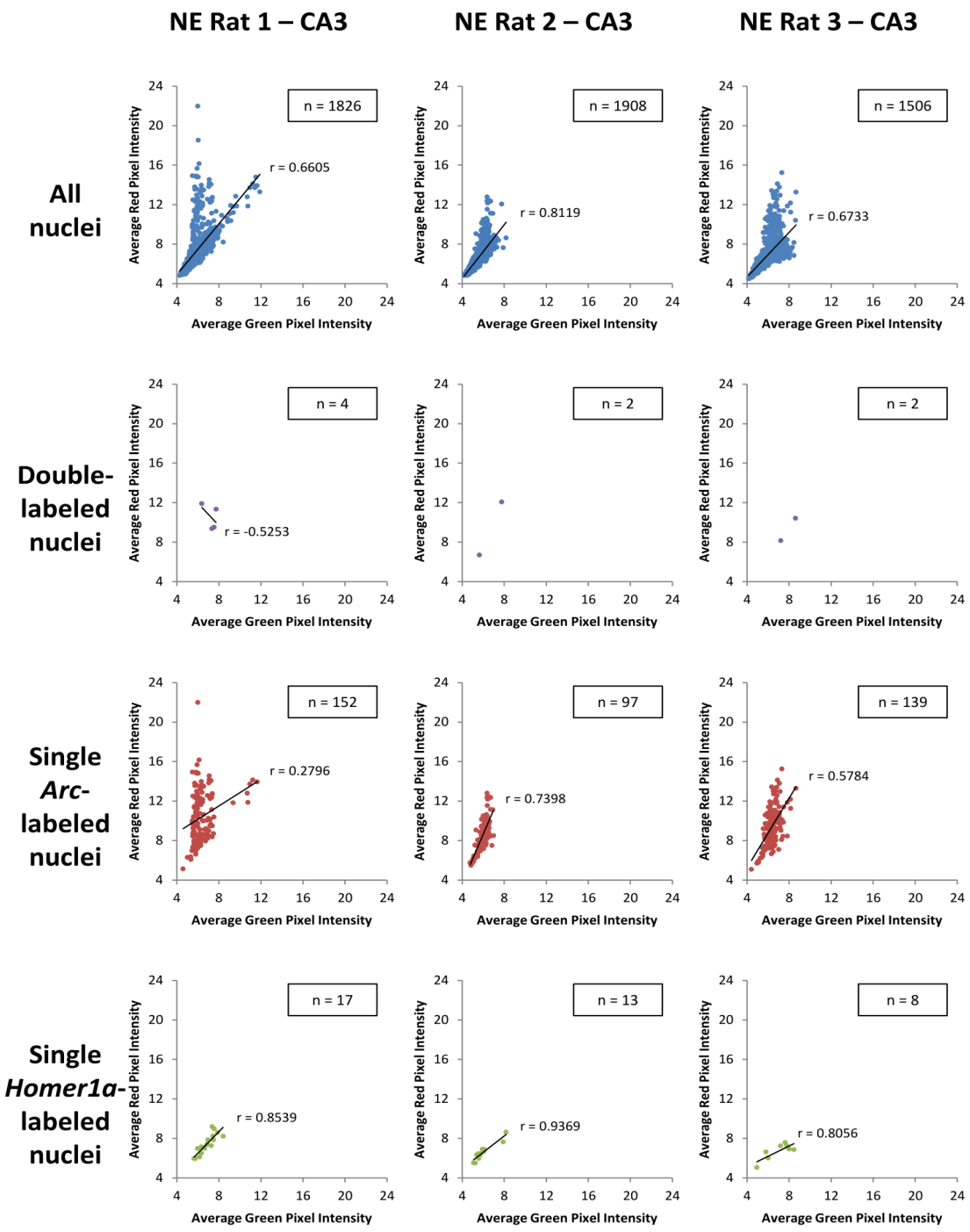

Figure 27: Correlations between nuclear average red and average green pixel intensities among all nuclei (both labeled and unlabeled), double-labeled nuclei, single *Arc*-labeled nuclei and single *Homer1a*-labeled nuclei in CA3 of the first cohort (Rats 1-3) of rats that explored a novel environment (NE) after a period of home cage rest. Individuals rats demonstrated a range of moderate to high correlations (*r*) between nuclear average red and green pixel intensities among subgroups of labeled nuclei (classified based on the foci analysis; n = number of nuclei).

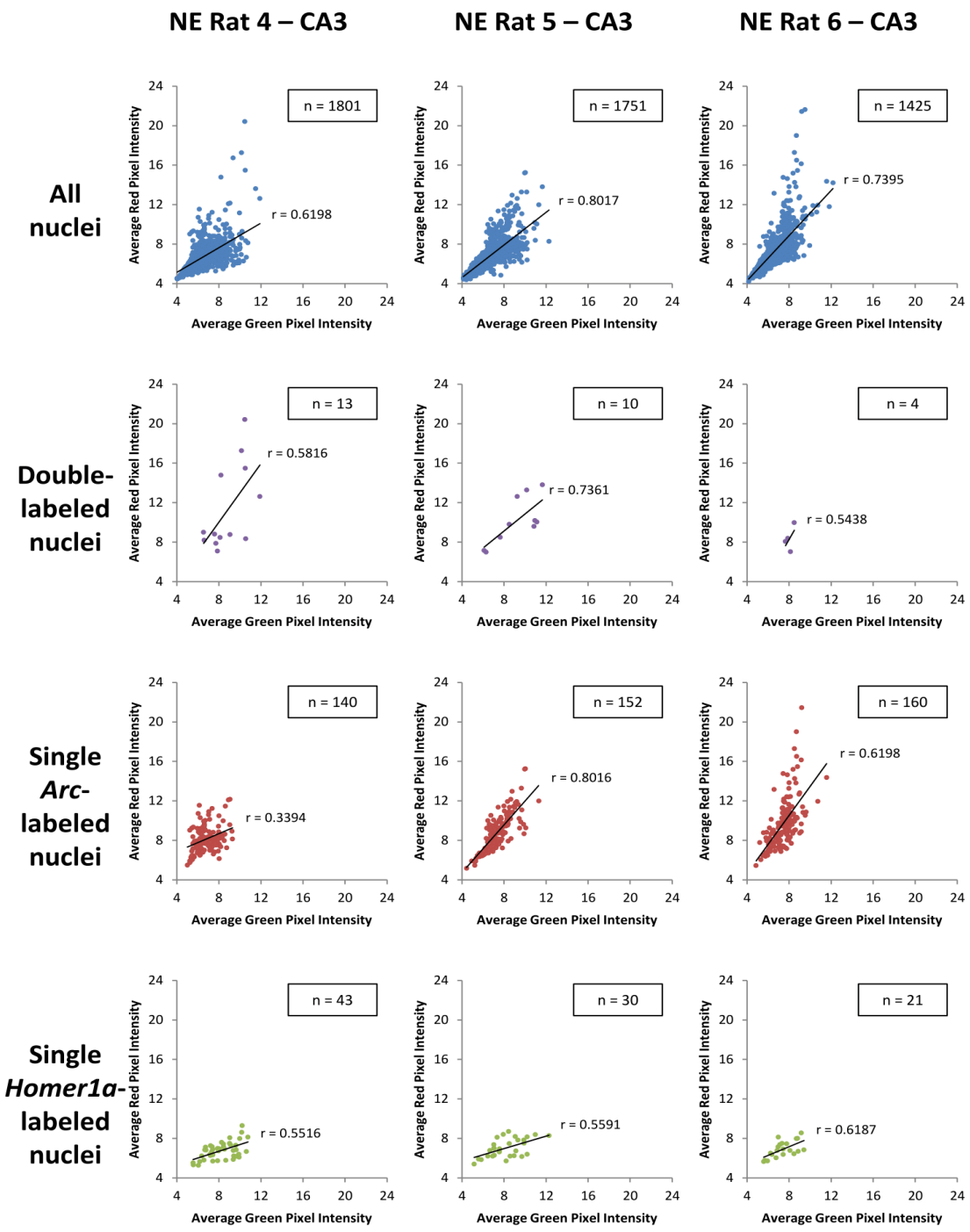

Figure 28: Correlations between nuclear average red and average green pixel intensities among all nuclei (both labeled and unlabeled), double-labeled nuclei, single *Arc*-labeled nuclei and single *Homer1a*-labeled nuclei in CA3 of the second cohort (Rats 4-6) of rats that explored a novel environment (NE) after a period of home cage rest. Individuals rats demonstrated a range of moderate to high correlations (*r*) between nuclear average red and green pixel intensities among subgroups of labeled nuclei (classified based on the foci analysis; n = number of nuclei).

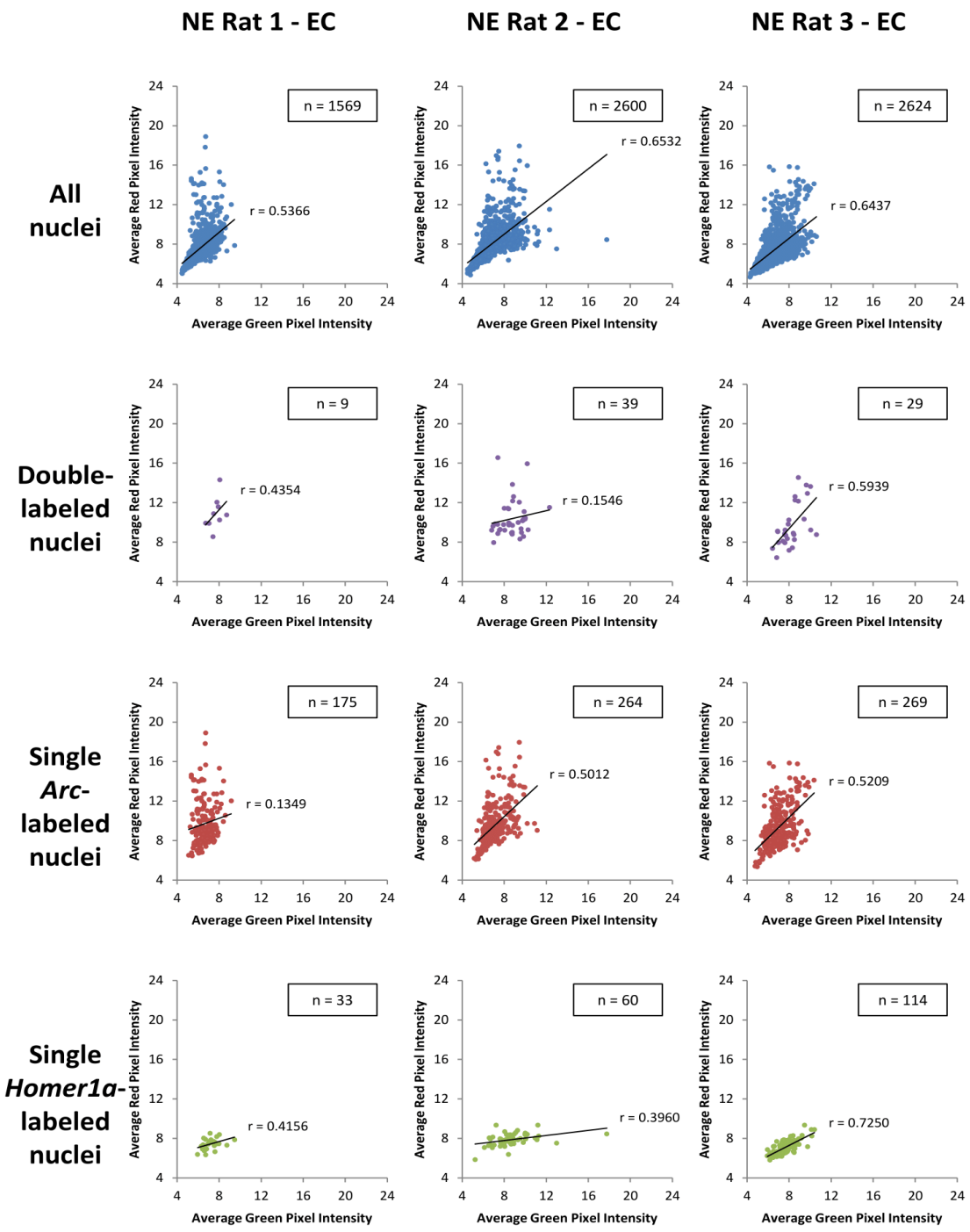

Figure 29: Correlations between nuclear average red and average green pixel intensities among all nuclei (both labeled and unlabeled), double-labeled nuclei, single *Arc*-labeled nuclei and single *Homer1a*-labeled nuclei in dorsolateral entorhinal cortex (EC) of the first cohort (Rats 1-3) of rats that explored a novel environment (NE) after a period of home cage rest. Individuals rats demonstrated a range of low to moderate correlations (*r*) between nuclear average red and green pixel intensities among subgroups of labeled nuclei (classified based on the foci analysis; n = number of nuclei).

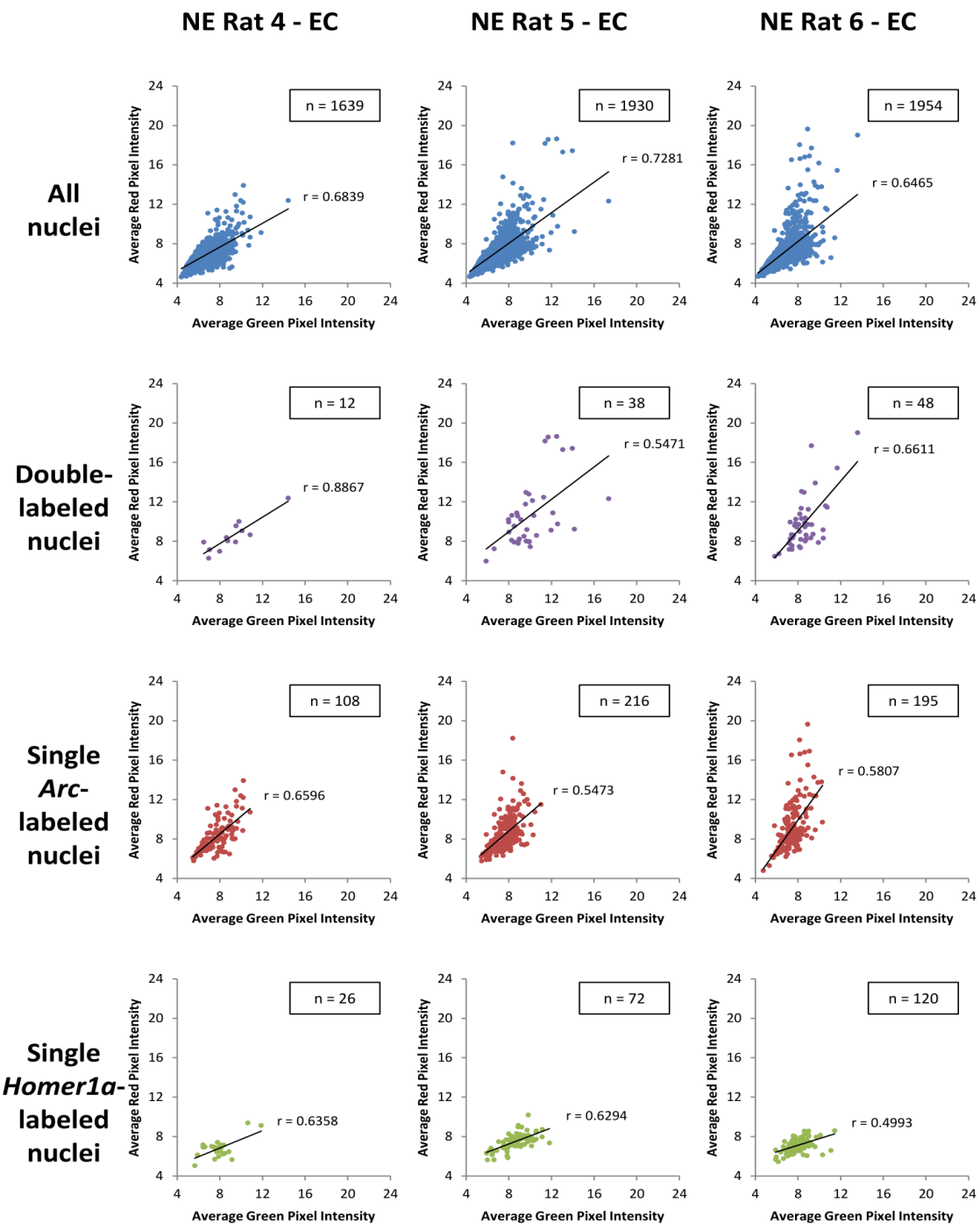

Figure 30: Correlations between nuclear average red and average green pixel intensities among all nuclei (both labeled and unlabeled), double-labeled nuclei, single *Arc*-labeled nuclei and single *Homer1a*-labeled nuclei in dorsolateral entorhinal cortex (EC) of the second cohort (Rats 4-6) of rats that explored a novel environment (NE) after a period of home cage rest. Individuals rats demonstrated a range of moderate to high correlations (*r*) between nuclear average red and green pixel intensities among subgroups of labeled nuclei (classified based on the foci analysis; n = number of nuclei).